UNLV | University Libraries
University of Nevada, Las Vegas

UNLV Theses/Dissertations/Professional Papers/Capstones

12-1-1999

Alteration associated with gold deposition at the Getchell, Carlin-type gold deposit, north-central Nevada

Tracy Lynn Cail
University of Nevada, Las Vegas

Follow this and additional works at: http://digitalscholarship.unlv.edu/thesesdissertations

 Part of the Geology Commons

Repository Citation

Cail, Tracy Lynn, "Alteration associated with gold deposition at the Getchell, Carlin-type gold deposit, north-central Nevada" (1999). *UNLV Theses/Dissertations/Professional Papers/Capstones*. Paper 1457.

This Thesis is brought to you for free and open access by Digital Scholarship@UNLV. It has been accepted for inclusion in UNLV Theses/Dissertations/Professional Papers/Capstones by an authorized administrator of Digital Scholarship@UNLV. For more information, please contact marianne.buehler@unlv.edu.

KINEMATICS AND TIMING OF OROGEN-PARALLEL FLOW, GROUSE CREEK MOUNTAINS, UTAH

by

Tonia Gail Arriola

Bachelor of Science
University of Nevada, Las Vegas
2002

A thesis submitted in partial fulfillment
of the requirement for the

Master of Science Degree in Geoscience
Department of Geoscience
College of Science

Graduate College
University of Nevada, Las Vegas
August 2008

ABSTRACT

**Kinematics and Timing of Orogen-Parallel Flow,
Grouse Creek Mountains, Utah**

By

Tonia G. Arriola

Dr. Michael L. Wells, Examination Committee Chair
Professor of Geology
University of Nevada, Las Vegas

Alternating contractional and extensional events in orogenic belts play a significant role in dynamically adjusting crustal thickness during regional contraction. Distinguishing between these two contrasting kinematic regimes is not only important for understanding the tectonic setting but also provides insights into the dynamics of evolving orogenic wedges. The earliest pervasive fabric, D_1, in the Grouse Creek Mountains of northwest Utah is interpreted to have played an integral role in accommodating such a dynamic adjustment. It is interpreted that focused crustal thickening led to differences in gravitational potential energy along strike, facilitating an episode of mid-Cretaceous synconvergent orogen-parallel extension. The D_2 event is a previously undocumented deformational event in the Pennsylvanian-Permian Oquirrh Formation and overprints the earlier D_1 fabric. D_2 is characterized by an axial planar cleavage, S_2, associated with east-verging north-northeast-trending large-scale folds at

Marble Peak, South Hill and the Rosebud area, and is interpreted to record a top-to-the southeast contractional event.

TABLE OF CONTENTS

ABSTRACT iii

LIST OF FIGURES vi

CHAPTER 1 INTRODUCTION 1
Purpose 4
Significance 5
Methodology 6

CHAPTER 2 REGIONAL GEOLOGIC AND TECTONIC SETTING AND GEOLOGY OF THE RAFT RIVER, ALBION, GROUSE CREEK MOUNTAINS 9
Previous work 10
Middle Mountain Shear Zone 12
Tectonostratigraphy 13

CHAPTER 3 MESOSCOPIC STRUCTURAL ANALYSES 14
Introduction 14
Spatial distribution of D_1 and D_2 fabric 15

CHAPTER 4 STRAIN AND KINEMATIC ANALYSES OF STRAIN FRINGES 22
Introduction 22
What are strain fringes? 22
Kinematic and petrographic analysis of strain fringes 26

CHAPTER 5 DISCUSSION 42
D_1: contraction or extension 42
Tectonic significance of D_1: orogen-parallel extension? 49
D_2: contraction or extension 57
Relative age of D_2 65
Tectonic implications for D_2 68

CHAPTER 6 CONCLUSIONS 72

REFERENCES 130

VITA 141

LIST OF FIGURES

Figure 1 Generalized geologic map of Raft River-Albion-Grouse Creek Mountains (RAG) showing distribution of the L_1 stretching lineation 75

Figure 2 Tectonostratigraphic column of Archean to Miocene rocks in the Grouse Creek Mountains 76

Figure 3 Geologic map of the Marble Peak klippe, showing the distribution and orientation of S_1, S_2, L_1, L_{mm} 77

Figure 4 Photographs A-E showing L_1 elongation lineation in Oquirrh Formation 79

Figure 5 Geologic map of North and South Hill, showing distribution and orientation of S_1, S_2, L_1, L_{mm} 81

Figure 6 Geologic map of Rosebud area, showing the distribution and orientation of S_1, S_2, L_1, L_{mm} 83

Figure 7 Photographs at Marble Peak showing relationship between S_1 and S_2, and parasitic folds within the upper limb of a west vergent fold 84

Figure 8 Geologic map, stereonets and photographs of east verging recumbent anticline within Pennsylvanian-Permian Oquirrh Formation at South Hill 86

Figure 9 Photomosaics of South Hill recumbent anticline, looking east 88

Figure 10 Geologic map of Rosebud area with stereonet data showing L_1 elongation lineation in red dots, poles to the S_1 planes in black dots and S_2 axial planar cleavage in blue lines 89

Figure 11 Shear sense indicators for D_1 deformation 90

Figure 12 Shear sense indicators for D_2 deformation 91

Figure 13 Contact between the Oquirrh Formation limestone and the Oquirrh Tectonite in the core of the fold at South Hill 92

Figure 14 Photomicrographs for face-controlled fibers versus displacement-controlled fibers, showing geometric difference between the two types 93

Figure 15 Figure showing the three principal planes of finite strain in relation to the strain fringes for Marble Peak and the Rosebud Creek ridge 95

Figure 16 Photomicrograph A is showing both D_1 and D_2 strain fringes within the XZ plane of S_1 at Marble Peak 96

Figure 17 Simplified geologic map of Marble Peak, showing D_1 top-to-the-north shear sense and D_2 top-to-the-south shear sense 97

Figure 18 Simplified geologic map of North and South Hill, showing D_1 top-to-the-south shear sense 98

Figure 19 Simplified geologic map of Rosebud, showing D_1 top-to-the-north shear sense and D_2 top-to-the-south shear sense 99

Figure 20 Photomicrographs illustrating the Rigid Fiber Model for incremental coaxial and object-center path method for non-coaxial strain fringes 101

Figure 21 Finite strain map of D_1 and D_2 deformation for Marble Peak 102

Figure 22 Finite strain map for D_1 and D_2 deformation for North and South Hill 103

Figure 23 Finite strain map of D_1 and D_2 deformation for the Rosebud area 105

Figure 24 Diagram illustrating the relationship between W_k with the flow apophyses and the orientation of the instantaneous stretching axes 106

Figure 25 A-B; Photomicrographs illustrating measurements used for vorticity analysis for the D_1 face-controlled strain fringes 108

Figure 26 Photomicrographs of D_1 strain fringes within the XY plane at Rosebud area 111

Figure 27 Geologic map of Rosebud area showing displacement path for D_1 and D_2 strain fringes within the XY plane of S_1 and S_2 respectively 112

Figure 28 Photomicrographs showing how the object center path method was used to determine the finite and incremental strain 113

Figure 29 Figure from Koehn et al. (2000) showing how increments of translation and rotation were measured and input into the "Fringe Growth" program 114

Figure 30 A-C; Simulations of fibrous strain fringes conducted using the program "Fringe Growth" to substantiate the object center path method, which was used to measure the incremental and finite strain 115

Figure 31 Cumulative incremental strain history diagrams within the XZ plane of S_1 for the folds at the northwest section of the map at Rosebud area 119

Figure 32 Cumulative incremental strain history diagrams within the XZ plane of S_1 for the folds at southeast section of the Rosebud area 121

Figure 33 Photomicrographs of D_2 displacement-controlled strain fringes within the XY plane of the S_2 axial planar cleavage at Rosebud area 122

Figure 34 Patterns of foliation trajectories 123

Figure 35 Generalized geologic map of Raft River-Albion-Grouse Creek Mountains (RAG) showing distribution of the L_1 stretching lineation 124

Figure 36 Vertical strain gradient for D_1 and D_2 at Marble Peak within the Oquirrh Formation in relation to the Middle detachment 126

Figure 37 Simplified tectonic model for development of orogen-parallel extension at mid-crustal levels in the interior of the Sevier orogen around ~100 Ma 127

Figure 38 Sequence of Mesozoic to early Cenozoic deformation proposed for relative constraints on timing for the "D_2" event 129

ACKNOWLEDGEMENTS

I would like to thank my advisor, Dr. Michael Wells, who deserves an award for tolerating me and my seemingly insurmountable quantity of edits. He deserves special recognition for his patience and encouraging words that helped guide me through this experience. Deep down, I am glad that I did not take the other field area offered to me; too many flowers, waterfalls and rainbows detract from the beauty of the outcrops. Thank you so much, Michael.

I would like to thank my committee members: Dr. Terry Spell, Dr. Michael Pravica, and Dr. Thomas Hoisch for serving on my committee. Extra thanks to Dr. Thomas Hoisch for serving on my committee and traveling back and forth from Arizona. In addition, I would like to thank my field assistants, Tiesa Dunlop, Dr. Michael Wells, and my brother James Arriola. I want to give special thanks to the best brother in the world for allowing me to use his brand new car as a field vehicle and for protecting me with his mighty stick against the mountain lion and rattlesnakes; lots of love.

I would like to thank my fellow graduate students, friends and the faculty members at UNLV. Special thanks to Maureen Yonovitz, Mandy Williams, Tricia Evans, Menghesha Beyene, Joe Kula, Nate Suurmeyer, and Aaron Hirsch for their help along the way. I would also like to thank Dr. Clay Crow for your assistance in the rock lab.

Last but definitely not least, I would like to thank my partner Lauren Izzo. I could not have done this without your patience, emotional support and encouraging words especially towards the end. Your turn.

This research was supported by the National Science Foundation, the Geological Society of America, and the UNLV Department of Geoscience.

CHAPTER 1

INTRODUCTION

Synconvergent extension parallel to the strike of orogenic belts is well recognized worldwide, but its causes are poorly understood (Ellis and Watkinson, 1987; Mancktelow, 1992; Murphy et al., 2002; Davis and Maidens, 2003; Merschat et al., 2005; Wells et al., 2008). Orogen-parallel extension has been documented in several tectonic settings such as: (1) accretionary prisms; (2) magmatic arcs; (3) arcuate orogenic belts; and (4) retroarc fold-thrust belts. The causes proposed for orogen-parallel extension include the following end members: (1) transpression (Sanderson and Marchini, 1984; Ellis and Watkinson, 1987; Teyssier et al., 1995; Fossen and Tikoff, 1998); (2) arcuation (Marshak, 1988; Ferrill, 1991; Ferrill and Groshong, 1993); (3) collisional and lateral escape (Molnar and Tapponier, 1975; Frisch et al., 1998; Seyferth and Henk, 2003; Rosenberg et al., 2004); and (4) gravitational relaxation due to unequal crustal thickening or thinning (Camilleri, 1998; Davis and Maidens, 2003; Miller et al., 2006; Wells et al., 2008). Although several insightful studies from various tectonic settings have been conducted in order to understand the processes controlling orogen-parallel extension (Ellis and Watkinson, 1987; Mancktelow, 1992; Murphy et al., 2002; Davis and Maidens, 2003; Merschat et al., 2005; Wells et al., 2008), the causes, which generate the spatial and temporal distribution of orogen-parallel extensional strain features common within mountain belts worldwide, remain insufficiently understood.

Mid-crustal levels of the interior of the Sevier orogenic belt are exposed in northwestern Utah and record deformation within deep levels of a retroarc non-collisional orogen. These exposures, along with the well-constrained tectonic framework of the western United States; including plate boundary location (Armstrong, 1968; Burchfiel, 1992; Decelles, 2004), convergent rates and direction, and inferred subduction angles (Engebretson, 1985; Decelles, 2004) through time; provide an excellent natural laboratory in which to study the driving mechanisms and the products of synconvergent orogen-parallel extension.

The earliest ductile deformation fabric (D_1) in the Grouse Creek Mountains of northwest Utah affects Archean to Permian rocks and records an episode of mid-Cretaceous deformation in the hinterland of the Sevier orogen. The mid-Cretaceous D_1 fabric developed during a top-to-the north mid-crustal shear and is characterized by a flat-lying penetrative foliation and a north-northeast-trending penetrative elongation lineation (L_1). Previous interpretations of the D_1 fabric have been offered, including top-to-the-east thrusting (Compton, 1977), top-to-the-north thrusting (Malavieille, 1987), and orogen-parallel extension (Wells et al., 1997; Wells et al., 2008).

Outcrops of the Pennsylvanian-Permian Oquirrh Formation of the Middle allochthon in the Grouse Creek Mountains were excellent sites for studying the D_1 fabric because: (1) the D_1 fabric is well developed in the Middle allochthon of the Grouse Creek Mountains, unlike exposures in the Raft River and Albion Mountains; (2) the D_1 fabric is well preserved in the upper plate of the Middle detachment, above the Cenozoic mylonite; (3) strain fringes in greenschist facies rocks, in which the original fiber geometries are preserved, record the incremental strain history; and (4) strain fringes

contain phlogopite fibers and are thus amenable to *in situ* laserprobe $^{40}Ar/^{39}Ar$ dating (Wells et al., 2000; Wells et al., 2008).

In addition to the D_1 fabric, a second deformational fabric is also present within the Pennsylvanian-Permian Oquirrh Formation in the field areas, to be referred to as D_2. The preservation of the D_2 fabric in these rocks provides an opportunity to determine the relationship between this fabric and large scale folds present in the field areas and to determine whether the kinematics of D_2 deformation are more compatible with extension or shortening.

Strain fringes are ubiquitous throughout the Pennsylvanian-Permian Oquirrh Formation and are important to determination of the kinematics and timing of the D_1 and D_2 deformational events. Strain fringes are useful kinematic indicators, providing information on incremental and finite strain (Ramsay and Huber, 1983), shear sense (Passchier and Trouw, 2005), flow vorticity, fold mechanics (Beutner and Diegel, 1985), and deformation age (Müller et al., 2000; Wells et al., 2008). Numerous studies have been conducted on these syn-kinematic features (Ramsay and Huber, 1983; Beutner and Diegel, 1985; Fisher and Anastasio, 1994; Aerden, 1996; Müller et al., 2000; Koehn et al., 2000, 2001, 2003). In particular, finite and incremental strain studies have provided important insights on the progressive deformational history of the host rock. Strain fringes have been used to determine the kinematics and reconstruction of regional and outcrop scale folds, adding to the understanding of the development of large-scale recumbent folds (Beutner and Diegel, 1985; Fisher and Anastasio, 1994). Fibrous strain fringes preserved in the greenschist facies Pennsylvanian-Permian rocks of the Middle allochthon provide an opportunity to contribute to the ongoing research of using strain

fringes to determine incremental and finite strain, shear sense, flow vorticity, and fold mechanics.

Purpose

The purpose of this study is to provide a more complete kinematic description of the earliest ductile fabric D_1 (as recorded in the Grouse Creek Mountains), and to test the hypothesis that the fabrics record an episode of mid-Cretaceous synconvergent orogen-parallel extension in the hinterland of the Sevier orogen. Additionally, I document a previously recognized but poorly studied ductile fabric, D_2, (associated with large scale folds) that records a reversal in shear sense. One of the principal research questions to be addressed here is whether or not the D_1 fabric in the Grouse Creek Mountains records a contraction or extension. This question is addressed by considering the following sub-questions: what is the overall distribution and orientation of the D_1 fabric, shear zone geometry and kinematics, sense of shear, degree of vorticity, and overall strain magnitude and gradient? Furthermore, what are the driving mechanisms and tectonic significance of the D_1 fabric? The other principal research question concerns the deformational history of the D_2 fabric. This is addressed by considering the following questions: what is the overall distribution and orientation of the D_2 fabric, kinematics, sense of shear, degree of vorticity, and overall strain magnitude and gradient? In addition, how is the D_2 fabric related to the earlier D_1 fabric and folds that are present throughout the field areas?

Significance

Over the past several years, there has been an increasing recognition of the importance of alternating contractional and extensional events in the evolution of orogenic belts and that these kinematic alternations play a significant role in dynamically adjusting crustal thickness during orogenesis. (Platt, 1986; Manctelow, 1992; Wells, 1997; Rey et al., 2001; Fergusson et al., 2007; Sullivan and Snoke, 2007) Knowledge of the strain distribution and kinematics for these events within crustal rocks provides insights into the driving mechanisms for these kinematic alternations. This study presents kinematic, petrographic, and geologic map data that provides evidence for both contractional and extensional events in the hinterland of the Sevier orogen. From these data, I propose that the earliest ductile fabric (D_1) in the Grouse Creek Mountains of northwestern Utah records an episode of mid-Cretaceous orogen-parallel extension, synchronous with orthogonal convergence of the Farallon plate with the North American plate. Synconvergent extension parallel to the strike of the Sevier orogenic belt played a significant role in dynamically adjusting crustal thickness during regional contraction. While synconvergent orogen-parallel extension is widely recognized in oblique plate margin settings, this study provides new insights on the development of orogen-parallel extension in retroarc non-collisional settings such as the hinterland of the Sevier orogen in a tectonic regime of orthogonal plate convergence. Furthermore, I interpret the D_2 folds and fabrics as related to the formation of a top-to-the-southeast contractional event, recording renewed crustal shortening following extension. Additionally, this study contributes to our understanding of the utility of syn-kinematic fibrous strain fringes in determining the progressive and incremental deformational history and kinematics of

tectonic processes. Moreover, it provides more documentation on the methods for quantifying incremental and finite strain using strain fringes. Finite and incremental strain values and kinematic reconstructions are significant in the study of crustal deformation. In particular, the majority of balance cross-sections and restorations of fold-and-thrust belts fail to incorporate the amount of internal strain, which therefore should be considered in order to produce accurate results.

Methodology

Both field and laboratory work were conducted in order to determine the kinematics of the D_1 and D_2 deformational events.

Field studies

Mississippian to Permian rocks of the Middle allochthon were mapped at a scale of 1:12,000 in three areas totaling about 26 square kilometers in the central Grouse Creek Mountains: the Marble Peak klippe, North and South hills, and the ridge south of Rosebud Creek, to be referred to as the Rosebud area (Figure 1). These locations were selected because they exhibit well developed D_1 fabrics. Mesoscopic structural features associated with D_1 and D_2 were measured, including two foliations (S_1 and S_2), two stretching lineations (L_1 and L_{mm}), intersection lineations, and relict bedding, with particular emphasis on determining whether folding was associated with D_1 or D_2 and whether S_1 or S_2 are axial planar to folds. Strain fringes were examined in the field as well as with a petrographic microscope, with an emphasis on determining the curvature of fibers within their respective cleavage (XY) planes, and asymmetries within their respective (XZ) planes. Fifty-seven oriented samples of fibrous strain fringes were

collected across transects from the Middle detachment to the highest structural levels throughout the three field locations. Thin sections were prepared parallel to L_1 and perpendicular to S_1, parallel to S_1, and where S_2 was well developed, parallel to S_2.

Laboratory studies

To represent and describe the kinematics of the D_1 and D_2 deformational fabrics, the field data were input into a geospatial ARCGIS database interactive map. This ARCGIS database contains all of the field data from Marble Peak, North and South Hill, and Rosebud Area, including GPS and sample locations, contacts of map units, S_1, S_2, L_1, L_{mm}, and field pictures. The user can choose a GPS location and select and view the measurements of the outcrops as well as the pictures that were taken at the chosen location. GPS locations from the collection sites of every strain fringe sample are also indicated on the map to represent the distribution throughout the field areas, both laterally and vertically within the shear zone. In addition, a field map was created in Adobe Illustrator CS3. Stereoplots for all three areas were completed using Stereowin 1.2, and provide information on the kinematics of the D_1 and D_2 deformational events. Stereographic projections were used to quantitatively display three dimensional geologic data such as the planar (relict bedding, foliations, cleavages) and linear (lineations, poles to foliations) features associated with D_1 and D_2 to determine fold axes and to assist with interpretations of the geologic history.

Thin sections prepared from all three field areas (Marble Peak, North and South Hill, and Rosebud Creek ridge) were examined with a petrographic microscope to determine the kinematics of the D_1 and D_2 events. Several digital photomicrographs of fibrous strain fringes were taken from every sample to aid in the kinematic study, and

measurements were made using ImageJ from NIH image company, developed by Larry Reinking. Methods and programs used for the kinematic study include: (1) rigid fiber model; (2) object-center path method; (3) Fringe Growth program; (4) and vorticity method. These methods will be discussed in greater detail under the appropriate heading in Chapter 4. Sense of shear was determined from digital photomicrographs for all of the fibrous strain fringe samples and from mesoscopic shear sense indicators measured in the field areas.

CHAPTER 2

REGIONAL GEOLOGIC AND TECTONIC SETTING AND GEOLOGY OF THE RAFT RIVER, ALBION, GROUSE CREEK MOUNTAINS

The Grouse Creek Mountains of northwest Utah are part of the Raft River-Albion-Grouse Creek metamorphic core complex, within the hinterland of the Late Mesozoic and early Cenozoic Sevier orogenic belt (Figure 1) (Armstrong, 1968; Wells, 1997). Prior to the onset of the Sevier orogeny, Archean and Proterozoic crystalline basement was overlain by a sedimentary wedge of Neoproterozoic, Paleozoic, and Lower Mesozoic platform, shelf, and slope deposits (Stewart et al., 1990) (Figure 2). During the Mesozoic, the development of a convergent plate margin created back arc intraplate crustal shortening and led to the development of the Sevier orogen (Burchfiel et al., 1992; Decelles, 2004). The Sevier orogen is characterized by east-vergent, decollement style low-angle thrust faults in the foreland fold and thrust belt marking the eastern limit (Armstrong, 1968), and contractional and extensional structures in the hinterland (Camilleri and Chamberlain, 1997; Wells, 1997). Following cessation of Sevier orogenesis, the Raft River-Albion-Grouse Creek Mountains underwent episodic crustal extension, magmatism, and metamorphism from the middle to late Eocene to the present (Compton, 1983; Wells et al., 1997). This produced metamorphic core complexes, which resulted in two opposing shear zones and detachments: the top-to-the-west Middle detachment and Middle Mountain shear zone, and the top-to-the-east Raft River

detachment and shear zone (Malavieille, 1987; Saltzer and Hodges, 1988; Wells et al., 2000). These Cenozoic shear zones and detachment faults exhumed the Mesozoic mid-crustal fabrics that are the subject of this research.

Previous work

In the past few decades, numerous structural studies of the Raft River-Albion-Grouse Creek metamorphic complex have been conducted, the majority of which focus on the Cenozoic extensional history, including multiple Cenozoic detachment faults and extensional shear zones (Malavieille, 1987a; Saltzer and Hodges, 1988; Manning and Bartley, 1994; Wells et al., 2000; Wells, 2001; Sheely, 2002; Egger et al., 2003). Studies of the Mesozoic geology have focused on metamorphic petrology and its tectonic implications, rather than on the Mesozoic fabrics (Dudash, 2001; Hoisch et al., 2002; Harris, 2003; Kelly, 2004; Harris et al., 2007). Specifically, the Cretaceous D_1 deformation event has received little study (Compton et al., 1977; Malavieille, 1987b; Wells, 1997; Wells et al., 2000b; Wells et al., 2008), despite being the most widespread and pervasive fabric in this core complex. A few interpretations of the D_1 fabric have been offered, including top-to-the-east thrusting, top-to-the-north thrusting, and orogen-parallel extension. This study focuses on this poorly understood aspect of the Mesozoic history and provides a better understanding of the widespread but currently enigmatic penetrative D_1 fabric.

An early study by Compton et al. (1977) interpreted the D_1 deformation fabric as recording top-to-the east thrusting in the late Mesozoic and early Tertiary. Compton suggested that at least three sets of folds formed during metamorphism and a fourth after

metamorphism. The oldest of the fold generations, D_1, is related to eastward thrusting and is documented to have fold axes and lineations that define a broad arc that rotates from east to northwest from the Raft River Mountains to the Grouse Creek Mountains.

Malavieille (1987) conducted strain and kinematics analyses across the entire Raft River-Albion-Grouse Creek metamorphic core complex in order to determine the geometry and kinematics of the ductile shearing events, referred to as D_1 and D_2. He interpreted the D_1 deformation event as related to thrusting to the north-northeast, corresponding to shortening in the Mesozoic. Malavieille's D_2 event is related to opposing Cenozoic extensional shearing events, eastward in the Raft River Mountains and westward in the Albion-Grouse Creek Mountains. For clarification purposes, the D_2 event recorded by the strain fringes in this thesis is not related to the "D_2" event described by Malavieille.

Wells (1997) interpreted the D_1 ductile shearing event present in the Grouse Creek, Raft River, and Albion Mountains as gravitational spreading of nappes linked to foreland shortening, based on studies in the eastern Raft River Mountains indicating a northeast-trend to L_1 lineations. Alternatively, kinematic studies of the D_1 fabric and a correlation of the fabric between allochthon and PreCambrian basement across the entire core complex indicate a dominant northward direction to the shear at mid-crustal levels, interpreted as resulting from gravitational collapse parallel to the orogen (Wells et al., 1997; Wells et al., 2008). A recent study by Wells et al. (2008) reinterprets the age of the D_1 deformational event as mid-Cretaceous (105 ± 6 Ma), recording a previously unrecognized event of mid-Cretaceous synconvergent orogen-parallel extensional flow in the Sevier hinterland. The D_2 fabric in the study area (Figure 1) has been previously

recognized (Wells et al., 2008) as a younger growth event in strain fringes, but its age, distribution, and kinematic significance remain unknown.

Middle Mountain shear zone

The Eocene and Oligo-Miocene Middle Mountain shear zone of the Raft River-Albion-Grouse Creek metamorphic core complex is exposed in the field areas (Figure 1). A low-angle normal fault, known as the Middle detachment, forms the upper boundary of the shear zone (Figure 2). This detachment places Mississippian-Pennsylvanian rocks over Late Proterozoic to Archean rocks within the field areas, thus creating a major unconformity in the stratigraphy. The Middle Mountain shear zone deforms Archean to Mississippian rocks; this is noted in the field by the overprint of northwest-trending stretching lineations (L_{mm}) (Figure 3). Two periods of movement during the Cenozoic are recorded within this shear zone (Wells et al., 2004). The older shearing event records a top-to-the-northwest movement ~N63W, whereas the younger event is more west directed at N87W (Saltzer and Hodges, 1988; Wells et al., 1997; Wells et al., 2004). Separation of the two events is based on the variation of the lineation trend, amount of deformation, and deformation temperature from the structurally deeper rocks to the structurally higher rocks (Wells et al., 1997; Wells et al., 2004), as well as their relationship with Oligocene plutons. These two ductile shearing events overprint the pervasive mid-Cretaceous D_1 top-to-the-north ductile fabric, with the exception of the Pennsylvanian-Permian Oquirrh Formation of the Middle allochthon. The Mesozoic fabrics within the Pennsylvanian-Permian Oquirrh Formation are well preserved

structurally above the Cenozoic Middle detachment and Middle Mountain shear zone in the study areas.

Tectonostratigraphy

The Grouse Creek Mountains expose three allochthonous sheets that overlie an autochthon consisting of predominantly Precambrian Adamellite (Compton et al., 1977; Todd, 1980) (Figure 1). There are four tectonostratigraphic units: the autochthon, the Lower allochthon, the Middle allochthon, and the Upper allochthon (Figures 1 and 2).

The autochthon is composed of Archean schist, amphibolite, trondjemite, and metamorphosed adamellite (orthogneiss) which is overlain by a Proterozoic package of, in ascending order, Elba Quartzite, schist of Steven Springs, and quartzite of Clarks Basin (Figure 2). Overlying the Proterozoic package is the Ordovician Pogonip Group (Garden City Formation and Swan Peak Quartzite from Wells, 1996), Eureka Quartzite, and the Ordovician/Silurian (?) dolomite (Figure 2). The highly strained, uppermost greenschist facies Pennsylvanian-Permian Oquirrh Formation tectonite within the Lower allochthon is below the Middle detachment (Figure 2). The Middle allochthon is composed entirely of lower grade (lower-middle greenschist facies) Oquirrh Formation, which is the focus of this study. The Oquirrh Formation was emplaced along the Middle detachment fault, structurally above the Middle Mountain shear zone. The Upper allochthon is comprised of unmetamorphosed Upper Permian-Triassic Gerster Formation, Thaynes Formation, and Tertiary sedimentary and volcaniclastic rocks, which are not exposed in the study areas (Figure 2).

CHAPTER 3

MESOSCOPIC GEOMETRIC AND KINEMATIC ANALYSES

Introduction

Kinematics is the study of the motion of an object or particles without the consideration of mass or force. During deformation, an object can undergo translation, rotation, dilation and distortion. A kinematic study can determine the sense of shear, tectonic transport direction and magnitude, and can provide information on the relative components of pure and simple shear within a shear zone.

The central Grouse Creek Mountains have experienced multiple Mesozoic and Cenozoic deformational events. This study focuses on the two ductile deformational events, known as D_1 and D_2. The D_1 fibers are mid-Cretaceous (Wells et al., 2008), and the age of the D_2 event is unknown. D_2 is a previously unrecognized deformational event that postdates the earlier top-to-the-north D_1 ductile event. Mesoscopic structural features associated with these deformational events, such as foliations and lineations, were measured in the field and plotted on stereoplots to aid in determining the kinematics of the two deformational events. Foliations are useful kinematic indicators, providing information on strain, metamorphic conditions and overprinting relationships, and are thought to record or lie parallel to the XY plane of the finite strain ellipsoid (Passchier and Trouw, 2005). Stretching lineations record the X direction of finite strain ellipsoid (Passchier and Trouw, 2005), and provide information on the direction of extension

within the shear zone but not the sense of shear. Lineation measurements are used in this study to record the transport direction of extension within the shear zone. The sense of shear for the D_1 and D_2 events was determined by a field study of mesoscopic shear sense indicators, including asymmetric porphryoclasts, calcite blebs, boudins, chert stringers, and quartz veins. Sense of shear for both D_1 and D_2 events was also determined by petrographic analysis of fibrous strain fringes within the XZ plane of the strain ellipsoid for each deformation event.

This thesis seeks to provide more documentation of the mid-Cretaceous ductile D_1 fabric and to determine the kinematics of the D_2 fabric.

Spatial distribution of D_1 and D_2 fabric

Throughout the study areas, the pervasive mid-Cretaceous D_1 ductile fabric is well preserved structurally above the Cenozoic Middle detachment within the Pennsylvanian-Permian Oquirrh Formation of the Middle allochthon (Figures 3-8). Structurally below the Middle detachment, the D_1 fabric is overprinted by the Eocene and Oligo-Miocene Middle Mountain shear zone (Figures 3-8). The D_1 fabric is also preserved in regions beneath the Cenozoic shear zones.

In the field areas, S_1 is predominantly a flat-lying foliation (Figure 3), sub-parallel to lithological layering, and dips are variable due to doming from exhumation of the Cenozoic metamorphic core complex as well as from folding during development of S_2 (Figure 3). In the Oquirrh Formation of the field areas, S_1 is defined by a variable pressure-solution to crystal-plastic foliation defined by dissolution creep of quartz and dynamic recrystallization of calcite. A penetrative, generally north-northeast trending

elongation lineation recorded by strain fringes, stretched fossils, and stretched minerals are within the S_1 plane (Figure 4). At the Rosebud area, the D_1 fibers are curved within the plane of S_1.

Within the field areas, S_2 foliation is axial planar to folds, and is defined by alignment of micas, calcite and quartz. The obliquity between S_2 and S_1 and the development of S_2 are dependent on the lithology and position about folds, and its development is heterogeneous. Throughout the field areas, the S_2 cleavages are at low angles to subparallel to the S_1 foliation within the marbles, and are at higher angles to S_1 within the silty lithologies. S_2 gently dips ~20°-40° to the east and west, on opposite limbs of folds present in the field areas, and is more pronounced in the southern parts of the field areas. The D_2 strain fringes are developed within the S_2 plane, thus indicating growth synchronous with the folding events. The D_2 fibers exhibit a counter-clockwise curvature within the XY plane of S_2. In addition, intersection lineations defined by the intersection of S_1 and S_2 trend north-northeast. L_1 elongation lineations are parallel to the locally developed hingelines of the folds exposed at Marble Peak, South Hill, and the Rosebud area (Figures 3, 5, 6).

Marble Peak

Marble Peak exposes a large-scale east-verging fold within the Pennsylvanian-Permian Oquirrh Formation. Through stereographic projection, the trend and plunge of the fold axis at Marble Peak is determined to be 184°, 06° (Figure 3). The interlimb angle determined by stereographic projection at Marble Peak is 140°. S_1 is predominantly a flat-lying foliation sub-parallel to lithological layering at Marble Peak. Strikes of the S_1 foliation at Marble Peak are variable due to doming, with a mean foliation of 098°, 07S°,

and dips ranging from horizontal to 58° (Figure 3). The trend of the L_1 elongation lineation at Marble Peak varies by 80°, from 162°-242°, with plunges ranging from horizontal to 38° to north and south (Figure 3). The mean vector trend and plunge are ~020°, 00° (Figure 3). S_2 foliation at Marble Peak is variable, with strikes predominantly to the north-northeast and to the northwest (mean foliation of 052°, 18SE°), and east and west dips ranging from 24° to 68°.

North and South Hill

Mesostructural measurements from North and South Hill are subdivided into two domains based on differences in orientations of S_1 and S_2 foliations and trends of L_1 elongation lineations. At North and South Hill, S_1 is predominantly a flat-lying foliation sub-parallel to lithological layering. The S_1 foliation at North Hill is variable with predominantly east-west strikes (mean foliation of 098°, 13S°), and dips ranging from horizontal to 58° (Figure 5). North Hill exhibits two sets of elongation lineation (L_1) trends; one set trends from (020° to 230°) and the other set trends (130° to 287°) to the northeast to northwest with plunges ranging from horizontal to 42°. S_2 at North Hill strikes predominantly to the southeast (mean foliation of 130°, 04S°), with dips ranging from 03° to 44° (Figure 5).

At South Hill, a large-scale closed recumbent anticline, overturned to the east, is exposed within the Pennsylvanian-Permian Oquirrh Formation (Figures 8 and 9). The S_1 foliation at South Hill is variable with strikes predominantly to the southwest (mean foliation of 239°, 13S°) and dips ranging from horizontal to 57° (Figure 5). The elongation lineation L_1 at South Hill exhibits a mean vector trend and plunge of 016 °, 06° (Figure 5). At South Hill, S_2 is an axial planar cleavage with strikes predominantly to the

southwest (mean foliation of 39°, 10W°) and dominantly westward dips ranging from 02° to 32°. The trend of the fold axis at South Hill is 001°, plunging 11° to the north (Figure 5).

Rosebud area

In the Rosebud area is a large-scale east-vergent tight antiformal fold in the northeastern part of the map area, with overturned limbs on the eastern side of an exposed cliff (Figure 10). The S_1 foliation at the Rosebud area is variable due to folding, with strikes predominantly to the north-northeast (mean foliation of 059°, 03SE°), and dips ranging from horizontal to 85° (Figure 6). The trend and plunge of the fold axis at Rosebud Hill is 213° and plunges 01° to the south, determined by stereographic projection of folded S_1 (Figure 6). The L_1 elongation lineation at Rosebud trends from 055° to 182°, and plunges from horizontal to 33° (Figure 6). The mean vector trend and plunge are 207° and 03°. S_2 at Rosebud is an axial planar cleavage with strikes predominantly to the west (mean foliation of 265°, 06S°) and dips ranging from 02° to 90°.

Discussion of folds

The folds at Marble Peak and South Hill trend similarly to the north, whereas the folds in the Rosebud area trend north-northeast (Figure 6). The fold at Marble Peak is not as well defined as the folds present at South Hill and the Rosebud area. A fold within the Marble Peak klippe is interpreted based on the relationship between S_2, S_1 foliation, and parasitic folds (Figure 7), the observation that S_2 elsewhere is an axial planar cleavage, and from the orientation of measurements plotted on the stereonet program (Figure 3). Unfortunately, no stratigraphic facing indicators were observed in the field,

making it difficult to determine the vergence direction. The interlimb angle of the fold present at Marble Peak, as determined by stereographic projection, is 140°, and as such is classified as a gentle fold (Figure 3). However, if the majority of the measurements are represented by one limb, then the interlimb angle is incorrect. The L_1 elongation lineations (vector mean 020°, 00°) are subparallel to the trend of the fold axis of 184°, 06° at Marble Peak (Figure 3). Based upon these relationships and assumptions of Sevier kinematics, the exposed Pennsylvanian-Permian Oquirrh Formation at Marble Peak is interpreted to represent an east-vergent fold, truncated by the Middle detachment (Figure 3).

South Hill exhibits a well exposed, east-vergent, tight recumbent anticline within the Pennsylvanian-Permian Oquirrh Formation (Figures 8 and 9). The interlimb angle of the fold at South Hill, determined by stereographic projection, is 32°, which classifies it as a tight fold (Figure 5). The L_1 elongation lineations (vector mean 016 °, 06°) are subparallel to the trend of the fold axis at South Hill (Figure 5). The trend and plunge of the fold axis at South Hill is 001°, 11°, determined by stereographic projection (Figure 5). The folded strata are cut by two low-angle westward dipping faults with eastward displacements; younger-on-older and older-on-younger (Todd, 1980).

The east-verging antiformal tight fold exposed at the Rosebud cliff face exposes an overturned limb. On the eastern side of the cliff, an east-vergent overturned tight fold is well exposed, whereas on the western side, the opposite overturned limb is not well exposed and is mostly covered by talus (Figure 10). The interlimb angle for the eastern limb at Rosebud is 23°, thus classifying the fold as tight. The L_1 elongation lineation

mean vector trend and plunge are 207°, and 03°, and is subparallel to the trend and plunge of the fold axis of 213° and 01° (Figure 10).

Syntectonic fibers from strain fringes were collected along the fold and are used in this study as kinematic and strain indicators for the mechanics and formation of the folds. Incremental strain data from displacement-controlled fibrous strain fringes have been fruitful in determining the kinematics of folds (Beutner and Diegel, 1985), and are displayed as Cumulative Incremental Strain History Diagrams (CISH), which are discussed in Chapter 4.

Shear sense indicators

Microscopic and mesoscopic features were used in this study to determine the sense of shear for the D_1 and D_2 deformational events. Sense of shear can be determined from the asymmetry of mesoscopic and microscopic features—shear sense indicators—which are produced during non-coaxial progressive deformation (Passchier and Trouw, 2005). Mesoscopic shear sense indicators, including asymmetric porphryoclasts, calcite blebs, boudins, chert stringers, and quartz veins, were measured at South Hill and the Rosebud area; these features record an overall top-to-the-north sense of shear for D_1 (Figure 11). Mesoscopic shear sense indicators are not present at Marble Peak; thus in this location, only microscopic shear sense indicators were used.

Asymmetric shear sense indicators, such as asymmetric porphyroclasts, are present at South Hill within the Oquirrh Formation tectonite, in proximity to the Mississippian Chainman Diamond Peak Formation lithologic contact. The tectonite contains dominantly sigma-type as well as delta-type porphyroclasts, recording a top-to-the-north sense of shear (Figure 12). The tectonite is exposed on the overturned limb of

the recumbent fold, as suggested by east-dipping cleavages present within the quartz rich siltite below the tectonite (Figure 13).

Mesoscopic shear sense indicators at the Rosebud area, such as asymmetric boudins (Passchier and Trouw, 2005), are associated with the D_1 fabric and record an overall top-to-the-north sense of shear (Figure 11). The asymmetric boudins of the earlier D_1 fabric are overprinted by the development of the D_2 fold within the Rosebud area. The measured mesoscopic shear sense indicators consistently record a top-to-the-north sense of shear. Microscopic shear sense indicators of D_1 and D_2 will be discussed in Chapter 4 of this thesis.

CHAPTER 4

STRAIN AND KINEMATIC ANALYSES OF STRAIN FRINGES

Introduction

A kinematic study of strain fringes was conducted in thin section to determine: (1) sense of shear; (2) finite strain; (3) amount of rotation for fibers and core objects in the XZ and to a lesser extent, the XY plane of the finite strain ellipsoid; (4) the progressive incremental strain history; and (5) the progressive incremental orientations within the XY plane of S_1 and S_2. A strain analysis is used to measure the changes in shape and size of an object due to deformation. Fifty-seven oriented samples were collected. Of these, 37 were selected for a finite and incremental strain analysis to determine the lateral and vertical strain gradient within the shear zone.

What are strain fringes?

Fibrous strain fringes contain fibrous minerals precipitated in low pressure sites adjacent to rigid objects, and are usually composed of a different mineral species from the rigid object (Kerrich, 1978; Davis and Reynolds, 1984; Groshong, 1988; Knipe, 1989; Passchier and Trouw, 2005). Strain fringes are useful kinematic indicators, providing information on flow and deformation history (Passchier and Trouw, 2005), and are used to estimate sense of shear and finite and incremental strain histories (Ramsay and Huber, 1983). Strain fringes form by the process of fluid assisted mass transfer. Dissolution

along grain boundaries oriented at high angles to the infinitesimal shortening direction within the matrix or core object occurs due to enhanced mineral solubility resulting from high elastic strain energy due to grain to grain interactions. Material is dissolved and transported by fluid-assisted diffusion from areas of high compressive stress to areas of low compressive stress, and is deposited as crystalline growths in the direction of the maximum instantaneous stretching axis (ISA) (Kerrich, 1978; Davis and Reynolds, 1984; Groshong, 1988; Knipe, 1989; Passchier and Trouw, 2005).

Four factors contribute to the fringe geometry: (1) the shape of the core object; (2) the type of strain fringe; (3) the flow regime in the surrounding matrix; and (4) whether fiber growth in the fringe is displacement controlled or face controlled (Passchier and Trouw, 2005). The growth sense of fringe structures can be syntaxial or antitaxial; fiber growth from the core object to the matrix is syntaxial, and fiber growth from the matrix to the core object is antitaxial. There are three types of strain fringes: pyrite type, crinoid type, and composite type. The most common type of strain fringes are pyrite type; since the strain fringes in this study are pyrite type, the discussion is restricted accordingly. Pyrite-type strain fringes are different from the other types in that fibers grow with crystallographic continuity from the matrix (antitaxial) towards the core object (Ramsay and Huber, 1983). There are two different end member types of fibers based on the relationship between their orientation, the shape of the core object, and the maximum instantaneous stretching axis: displacement-controlled fibers and face-controlled fibers or a combination of both, intermediate fibers (Ramsay and Huber, 1983, Koehn et al., 2000, 2001, 2003).

Displacement-controlled fibers are typically very narrow, the fibers consist of one or more mineral species growing sub-parallel, and they can be used to determine the progressive strain history (Ramsay and Huber, 1983) (Figure 14). Displacement-controlled fibers grow parallel to the relative displacement between the matrix and the core object and are thought to record the incremental and finite strain history (Ramsay and Huber, 1983; Koehn et al., 2000, 2001, 2003). Recent studies have focused on displacement-controlled fibers to determine their use for strain history, growth, and what the fibers actually trace (Aerden, 1996; Koehn et al., 2000, 2001, 2003).

Koehn et al., (2000, 2001) has modeled strain fringes numerically using a two dimensional computer model "Fringe Growth" (Koehn et al., 2000, 2001), and by analog using wooden objects in a simple shear box with a Polydimethylsiloxane substance (Koehn et al., 2003). The "Fringe Growth" program simulates the incremental growth of undeformed antitaxial strain fringes and users can change the parameters of growth. Moreover, ostensibly, the user can create self made core objects by converting the shape into a text file and uploading into the program.

Several attempts were made to create core objects from the Grouse Creek samples to input into the program Fringe Growth, but unfortunately they were unsuccessful. While the program works well with pre-defined shapes, self-created complex core objects do not work properly (Koehn, personal communication). Koehn determined through modeling that face-controlled fibers show a tendency to grow around smooth core objects, and fringe structures with both displacement-controlled fibers and face-controlled fibers grow around rough core objects (Koehn et al., 2000). Furthermore, the surface roughness determines whether or not the fibers track the instantaneous stretching

direction (Koehn et al., 2000). According to Koehn et al. (2000), the long axis of displacement-controlled fibers records the opening direction and rotation of the core object and the fringes with respect to the maximum instantaneous stretching axis (ISA). Modeling of strain fringes using polydimethylsiloxane wax illustrated that fringes and core objects can rotate relative to each other, and the aspect ratio of the core object and fringe structure influences the amount of rotation that occurs (Koehn, et al., 2003). In addition, hook-shaped object-center paths can result from variable rotation rates of non-equant core objects and therefore do not always represent a change in orientation of the instantaneous stretching axis (Koehn, et al., 2003). Consequently, such hook-shaped object-center paths cannot always be attributed to multiple deformation phases, contrary to the interpretation of strain fringes from the Pyrenean shear zone (e.g., Aerden, 1996; Müller et al., 2000).

Face-controlled fibers are typically fairly wide (>30 μm) with fibers forming perpendicular to the face of the core object (Figure 14). Determining the strain history of face-controlled strain fringes is more complicated, and only in some cases can the infinitesimal strain history, in addition to magnitude of finite extension, be determined (Ramsay and Huber, 1983). Strain history cannot be determined from the directions of face-controlled fibers, but rather is determined from the geometry of the contact suture, which records the progressive displacement history (Ramsay and Huber, 1983). A suture is the surface separating two parts of a strain fringe, each originating from a different core object face and with a different orientation of fibers (Passchier and Trouw, 2005) (Figure 14). The suture is trapped by corners of the core object (Koehn et al., 2000). Face-controlled fibers sometimes contain inclusion trails known as "ghost" fibers, which

appear to mark out displacement paths, similar to displacement-controlled fibers, and can be used to determine the strain history (Ramsay and Huber, 1983). Therefore, face-controlled fibers, by themselves, can be used to determine the magnitude of extension but not the displacement path and history. Only the suture or the "ghost" fibers can be used to track the displacement path and determine the strain history.

Kinematic and petrographic analysis of strain fringes

Thin sections of fibrous strain fringes were analyzed within the principal planes of the finite strain ellipsoid from the Pennsylvanian-Permian Oquirrh Formation at Marble Peak, North and South Hill, and the Rosebud area (Figure 15). Two sets of fibers, known as D_1 and D_2, are present within the strain fringes (Figure 16). D_1 fibers exhibit dominantly face-controlled fibers as well as displacement-controlled fibers (Figure 14). D_2 fibers exhibit displacement-controlled fibers (Figure 14).

Depending on the type of fiber growth, face-controlled or displacement-controlled, different methods were used to measure the finite and incremental strain history of each strain fringe. The different methods used were based on the relationship between their orientation, the shape of the core object, and the maximum infinitesimal strain orientation (Ramsay and Huber, 1983). Methods and results for both D_1 and D_2 will be separated and discussed below.

D_1 sense of shear

Face-controlled strain fringes are useful microstructural features for providing sense of shear during non-coaxial progressive deformation (Ramsay and Huber, 1983). Face-controlled strain fringes are used in this study to provide the sense of shear for the

D_1 event and to provide information on the incremental strain paths. Sense of shear for D_1 was determined microscopically from samples within the XZ plane of the finite strain ellipsoid, parallel to lineation in the X direction and perpendicular to foliation. Samples were collected across the three field areas at Marble Peak, North and South Hill, and the Rosebud area.

Throughout the field areas, D_1 fibers dominantly record a top-to-the-north sense of shear as seen from asymmetric fiber packages and contact sutures. At Marble Peak, D_1 face-controlled fibers are undeformed and well preserved, recording top-to-the-north sense of shear (Figure 17). North and South Hill preserves both top-to-the-north and top-to-the-south D_1 fibers (Figure 18). However, the top-to-the-south D_1 fibers are within the east-verging overturned limb of the recumbent anticline at South Hill. The D_1 fibers at the Rosebud area consistently record a top-to-the north sense of shear (Figure 19).

D_1 finite strain

The Durney and Ramsay method (1973) was used on all of the D_1 fibers exhibiting face-controlled undeformed strain fringes that do not exhibit a suture or "ghost fiber." This method is based on the assumption that previously formed fibers behave rigidly and are undeformed. Measurements were made from digital photomicrographs taken from a petrographic microscope and analyzed in two graphics programs (Adobe Illustrator CS2 and ImageJ). Only the finite stretch, and not the incremental strain history, can be measured with this method. The total finite extension is derived by dividing the total length of the strain fringe (l_{sf}) structure by the diameter of the pyrite core object (D_{co}) and multiplied by 100 to gain an extension percent (Figure 20).

Finite extension $= (l_{sf}/D_{co}) \times 100\%$

Finite strain analysis was conducted on 37 samples of fibrous strain fringes throughout the field areas. Finite strain results were determined from samples within the XZ plane of the finite strain ellipsoid. Overall results for the finite strain analysis on fibrous strain fringes showed an increase in strain magnitude southward within the field area for the D_1 fibers.

Uncertainties

Finite strain values per sample will fluctuate depending on whether or not the thin section recording the principal plane of finite strain (XZ) was cut through the centroid of each strain fringe. In addition, curvature of the fibers in and out of the plane (XZ) will also influence the fiber geometry and the amount of strain that was recorded. Therefore, for each sample, the maximum finite strain values were used as the minimum amount of extension that was recorded by each strain fringe within the thin sections.

Marble Peak

At Marble Peak within the Pennsylvanian-Permian Oquirrh Formation, finite strain magnitudes from D_1 fibrous strain fringes ranged from 49% to 165% extension, with significantly greater magnitudes evident in the Oquirrh limestone of the lowest part of the Middle allochthon (Figure 21). Greater magnitudes of 408% extension of the D_1 fibers were found in the northern part of Marble Peak resulting from overprinting from the D_2 event (Figure 21). These face-controlled strain fringes are deformed by a crenulation cleavage, S_2, and therefore are recording an inaccurate finite strain magnitude for D_1. Vertically within the allochthon at Marble Peak, strain magnitudes are heterogeneous with higher magnitudes for the D_1 fibrous strain fringes within the central to western side of the klippe.

North and South Hill

At North and South Hill, finite strain magnitudes of D_1 fibrous strain fringes ranged from 107% to 322% extension (Figure 22). It is unclear how homogenous or heterogeneous strain magnitudes are at North and South Hill due to the lesser abundance of strain fringes as compared to the other field localities.

Rosebud area

Further south at the Rosebud area, finite strain magnitudes for the D_1 fibrous strain fringes increase considerably, ranging from 184% to 634% extension (Figure 23). It is unclear whether or not a vertical strain gradient exists at the Rosebud area, due to the lack of vertical exposure of strain-fringe-bearing rocks. However, there is a lateral strain gradient across the field areas within the Oquirrh Formation, with higher magnitudes for the D_1 fibrous strain fringes in the southeastern part of the Rosebud area.

D_1 amount of rotation (vorticity analysis)

Vorticity records the amount of rotation relative to the amount of stretching at a point in space and time and is used to determine the degree of non-coaxiality of a ductile flow (Tikoff and Fossen, 1995). In order to conduct a vorticity analysis, the flow apophyses, the orientation of the instantaneous stretching axes, and the angle between the maximum instantaneous stretching axis and the shear zone boundary need to be established (Figure 24). A vorticity analysis was conducted on the D_1 strain fringes from Marble Peak, in order to establish whether the D_1 deformational event is associated with extension or shortening. The use of three dimensional kinematic vorticity analysis was first established by Ramberg (1975) and McKenzie (1979). The framework for three dimensional kinematic vorticity analyses was established by Tikoff and Fossen (1995),

whose study discusses the use and limitations of three-dimensional kinematic vorticity analysis. Tikoff and Fossen (1995) conclude that the internal kinematic vorticity number is useful for a two-dimensional analysis, but that it is less precise and consequently less useful in most three-dimensional deformations.

In order to conduct a vorticity analysis, certain assumptions must be made. First, a reference frame needs to be determined. Therefore, for purposes of this study, the reference frame is assigned to the foliation, which represents the boundary of the shear zone. Other studies have assumed that the foliation records the X axis of the finite strain ellipsoid, which represents the shear zone boundary. (Simpson and DePaor, 1993; Tikoff and Fossen, 1995). Determining the orientation of the instantaneous stretching axes is also necessary. Displacement-controlled fibers and sutures within face-controlled fibers have been documented as providing information on tracking the orientation of the instantaneous stretching axes (Durney and Ramsay, 1973; Ramsay and Huber, 1983; Tikoff and Fossen, 1995; Wallis, 1995). The last incremental orientation of the displacement-controlled fibers or sutures is thought to record the approximate orientation of the maximum instantaneous stretching axis (Wallis, 1995). The kinematic vorticity number can be determined if the angle between the shear zone boundary and the extensional instantaneous stretching axes is known (Figure 24).

Face-controlled strain fringes exhibiting sutures were used for the vorticity analysis of the D_1 deformational event. Four samples were analyzed within the XZ plane of the finite strain ellipsoid. Angles between the S_1 foliation, which parallels the shear zone boundary, and the last increment of the suture ranged between 8° and 44°. Angles plotted on the vorticity diagram (Tikoff and Fossen, 1995) (Figures 25a and b), yielded

kinematic vorticity numbers (W_k) between 0.28 and 0.99. For pure shear, $W_k = 0$ and for simple shear, $W_k = 1$. Sample MW00-GC-16-01 yielded a kinematic vorticity number of 0.28. Sample TA-06-MP-06-02 yielded a kinematic vorticity number of 0.77. Sample TA-06-07-04-01 yielded a kinematic vorticity number of 0.47. Sample TA-06-MP-01-3A-02 yielded a kinematic vorticity number of 0.99. The values recorded ranged from pure to simple shear deformation within the extensional realm, collectively recording a thinning shear zone, and thus interpreted to record extension.

Uncertainties

Errors in the vorticity analysis could result if there is an inaccurate reference frame under the assumption that the foliation records the shear zone boundary, if the last increment of the suture within face-controlled fibers does not record the instantaneous stretching axis, if the aspect ratio of the rigid core object influences the orientation of the ISA, or if the assumption of steady state deformation is inaccurate. These assumptions and factors could all produce an inaccurate kinematic vorticity number.

Orientations within S_1 (XY plane)

Incremental orientations of the long axes of the strain fringes were measured within the S_1 plane at the Rosebud area (Table 1). Within the XY plane of D_1 (S_1), D_1 fibers exhibit a clockwise curvature, which can be seen in Figure 26. In the D_1 Rosebud samples, a northeast elongation lineation is recorded in the distal parts of the fiber ranging from (~270°-343°), and an orientation in the proximal parts records a northeast elongation lineation (~354°-024°) (Table 1) (Figure 26). Distal parts of the strain fringe record a mean orientation of 312°, and proximal parts record a mean orientation of 032°

(Figure 26). The clockwise rotation displacement path recorded by the D_1 strain fringes can be seen in Figure 27.

Sample XY	S_1	S_1	S_2	S_2	Measurement technique
	D_1 old	D_1 young	D_2 old	D_2 young	
Rosebud Area					
RB-10A-01	NA	NA	240	145	Object-center path
RB-13-10A-03	NA	NA	218	113	Object-center path
RB-18-03b-01	NA	NA	210	147	Object-center path
RB-19-06-02	NA	NA	204	115	Object-center path
RB-23-08-01	311	024	243	125	Medial lines through centroid & OCP
RB-13-07-01	326	047	NA	NA	Medial lines through centroid
RB-25-01-01	326	027	175	138	Medial lines through centroid & OCP
RB-06	343	044	NA	NA	Medial lines through centroid
RB-24	300	354	NA	NA	Medial lines through centroid
RB-14	285	033	NA	NA	Medial lines through centroid
RB-20B	270	033	NA	NA	Medial lines through centroid
RB-21	326	045	NA	NA	Medial lines through centroid
RB-03-08-01	320	045	NA	NA	Medial lines through centroid
Mean	312	032	215	131	

Table 1. Recorded incremental orientations of D_1 and D_2 fibrous strain fringes within the XY plane of S_1 and S_2. Measurement techniques were from object-center path method (OCP) for displacement-controlled fibers, and medial lines through the centroid for face-controlled fibers. Proximal parts of strain fringes are younger and distal parts are older. Samples from Rosebud area.

D_2 sense of shear

Displacement-controlled strain fringes are fruitful microstructural features that are used to determine sense of shear during coaxial and non-coaxial progressive deformation (Ramsay and Huber, 1983). Displacement-controlled fibers are used to determine the sense of shear for the D_2 event and to provide information on the incremental strain paths. As previously discussed for the D_1 fibers, sense of shear for D_2 fibers was determined within the XZ principal plane of the finite strain ellipsoid. Throughout the field areas, D_2 fibers consistently record a top-to-the-south shear sense (Figures 18-20). D_2 fibers at Marble Peak are displacement-controlled fibers recording top-to-the-south sense of shear with lesser strain magnitudes than the D_1 fibers (Figure 17). D_2 fibers record a top-to-the-south sense of shear further south, within the field area at North and South Hill (Figure 18). In the southernmost extent of the field areas, in the Rosebud area, the D_2 fibers record a top-to-the-south sense of shear (Figure 19).

D_2 finite strain

The object-center path method was used in the analysis of non-coaxial displacement-controlled D_2 fibers, which track the opening direction of the maximum instantaneous stretching axis (Figure 20). The object-center path method was initially developed by Aerden (1996), further developed by Koehn et al. (2000), and was developed to separate the opening paths of fringes from rotation of the core object. The object-center path length along the path can be used to determine the incremental and finite strain. The curvature along the path and the core object relative to the fringes is used to determine the amount of rotation. According to Aerden (1996), single displacement fibers should not be used, so the fringe structure must be treated as a whole.

This method reconstructs polyphase deformation histories for displacement-controlled fibrous strain fringes by rotating a traced rigid core object along marginal points reproducing the natural fiber pattern from a photomicrograph (Figure 28) (Aerden, 1996). The center of the core object is plotted on each increment tracing the displacement path and showing the translation between the core object and the fringes (Figure 29).

Six simulations were conducted using the "Fringe Growth" program to substantiate that the object-center path method, as applied, accurately reveals the incremental strain paths (Figure 30a-c). Pre-defined shapes similar to Grouse Creek samples were used for modeling the strain fringes. Measurements for incremental and finite strain were completed using Adobe Illustrator CS2 and the ImageJ program. Measurements were taken along the object-center path trajectory for each increment of finite strain (Figure 29).

A finite strain analysis was performed on displacement-controlled fibrous strain fringes following the object-center path method. Overall results for the finite strain analysis on the D_2 fibrous strain fringes indicate an increase in strain magnitude southward within the field area.

Marble Peak

Finite strain magnitudes from D_2 fibrous strain fringes ranged from 17% to 61% extension within the Oquirrh Formation at Marble Peak (Figure 21). Overall, there are no apparent trends for strain gradient throughout the Marble Peak klippe. These finite strain magnitudes are much lower than the finite strain magnitudes recorded at North and South Hill and the Rosebud area.

North and South Hill

At North and South Hill, finite strain magnitudes of D_2 fibrous strain fringes ranged from 28% to 73% extension (Figure 22). It is inconclusive whether or not a strain gradient or pattern exists for the D_2 fibers, due to the lack of a sufficient number of suitable samples.

Rosebud area

At the furthest south of the field areas at the Rosebud area, finite strain magnitudes for the D_2 fibrous strain fringes ranged from 52% to 511% extension (Figure 23). With the exception of three samples from two separate locations, all samples were collected from the upright limb of the east-verging fold. Samples TA-06-RB-13, 18, and 19 were collected at hinge zones and indicate higher amounts of finite strain (Figure 23). Finite strain results yield higher strain magnitudes at the Rosebud area than at the areas further north at North and South Hill and at Marble Peak. Therefore, a lateral strain gradient from the southern extent of the field area to the northern part is obviously present. Unfortunately, due to a lack of vertical exposure of strain-fringe-bearing rocks, the question of a vertical strain gradient for the D_2 cannot be determined.

D_2 incremental strain and vorticity analysis

Incremental strain analysis was determined for 12 samples of fibrous strain fringes throughout the field areas within the XZ plane of the finite strain ellipsoid. These incremental strain histories are used to quantify temporal variations in the magnitude and orientation of elongation as a function of structural position around the fold at Rosebud. Analyses were performed on face-controlled and displacement-controlled fibrous strain fringes following the object-center path method. Results from the incremental strain

analyses from displacement-controlled fibrous strain fringes were plotted on Cumulative Incremental Strain History Diagrams (CISH), which will be discussed below. The upper numerical value of finite strain was used, per sample, recording the minimum amount of extension, due to the amount of error that will occur when the samples were not cut through the pyrites centroid. Results for the incremental strain analysis on fibrous strain fringes indicate an overall increase in strain magnitude southward within the field area for the D_2 fibers.

Uncertainties

Incremental strain values per sample will vary depending on how the increments were segmented. Incremental segmentation was based on angular change of fibers and determined by the object-center path method, which separates the movement between the pyrite and the fringe into components of translations and rotations. Possible human errors exist when separating the increments of rotation versus translation along the displacement path. Use of the object-center path method was verified by modeling strain fringes with the "Fringe Growth" program. Modeling the components of both translation and rotation obtained by the object-center path method produced strain fringes very similar to the natural samples. The shape and smoothness of the core object greatly influences the morphology of the fibers. Therefore, the pre-defined shapes that were used to most represent the core objects, also introduces some amount of error with the outcome of the fiber morphology as seen with the results.

CISH

Cumulative Incremental Strain History diagrams (CISH) were used to determine how strain accumulates (y axis) relative to the changes of the orientation of the

incremental extension direction from the horizontal reference frame (x axis) (Clark et al., 1993; Fisher and Anastasio, 1994; Anastasio et al., 1997). These graphs depict extension versus orientation with respect to a horizontal reference frame (S_2) (Clark et al., 1993; Fisher and Anastasio, 1994; Anastasio et al., 1997). Measurements for the CISH diagrams were taken from D_2 fibrous strain fringe samples from the field areas that exhibited displacement-controlled growth. The reference frame for all measurements was taken viewing west with north to the right. Therefore, clockwise rotation on the graphs is positive and counter-clockwise is negative. This reference frame reverses that of Fisher and Anastasio (1994) and Clark et al. (1993) due to a change in viewing direction. This reference frame was chosen for a more intuitive graphical representation of the CISH diagrams. The slope of the curve determines the amount of external vorticity and gives information on the reorientation of the extension direction and rate of rotation (Clark et al., 1993; Fisher and Anastasio, 1994; Anastasio et al., 1997). Vertical paths represent coaxial deformation, that is a constant orientation of extension, and horizontal paths represent non-coaxial deformation with little or no accumulation of strain (Clark et al., 1993; Fisher and Anastasio, 1994; Anastasio et al., 1997).

CISH results

Incremental strain histories for D_2 strain fringes at the Rosebud area were plotted on CISH diagrams to determine the degree of non-coaxiality of the D_2 event (Figure 31 and 32). The results clearly demonstrate a non-coaxial strain history and provide information on the incremental strain history and kinematics during the development of the D_2 event. Two locations were sampled at the Rosebud area—within an upright limb of a fold at the northwest side and an upright limb of the southeast side—and will be

discussed separately. Due to the lack of exposure, no samples were collected from the overturned limb at the Rosebud area. At both locations, the D_2 fibrous strain fringes undoubtedly display an overall top-to-the-south shear sense.

At the northwest side of the Rosebud area within the upright limb of the fold, the slopes determined from the nine CISH diagrams clearly demonstrate a non-coaxial strain path, with one exception from a hinge zone (TA-06-RB-18). This sample has an initial path reflecting a non-coaxial slope and progressively rotates into a coaxial path approaching subparallelism to the S_2 cleavage. This sample was collected from a hinge zone of the fold, which is evidenced by the mutually perpendicular relationship of S_1 and S_2, and by the presence of D_1 asymmetric boudins overprinted by a component of pure shear during D_2. The CISH diagrams display an overall amount of rotation that varies throughout the samples, ranging from 0° to 96° (difference between initial orientation and final orientation). The overall average rotation for these samples is ~50°. Samples TA-06-RB-22-05-01 and 02 record a total rotation of 0° and 1° respectively, and sample TA-06-RB-16-05-03 records a 2° rotation. These samples being much different than the majority of samples, cause a shift in the overall averages; by eliminating them, the overall averages increased to ~60°. Nearly all of the youngest fiber increments displayed in the CISH diagrams are inclined ~65° to the S_2 cleavage planes and rotate into sub-parallelism (older distal fibers) with the cleavage plane, which is consistent with progressive rotation of fiber segments toward S_2. In a simple shear flow, the infinitesimal shortening and extension directions are inclined 45° to the shear plane. The youngest parts of the fringe structures will initially develop parallel to the maximum instantaneous stretching axis. Studies document this relationship and propose that the youngest parts of the fibers

record the orientation of incremental extension relative to the final orientation of bedding (Etchecoper and Malievielle, 1987; Fisher and Byrne, 1992; Fisher and Anastasio, 1994; Anastasio et al., 1997). In other words, earliest formed fibers rotate into the shear direction, and only the orientation of youngest part of the fibers relative to bedding last increment of strain reflect (Fisher and Anastasio, 1994). Therefore, during simple shear, fiber growth should initiate at a 45° angle to the shear plane (D_1 cleavage) and rotate into parallelism with the cleavage, if the fibers are recording contemporaneous development of the cleavage.

However, fibers do not always rotate into parallelism with cleavage, as documented by a large scale leading edge fold in the Sevier orogen from the Lost River Range (Fisher and Anastasio, 1994; Anastasio et al., 1997). This relationship is attributed to the following: (1) mineral fibers in strain fringes are deformed; (2) strain fringes developed after folding began, and growth is not synchronous with initial development of folds; and (3) fiber shape is a consequence of general shear. If the younger parts of the fibers inclined 65° to the cleavage plane are recording the opening direction of the extensional instantaneous stretching axis and the cleavage plane represents the flattening plane, then the maximum principal stress direction is oriented at a subhorizontal angle to the shear plane. These fibers record the maximum instantaneous stretch direction, which makes the minimum instantaneous stretch direction (instantaneous shortening) oriented at a subhorizontal angle to the shear plane. Therefore, this orientation is recording horizontal shortening 25° to the shear plane. Few exceptions include samples TA-06-05-03 and TA-06-RB-23-03, which show the opposite. In these cases, youngest fiber increments are sub-parallel to the S_2 cleavage

plane and rotate approximately 70° to S_2. Fisher and Anastasio (1994) and Anastasio et al. (1997) determined that this could possibly indicate that fiber growth did not occur during the early stages of folding, that the fibers over rotated during fold development, or that the fibers are deformed.

At the southeast side of the Rosebud ridge area, the strain histories depict variations in the orientation of incremental extension. The majority of the samples demonstrate a higher degree of coaxial character TA-06-RB-11 and 13 with lesser amounts of rotation, with one exception TA-06-RB-14. This particular sample demonstrates a higher degree of non-coaxiality than the other samples from the area. Sample TA-06-RB-13 was collected from a hinge zone of the fold, evidenced by a mutually perpendicular relationship between S_1 and S_2. The D_2 fibrous strain fringes from the southeast side of the Rosebud area demonstrate a top-to-the-south shear sense. An overall amount of rotation varies from 5° to 77°. The overall average rotation from these samples is ~38°. Sample TA-06-RB-11A-02-01 records a 5° rotation, and sample TA-06-RB-13-10A-02 records a 10° rotation. These two samples record the overall averages; by eliminating them, the overall averages increased to 60°. However, these samples reflect a coaxial strain history, so eliminating them would be erroneous. Of the few samples collected at the southeast side of Rosebud area, there was only one sample displaying rotation TA-06-RB-14-07. The youngest fiber increments displayed in the CISH diagram are inclined ~65° to the S_2 cleavage planes and older segments are rotated into sub-parallellism with the cleavage plane. The other samples display a coaxial strain history. As previously mentioned, the younger parts of the fibers inclined 65° to the cleavage plane are recording the opening direction of the extensional instantaneous

stretching axis and the cleavage plane represents the flattening plane. These fibers record the maximum instantaneous stretch direction, which makes the minimum instantaneous stretch direction (instantaneous shortening) oriented at a subhorizontal angle. Therefore, the maximum principal stress direction is oriented 25° to the shear plane and is recording a horizontal shortening component parallel to bedding.

Orientations within S_2 (XY plane)

The large scale folds within the field areas display an axial planar cleavage, known as the S_2 foliation. Within the S_2 plane, D_2 fibers exhibit a curvature recording progressive incremental changes in infinitesimal strain orientation (Figure 33). Incremental orientations of the long axis of the strain fringes were measured within the XY plane from samples at the Rosebud area. Samples from the Rosebud area were selected based on the maximum obliquity between S_1 and S_2. These samples exhibited the greatest resolvable distinction between the D_1 and D_2 fibers within the S_1 and S_2 planes. The D_2 fibers lie within the S_2 plane and exhibit a progressive curvature from northeast-southwest (204°-240°) within the older distal parts to an orientation of northwest-southeast (147°-113°) in the proximal younger fibers (Table 1) (Figure 33). Distal parts of the strain fringe record a mean orientation of 215°, and proximal parts record a mean orientation of 131° (Figure 33). The distal parts of D_2 fibers are sub-parallel to the fold hinge (215°) at Rosebud and progressively rotate perpendicular (147-113°) to the fold hinge in the proximal parts, thus recording a counter-clockwise vertical rotation about the Z axis of the finite strain ellipsoid (Figure 33). The counter-clockwise rotation displacement path recorded by the D_2 strain fringes can be seen in Figure 27.

CHAPTER 5

DISCUSSION

D_1: contraction or extension?

One of the principal research questions addressed by this thesis is whether the D_1 fabric in the Grouse Creek Mountains records contraction or extension. Distinguishing contraction from extension is a critical matter in the study of mid-crustal shear zones and relies on establishing the tectonic significance of ductile fabrics in metamorphic rocks. Several studies have analyzed the structural, metamorphic, and geochronological patterns observed in shear zones to distinguish extension from contraction (Wallis et al., 1992; Wheeler and Butler, 1994; Wells et al., 2005). Structural criteria include analyzing the shear zone geometry and kinematics, hanging-wall deformation, and the overall thinning or thickening of a shear zone (Wallis et al., 1992; Wheeler and Butler, 1994; Wells et al., 2005). In particular, kinematics of the shear zone can be determined by the relative movement of the hanging wall and footwall, or from kinematic indicators or offset markers (Wheeler and Butler, 1994). Metamorphic criteria include observations of pressure and temperature differences between the hanging wall and footwall that distinguish whether the hanging wall contains structurally deeper or shallower rocks with respect to their pre-faulting configuration. Similarly, geochronological criteria allow this distinction to be made, including observations of discordance between hanging-wall and

footwall thermal histories. This study focuses primarily on the structural criteria used to distinguish contractional from extensional origins for the D_1 fabric.

Previous workers suggest that the D_1 fabric is related to thrusting produced during Mesozoic contraction; Compton et al. (1977) interpreted top-to-the east thrusting, whereas Malavieille (1987) interpreted top-to-the north-northeast thrusting. Alternatively, the fabrics may be extensional in origin (Wells et al., 2008). To test these alternative hypotheses, the strain geometry, kinematics, and vorticity of the shear zone is discussed below.

Shear zone geometry and kinematics

The traditional approach of using the geometry and kinematics of shear zones as criteria for distinguishing contraction from extension cannot be used for the D_1 shear zone because there are no indications of whether the shear zone cuts up or down section to the north or whether there are changes in structural depth in the shear direction (Lister and Davis, 1989; Wheeler and Butler, 1994; Butler and Freeman, 1996). However, the geometry of the shear zone, its foliation and lineation orientations, and the kinematics of shearing, when viewed in the context of their orientation and position within the orogenic belt, allow some constraints on whether the shear zone records contraction, transpression, or extension.

The overall orientation, the characteristic curved shape, and the geometry of foliations are used to determine the shear sense and allow some predictions of the geometry of the shear zone (Sanderson, 1982; Passchier and Trouw, 2005). Foliations are thought to record or lie parallel to the XY plane of the finite strain ellipsoid (Passchier and Trouw, 2005), and consequently are useful shear sense indicators within a shear zone

when analyzing sigmoidal foliation trajectories, the geometry of the foliation relative to the shear zone boundary, and shear band cleavages. Furthermore, and most importantly, they are used to determine whether or not the fabrics developed within the shear zone record contraction or extension. Conventionally, during heterogeneous simple shear, foliations may show a characteristic sigmoidal curved shape in the overall shear zone. This reflects the orientation of the finite strain axes (specifically, XY principal plane), and develops as a result of the foliations rotating from the instantaneous stretching axis towards the fabric attractor with increasing non-coaxial strain (Ramsay and Graham, 1970; Passchier and Trouw, 2005). However, a study by Yonkee (2005) suggests that foliation patterns in heterogeneous simple shear with downward increasing shear strain are commonly subhorizontal at the base of the shear zone, and rotate to ~45° toward the top of the shear zone, reflecting the variations in orientation of the finite strain ellipsoid (Figure 34a).

In contractional settings where overall thickening of the shear zone occurs, foliation patterns are at higher angles to the shear zone boundary than in heterogeneous simple shear regimes (Sanderson, 1982; Yonkee, 2005). Thickening shear zones undergo layer parallel shortening and simple shear producing higher angle foliations at the base of the shear zone that rotate to nearly vertical at the top (Figure 34b) (Sanderson, 1982; Yonkee, 2005). Alternatively, in extensional settings where thinning of a shear zone occurs, foliations are at a much lower angle than observed in contractional settings (Sanderson, 1982; Yonkee, 2005). Thinning shear zones undergo layer parallel extension and simple shear, producing foliations that are subhorizontal at the base of the shear zone, increase in angle within the middle, and eventually flatten out at the top (Figure 34c)

(Sanderson, 1982; Yonkee, 2005). In a transpressional setting, theory predicts that high-angle foliations should be dominant over low-angle foliations, as transpressional zones record a component of shear zone-perpendicular contraction (Sanderson and Marchini, 1984; Yonkee, 2005).

The base and top of the D_1 shear zone cannot be established due to overprinting by the Cenozoic MMSZ and detachment of the base and lack of exposures defining the top of the shear zone. For that reason, interpretation relies on predictable foliation trajectory patterns for contractional and extensional regimes that develop during non-coaxial deformation as discussed below (Figure 34).

The D_1 fabric is characterized by a flat-lying foliation (S_1) sub-parallel to bedding and a generally north-northeast-trending penetrative elongation lineation (L_1). However, the mere presence of flat-lying foliations is not necessarily definitive of extension or contraction since flat-lying foliations sub-parallel to a shear zone boundary can develop both during coaxial deformation and non-coaxial deformation. For instance, during non-coaxial deformation, flat-lying foliations are developed in zones of high shear strains where the foliation rotates into parallelism with the shear zone. Alternatively, flat-lying foliations may be produced during coaxial deformation, where a higher component of pure shear in which the shortening axes is perpendicular to the shear zone boundary producing layer perpendicular shortening.

Assuming that the S_1 foliation, which is parallel to bedding, represents the shear zone boundary, then an interpretation can be made as to whether the shear zone records extension or contraction (Simpson and DePaor, 1993; Tikoff and Fossen, 1995). S_1 is a flat-lying foliation that is sub-parallel to bedding regardless of vertical or lateral strain

gradients within the shear zone. The S_1 foliation does not record the amount of high shear strains required to have rotated foliation towards parallelism with the shear zone boundary. Moreover, coaxial strain without a component of simple shear must be ruled out based on the asymmetric shear indicators within the shear zone, which will be discussed later on. Therefore, when comparing the orientation of the S_1 foliation to the previously mentioned models, the flat-lying foliation is more indicative of an extensional thinning shear zone than of a contractional shear zone. A flat-lying foliation (S_1) that is parallel or subparallel to bedding with a significant component of pure shear has been previously interpreted to record extension (Wallis, 1995; Camilleri, 1998; Davis and Maidens, 2003; Wells et al., 2008). Studies have documented that within footwalls of large thrust sheets, collapse occurs in response to loading, producing flat-lying foliations (Camilleri, 1998; Wells et al., 2008). Therefore, the S_1 foliation is interpreted to have developed within an extensional flow.

In addition to foliations, lineations are good strain indicatos recording the X (maximum finite stretch) direction of the finite strain ellipsoid (Passchier and Trouw, 2005). Within the S_1 plane of the foliation lies a north-northeast-trending penetrative elongation lineation (L_1) recorded by strain fringes, stretched fossils, and stretched minerals. Within the XY plane of D_1 (S_1), D_1 strain fringe fibers at the Rosebud area exhibit a clockwise rotation of infinitesimal strain. The variable trend of the elongation lineation (L_1) throughout the field areas and the clockwise rotation of infinitesimal strain in the XY plane provide information on the direction of extension and are consistent with N-S gravitational flow (e.g., Camilleri, 1998; Davis and Maidens, 2003), as opposed to kinematics governed by E-W plate convergence (Figure 35). Therefore, it is interpreted

that the flat-lying foliation and north-northeast trending elongation lineation records a component of vertical shortening accompanied by north-south elongation related to gravitational collapse within a extensional setting.

Asymmetric shear sense indicators support the hypothesis that the D_1 fabric records a top-to-the-north shearing event. Measurements of mesoscopic sense of shear indicators (asymmetric boudins, chert stringers and porphyroclasts) and microscopic shear sense indicators (strain fringes) within the D_1 fabric consistently demonstrate a top-to-the-north shear sense. Determination of sense-of-shear in a flat-lying shear zone cannot in itself distinguish between shortening and extension. However, since the Sevier fold-thrust belt is dominantly north trending, and has traditionally been interpreted to record east-directed shortening (Royse, 1993; Yonkee, 1997), top-to-the-north shear in the hinterland of an N-trending curvilinear orogen is most consistent with extensional rather than contractional deformation.

Vorticity study

Another criterion that was used to determine whether the D_1 fabric records compression or extension is the vorticity of ductile flow.

The vorticity study conducted on face-controlled strain fringes from Marble Peak show results ranging from simple to pure shear, recording a thinning shear zone, and thus extension. Previous strain studies indicate that a thinning shear zone behavior, while not diagnostic by itself, commonly occurs within extensional shear zones (Wallis et al., 1992; Wells, 2001; Wells et al., 2005). If the D_1 fabric was produced during contraction, angles greater than 45° would have resulted between S_1 and the sutures within the strain fringes and would have recorded thickening in the shear zone. Vorticity results of the D_1 strain

fringes indicate a non-coaxial strain path and that they were produced during layer parallel extension. Therefore, the vorticity study supports the hypothesis that the D_1 ductile fabric was produced during extension as opposed to contraction.

Finite strain

Finite strain results for D_1 strain fringes indicate that they are heterogeneous both laterally and vertically within the allochthon, with values for extension ranging from 28% to 634%. Higher amounts of strain are present in the Rosebud area, which is the southernmost part of the field areas, and at one locality north at Marble Peak. As previously discussed for the D_1 strain gradient, the question arises whether or not the lateral or vertical increase in strain is due to variable depths exposed within the shear zone or rather, are truly a mixture of lateral strain gradients at constant structural level.

At the Marble Peak, North and South Hill localities, section is locally omitted along the Middle detachment. To a first order, Marble Peak comprises stratigraphically higher rocks than the Rosebud area. In addition, the D_1 fabric in the Grouse Creek Mountains is evident in Archean to Ordovician rocks in areas unaffected by Cenozoic extension and is not developed in the Middle allochthon in the Raft River or Albion Mountains. Using these parameters, there appears to be a strain gradient both laterally and vertically within the shear zone, even though section is discontinuous across the field areas. Laterally across the field areas, strain magnitude increases southward into the Rosebud area. Vertically within the allochthon, a strain gradient is evident at Marble Peak, with increasing strain magnitude deeper into the shear zone in close proximity to the Middle detachment (Figure 36). It was difficult to determine whether a vertical strain

gradient was present at the Rosebud area due to the lack of exposure of the base of the Oquirrh Formation and underlying units.

Tectonic significance of D_1: orogen-parallel extension?

Another principal research question addressed is the driving mechanisms and tectonic significance of the D_1 orogen-parallel extensional event. Although widely recognized in the hinterlands of orogens (Ellis and Watkinson, 1987; Mancktelow, 1992; Murphy et al., 2002; Davis and Maidens, 2003; Merschat et al., 2005; Wells et al., 2008), the causes of orogen-parallel extension are not well understood. The end member causes proposed for driving orogen-parallel extension are: (1) transpression (Sanderson and Marchini, 1984; Ellis and Watkinson, 1987; Teyssier et al., 1995; Fossen and Tikoff, 1998); (2) arcuation (Marshak, 1988; Ferrill, 1991; Ferrill and Groshong, 1993); (3) collisional and lateral escape (Molnar and Tapponier, 1975; Frisch et al., 1998; Seyferth and Henk, 2003; Rosenberg et al., 2004); and (4) gravitational relaxation due to unequal crustal thickening (Coleman, 1996; Camilleri, 1998; Davis and Maidens, 2003; Wells et al., 2008). In order to determine the driving mechanisms responsible for orogen-parallel extension within the hinterland of the Sevier orogen, the proposed tectonic models will be explored within the context of the well-constrained tectonic framework of the western United States. First, the tectonic framework of the western United States will be discussed.

Tectonic framework

The tectonic framework for the western United States, including plate boundary location and convergent rates and direction, are reasonably well constrained (Armstrong,

1968; Burchfiel, 1992; Decelles, 2004). The positions of the mid-Cretaceous North American plate boundary and its retroarc fold-thrust belt have been well established by numerous studies through palegeographic reconstructions (e.g., Armstrong, 1968; Burchfiel, 1992; Decelles, 2004). The area of proposed orogen-parallel extension occurred within mid-crustal levels of the retroarc setting of the Sevier orogen. Although intrabatholithic strike-slip faulting occurred within the Sierran arc as early as 105 Ma (Decelles, 2004), there is no evidence for strike-slip faults and related transpressional shear zones within the retroarc setting of the hinterland of the Sevier orogen. Furthermore, paleomagnetic reconstruction of the Farallon/Kula plates indicate dominantly orthogonal convergence with the North American plate during the proposed 105 Ma orogen-parallel extension (Engebretson, 1985; Decelles, 2004). In addition, convergent rates were constant at 50 mm/yr during mid-Cretaceous time of orogen-parallel extension and increased abruptly to 100 mm/yr at ~100 Ma (Müller et al., 1997; Decelles, 2004) (Decelles Figure 4B showing rate). This well-constrained tectonic framework for the western United States provides an excellent opportunity to determine the driving mechanisms and tectonic significance for the D_1 orogen-parallel extensional event.

Transpression

Orogen-parallel extension has been documented in transpressional settings resulting from oblique plate convergence. Ellis and Watkinson (1987) summarize several localities documenting orogen-parallel extension and attribute extension to oblique plate convergence during collision. These localities include the western Alps, the Variscides of Ireland and France, the Himalaya, and the south-central Canadian Cordillera. These

settings are characterized by wide orogenic zones with major strike-slip faults subparallel to the plate boundary (Sanderson and Marchini, 1984; Teyssier et al., 1995; Fossen and Tikoff, 1998). These zones undergo wrench shear accompanied by horizontal shortening and vertical lengthening (Sanderson and Marchini, 1984; Fossen and Tikoff, 1998). Within these zones, the type of deformation that occurs is dependent on the angle of plate convergence relative to the plate margin. Vertical foliations and a vertical or horizontal lineation are predictable observations in transpressional settings (Fossen and Tikoff, 1998). Vertical foliations are more conclusive criteria used for determining a transpressional setting than are stretching lineations (Fossen and Tikoff, 1998).

This tectonic scenario can be ruled out based on the geometry and kinematics of the D_1 shear zone, which are inconsistent with the predictions of high angle foliations and strike-slip faults in transpressional zones. The D_1 shear zone is characterized by flat-lying foliations parallel to lithological layering, and there are no documented strike-slip faults in the back arc setting. In addition, paleomagnetic reconstruction of the Farallon plate indicates dominantly orthogonal convergence with the North American plate during the mid-Cretaceous at the time of the D_1 orogen-parallel extensional event, not oblique plate convergence (Engebretson, 1985; Decelles, 2004). Therefore, transpression was not the driving mechanism responsible for the development of the D_1 orogen-parallel extensional event.

Arcuation

Extension parallel to the strike of orogenic belts occurs in arcuate orogens, which can develop primary arcuation or undergo secondary arcuation. Primary arcs are fold-thrust belts that are initially curved during their early development and secondary arcs are

initially straight fold-thrust belts that undergo arcuation. Examples of primary arcs where orogen-parallel extension has been described are the forearc of Sumatra, the fold-thrust belt of the Himalayas, and the eastern Carpathians (McCaffrey, 1996; Zweigel et al., 1998; McCaffrey and Nabelek, 1998). Examples of secondary arcs where orogen-parallel extension has been described are the Cantabria-Asturias arc of southwestern Europe, and the northern Subalpine chain in France where the fold-thrust belt was initially straight and underwent oroclinal bending (Marshak, 1988; Ferrill and Groshong, 1993). A study by Zweigel et al. (1998) documents < 20% orogen-parallel extension in the eastern Carpathians. It has been suggested that lower values of orogen-parallel extension are indicative of primary arc settings rather than secondary arc settings, through the use of sand wedge modeling (Zweigel, 1998). In addition to determining the magnitude of extension, the structural geometry of folds was documented as generally trending subparallel to the primary arc.

Most orogenic belts around the world display map-view curvatures that have been the subject of a great deal of study. Several explanations for these curvatures include rigid plate indentor, rigid basement obstacle or a precursor basin geometry, change in sedimentary wedge thickness, changing thrust direction, and oroclinal bending, which is also known as secondary arcuation.

The argument could be made that the curvature seen in the Cordilleran fold-thrust belt evolved during secondary arcuation, not primary arcuation, and if so, produced the D_1 extensional fabric as seen in the Raft-River-Albion-Grouse Creek Mountains. Primary and secondary arcuation can be distinguished by characterizing the overall geometry, kinematic, distribution and magnitude of strain along an arcuate orogen.

Therefore, in order to determine whether or not the D_1 fabric is the remnant of arcuation or developed during a primary arcuate setting, the overall geometry of the salients and re-entrants in the Mesozoic frontal Sevier fold-thrust belt will be discussed.

East of the study area, the Idaho-Wyoming-Utah salient spans northeastern Utah, western Wyoming and southeastern Idaho and is represented by arcuate folds and thrusts of the frontal belt of the east-verging Sevier fold-and-thrust belt (Decelles, 2004). The Idaho-Wyoming-Utah salient contains eight major thrust systems. The strain magnitudes observed parallel to the trend of the salient have been documented as recording along strike-parallel extension of less than 10% (Dixon, 1982; Coogan and Royse, 1990; Mitra, 1994; Apotria, 1995; Paulsen and Marshak, 1999; Yonkee, 2005). Total shortening across the salient has been recorded as high as 100 kilometers (Coogan and Royse, 1990). In particular, a study by Apotria (1995) documented fold axis trend sub-parallel to the arc in both the hanging wall and footwall of the Idaho-Wyoming-Utah salient. In addition, principal shortening axes determined by styolite measurements and calcite strains provided evidence of shortening directions, regional transportation, and counter-clockwise rotation resulting from oblique ramps (Apotria, 1995).

If the present ~232 mile (arcuate length) Idaho-Wyoming-Utah salient was initially straight (~200 miles from mapview endpoints) and underwent arcuation, the magnitude of line parallel strain would only be ~16%. Finite strain magnitudes recorded from the D_1 fibers are at a much higher magnitude of ~227% and are not compatible with the low estimate based on radius of curvature and low documented values of 10% (Yonkee, 2005). Furthermore, since analog modeling of orogen-parallel extension in sand wedge models determines a much higher value of strain from arcuation than from

primary arcs, the strain magnitude of the Idaho-Wyoming-Utah salient is not compatible with arcuation. Therefore, orogen-parallel extension recorded by the D_1 fabric could not have resulted from arcuation of the Idaho-Wyoming-Utah salient.

Collision and lateral escape

Synconvergent orogen-parallel extension occurs in continental collision zones where intense crustal deformation leads to the lateral flow of orogenic material; this is known as lateral escape. Modeling of lateral extrusion reveals the strain distribution within the internal structure of the orogen and highlights the areas where lateral extrusion is significant in the lower part of the crust (Seyferth and Henk, 2003). Localization of lateral extrusion is due to the lack of a rigid block impeding extension. Several studies document the existence of lateral extrusion within active collisional zones. The most prominent example of lateral extrusion is in Southeast Asia where the Indian and Eurasian plates converge, producing the largest collisional zone and orogen in the world. A study by Molnar and Tapponier (1975) from this area estimates a 1500 km amount of displacement from lateral extrusion. Another example of lateral extrusion is in the Eastern Alps and Carpathians, where 170 km of displacement from lateral extrusion have been documented (Frisch et al., 1998). An additional example of lateral extrusion caused by oblique collision is the Tauern Window of the Eastern Alps (Rosenberg et al., 2004). Rosenberg et al., (2004) modeled the effects of an oblique indentor and observed the strain patterns produced during this type of motion.

It is well documented that during the Late Mesozoic, the Sevier orogen was developed during a non-collisional plate margin setting (Burchfiel et al., 1992; Decelles, 2004). There is no documentation of a rigid plate collision or accretionary events during

the Mesozoic Sevier orogen or the western United States that could have resulted in extrusion. Consequently, the D_1 extensional fabric could not be the product of lateral extension formed as the result of an indenter.

Gravitational relaxation

Gravitational collapse is defined as the gravity driven ductile flow that effectively reduces lateral contrasts in gravitational potential energy (Rey et al., 2001). During orogenesis resulting from plate convergence, gravitational potential energy is stored in the isostatically compensated overthickened crust and can be released laterally by extension from areas of high potential energy to areas of low potential energy (Platt and England, 1993; Rey et al., 2001; Vanderhaeghe and Teyssier, 2001). The overthickened crust produced during orogenesis through time increases the geothermal gradient (thermal relaxation) causing gravitational flow. This fundamental process can result in orogen-parallel extension in the interior of orogens during mountain building processes (Coleman, 1996; Davis and Maidens, 2003; Wells et al., 1997; Wells et al., 2008).

Camilleri (1998) investigated the effects of gravitational relaxation in the footwall of the Mesozoic Windermere thrust sheet from the Sevier hinterland in northeast Nevada. The results of that study suggested that with a sufficient amount of loading from thrust sheets, the rocks in the footwall weaken due to thermal relaxation and ultimately collapse in gravitational flow. Barrovian-style metamorphic fabrics, S and SL tectonites formed during prograde metamorphism. During thermal relaxation and prograde metamorphism, the rocks in the footwall underwent primarily coaxial deformation that produced foliations parallel or sub-parallel to bedding (Camilleri, 1998). Moreover, Camilleri

(1998) documented a variability of stretching lineation regionally, with no evidence of rotation of lineation after their formation.

A study by Davis and Maidens (2003) of the Eastern Goldfields Province in Western Australia documents orogen-parallel extension as the result of gravitational collapse during orogenesis. In this situation, thermal weakening of the crust was associated with granite emplacement and not from overthickening of the crust; however, the same basic principle produced gravitational collapse (Davis and Maidens, 2003). This study also documented flat-lying foliations and lineations that recorded tectonic transport produced during gravitational collapse (Davis and Maidens, 2003).

Gravitational relaxation due to unequal crustal thickening appears to be the most logical tectonic scenario producing the D_1 fabric. Flat-lying foliations sub-parallel to bedding are more consistent with gravitational flow than with a transpressional setting (Camilleri, 1998; Davis and Maidens, 2003; Wells et al., 2008). Furthermore, the variable trends of the L_1 lineations across the Grouse Creek Mountains are also more consistent with gravitational flow responding to differences in potential energy gradients, than from tectonically induced shearing (e.g., thrust faults) parallel to the orogen (Camilleri, 1998; Davis and Maidens, 2003). The D_1 fabric, S_1 and L_1 are interpreted to have developed from thermal relaxation of the overthickened crust in the footwall of coeval Mesozoic thrusts within the Sevier fold-thrust belt. For instance, multiple motions on the Williard thrust, one of the major thrust sheets within the Idaho-Wyoming-Utah salient, carried thick Proterozoic and Paleozoic rocks eastward between ~120-110 Ma and ~115-100 Ma (Decelles, 2004). Another thrust fault known as the Basin-Elba fault, the remnant of a once areally extensive thrust nappe, is located in the Northern Albion

Mountains at Mount Harrison (Miller, 1980; Saltzer and Hodges, 1988; Wells et al., 1997). This thrust nappe is thought to be responsible for much of the thrust burial within the Raft-River-Albion-Grouse Creek Mountains and was later removed by the Middle detachment fault (Wells et al., 1997; Harris et al., 2007). Therefore, the driving mechanism responsible for the development of the top-to-the north D_1 orogen-parallel fabric is interpreted to be the result of gravitational relaxation within the footwall of the overlying hinterland Mesozoic thrusts. The overall tectonic framework of the western United States, along with the strain geometry, kinematics, and vorticity of the shear zone of the D_1 ductile event, provides the evidence supporting the hypothesis that the D_1 fabric records an episode of mid-Cretaceous synconvergent orogen-parallel extension within the hinterland of the Sevier orogen (Figure 37).

D_2: contraction or extension?

Alternating contractional and extensional events in orogenic belts play a significant role in dynamically adjusting crustal thickeness during regional contraction. The D_1 event is interpreted to play an integral part in this dynamic adjustment and to have resulted from focused crustal thickening leading to differences in gravitational potential energy along strike, which further lead to extension parallel to the orogen. The D_2 event within the field areas is a previously undocumented deformational event in the Pennsylvanian-Permian Oquirrh Formation of the Grouse Creek Mountains and overprints the earlier D_1 fabric. D_2, as demonstrated in this thesis, is characterized by an axial planar cleavage, S_2, associated with east-verging north-northeast-trending large-scale folds at Marble Peak, South Hill and the Rosebud area.

The principal research question regarding the D_2 deformation to be addressed is whether the D_2 event in the Grouse Creek Mountains records contraction or extension. Distinguishing contraction from extension is important in that it will allow the tectonic significance of the deformational event to be established, and furthermore, will allow some relative temporal constraints to be made through correlation of the kinematic sequence determined in the field area to dated kinematic sequences determined elsewhere in the RAG (Wells, 1997; Harris et al., 2007).

In order to establish whether the event is caused by contraction or extension, interpretation of the kinematics of the D_2 deformation and development of the east-verging folds and associated S_2 and D_2 fibrous strain fringes is necessary. Proper interpretation of these folds is of utmost importance for the structural and tectonic analyses. Previous studies of the folds present at South Hill and the Rosebud area have interpreted them to have resulted from eastward tectonic thrust transport between 20 to 12 Ma (Compton et al., 1977) and from emplacement of the Oligocene Red Butte stocks (Todd, 1980). The argument could be made that the folds developed during crustal shortening or developed during extension. Recumbent folds, such as the one seen at South Hill, have been documented in numerous mountain belts, and while most are interpreted as recording contraction, there is an increasing recognition that such folds can develop during extension (Malavieille, 1987; Froitzheim, 1992; Mancktelow, 1992; Janecke et al., 1998). Synextensional folds, such as sheath folds, are not uncommon in progressive simple shear regimes within orogenic belts, and most have hinge lines subparallel to the extension direction (Cobbold and Quinquis, 1980; Lacassin and Mattauer, 1985; Malavieille, 1987; Ghosh et. al, 1999; Alsop and Holdsworth, 2004;

Alsop and Holdsworth, 2006). Sheath folds are thought to initially form at high angles to the shear direction and to progressively rotate up to 90° during progressive non-coaxial shear into orientations with hinge lines parallel to the direction of transport (Cobbold and Quinquis, 1980; Lacassin and Mattauer, 1985; Malavieille, 1987; Ghosh et. al, 1999; Alsop and Holdsworth, 2004; Alsop and Holdsworth, 2006). Malavieille (1987) documented kilometer scale sheath folds and "a" type folds within the Raft River Mountains and attributes formation to top-to-the-east noncoaxial strain across an inclined surface. Additionally, synextensional recumbent folds have been interpreted to develop where initially steep layering is subjected to horizontal extension and subvertical shortening (Froitzheim, 1992). More commonly, extensional folds are closely related to faults and have been attributed to eight common mechanisms. These mechanisms are: (1) isostatic folds, (2) fault-bend folds, (3) fault-propagation folds, (4) fault-drag folds, (5) constrictional folds, (6) displacement gradient folds, (7) transtensional folds and (8) compound folds (Janecke et al., 1998).

Alternatively, and most commonly, these folds and associated fabrics could record subhorizontal shortening related to crustal shortening as previously interpreted by Compton (1972) and Todd (1980), although of a significantly older age. Recumbent folds have been recognized throughout the Raft River-Albion-Grouse Creek Mountains by numerous authors (Compton, 1972; Todd, 1980; Miller, 1980; Malavielle, 1987; Wells, 1997). In particular, a study by Wells (1997) interprets recumbent folds from the Raft River Mountains as developing during a contractional event known as D_3, and assigns an age of 60-45 Ma based on a structural sequence relative to dated structural events. Furthermore, recumbent folding of the Mahogany Peaks fault in the footwall of

the Basin-Elba fault at Mount Harrison in the northern Albion Mountains may be associated with a period of pressure increase evident in P-T paths constructed from growth zoned garnets (Hoisch et al., 2002; Harris, 2008).

To test these alternative hypotheses, the strain geometry, kinematics, and vorticity of the D_2 folds and associated fabric will be discussed below.

D_2 geometry and kinematics

Foliations are used in this study to determine the shear sense and allow some predictions of the geometry of the D_2 structures. A relatively flat-lying axial planar cleavage, S_2, within east-verging north-northeast trending large-scale folds at Marble Peak, South Hill, and the Rosebud area, distinguishes D_2. Orientations of axial planar cleavages show a consistent geometrical relationship with axial planes of folds, can be used to trace the axial plane, and provide the orientation and geometry of the folds. Marble Peak exposes a limb of a large-scale east-verging fold with S_2 axial planar cleavages striking predominantly to the north-northeast and to the northwest (mean foliation of 052°, 18SE°), and east and west dips ranging from 24° to 68°. At South Hill, within a large-scale east-verging recumbent anticline, S_2 strikes are predominantly to the southwest (mean foliation of 219°, 10S°), with dominantly westward dips ranging from 02° to 32°. At Rosebud, S_2 is within a large-scale east-verging fold displaying strikes predominantly to the west (mean foliation of 265°, 06S°) and dips ranging from 02° to 90°. The average trend and plunge of fold axes at Marble Peak, South Hill, and Rosebud is (184°, 06°), (001°, 11°) and (213°, 01°) respectively. Marble Peak, South Hill, and the Rosebud area exhibit relatively flat-lying S_2 mean foliations, indicating that the folds are recumbent. Based on the mean orientations of S_2 and the trend and plunge of the fold

axes from Marble Peak, South Hill, and Rosebud, these folds are correlated to the same D_2 contractional event.

The obliquity between S_2 and S_1 and development of S_2 is dependent on the lithology and position about folds, and its development is heterogeneous. For instance, within the Oquirrh Formation, S_2 is at a higher angle to S_1 within the competent sandstone lithology and at lower angles in the less competent siltstone and marble lithology. S_2 is interpreted to be a pressure solution cleavage, and is more pronounced in the southern parts of the field areas at North and South Hill and the Rosebud area. S_2 is weakly developed throughout the Oquirrh Formation at Marble Peak, except for one locality north of Marble Peak where S_2 is strongly developed and overprints the D_1 fabric. At this location, S_2 is at a high angle to S_1 associated with a well developed crenulation cleavage.

The overall orientation of foliations is used to determine the shear sense and allows some predictions of the geometry of the D_2 event. Previously the predictable patterns of foliations for contractional and extensional settings were presented in the D_1 discussion. In contractional settings where overall thickening of the shear zone occurs, foliation patterns are at higher angles than in hetereogenous simple shear regimes. In extensional settings, foliations are at a much lower angle. Thickening shear zones undergo layer parallel shortening and simple shear producing higher angle foliations at the base of the shear zone that rotate to nearly vertical at the top, where the component of simple shear progressively lessens upwards (Figure 34b). Therefore, the higher angle S_2 foliations, in particular in the lower strained rocks at Marble Peak, are more consistent with a contractional setting indicating vertical thickening.

In addition to foliations, lineations were used to indicate strain recording the X (maximum finite stretch) direction of finite strain ellipsoid (Passchier and Trouw, 2005). Within the S_2 plane of foliation, D_2 fibrous strain fringes are developed, thus indicating growth of strain fringes synchronous with the folding events. Within the XY plane of S_2, the D_2 fibers exhibit a counter-clockwise curvature from northeast-southwest (204° to 240°) within the older distal parts to an orientation of northwest-southeast (147°-113°) in the proximal younger fibers. The distal (older) parts of the D_2 fibers are sub-parallel to the locally developed fold hingeline at Rosebud (215°) and progressively rotate perpendicular (147° -113°) to the fold hinge in the proximal (younger) parts. The counter-clockwise rotation of the infinitesimal strain in the XY plane of the D_2 fibers provides information on the progressive change in the direction of maximum incremental stretch or alternatively, the rotation or rocks within a strain field of constant orientation. Documentation of rotation of stretching lineations within the XY axial planar cleavage in other studies has been attributed to changing shear direction produced by nappe transport (Dietrich and Durney, 1986). The tectonic significance of the rotational component recorded by the D_2 strain fringes will be discussed later on.

Shear sense indicators

Measurements of microscopic fibrous strain fringes (D_2) throughout the field areas consistently record a component of top-to-the-south sense of shear. That is, the shear direction and sense varies from top-to-the-southwest during early D_2 to top-to-the southeast during late D_2, as the orientation of the fiber stretching direction changed. The degree of non-coaxiality and vorticity will be discussed below.

Finite and incremental strain results

Finite strain results of D_2 strain fringes are heterogeneous both laterally and vertically within the Oquirrh Formation with finite extensions ranging from 17% to 511%. Higher strain magnitudes are present in the southern extent of the field area (Rosebud). Section is locally omitted along the Middle detachment at Marble Peak and North and South Hill. Samples from the Rosebud area are within the pyrite bearing sandstone unit of the Oquirrh Formation just above the fossiliferous limestone unit that forms the base. The fossiliferous basal unit is missing at Marble Peak and is locally exposed at South Hill. Results from finite strain measurements in conjunction with map data indicate that the D_2 strain fringes display a lateral strain gradient, increasing in magnitude toward the south. Although not very well represented, finite strain magnitudes plotted against structural level indicate that there is a vertical strain gradient as well. The Middle detachment introduces discrepancies due to the fact that at Marble Peak, it truncates the stratigraphic and inferred structural section at shallower levels whereas at Rosebud, deeper levels are preserved, making a vertical gradient from a single locality difficult to determine. However, if Marble Peak represents the upper part of the section and Rosebud is the lower part of the section, then a vertical strain gradient is evident. Therefore, both a vertical strain gradient and a lateral strain gradient increasing in magnitude to the south are present throughout the field areas.

Incremental strain results from displacement-controlled fibrous strain fringes (D_2) document the vorticity of the D_2 ductile flow. At Marble Peak, the displacement-controlled D_2 fibers exhibit a lesser magnitude and curvature of fibers and CISH diagrams were not used. Strain fringes at the Rosebud area exhibit higher amounts of strain

magnitude and curvature of fibers, therefore allowing a more complete analysis. Results of incremental strains were plotted on Cumulative Incremental Strain History diagrams to exhibit the degree on non-coaxiality of the D_2 fibers. Based on the slopes of the CISH diagrams from the Rosebud samples, it is evident that the D_2 fibers record a southward non-coaxial flow with an average (horizontal axis) rotation of ~60°. In addition, the youngest parts of the D_2 fibers are inclined 65° to the cleavage plane. These fibers record the maximum instantaneous stretch direction, which makes the minimum instantaneous stretch direction (instantaneous shortening) oriented at a subhorizontal angle. This relationship is more indicative of contraction as opposed to extension, therefore indicating that shortening produced the D_2 folds and fabric.

Folds

Are the east-verging D_2 folds contractional or extensional? The D_2 geometry, kinematics, and vorticity were previously established; now the discussion focuses on whether the D_2 folds formed from contractional (Compton, 1972; Todd, 1980) or extensional processes. The observed curvature of the strain fringes within the XY plane is opposite to what would be expected during hinge rotation of an extensional sheath fold. Hinge lines of a sheath fold typically initiate perpendicular to the flow direction, and rotate into parallelism with the direction of the extensional flow; this would predict strain fringe lineations to initiate perpendicular to fold hinge lines and to progressively rotate into parallelism with the hinge lines. The opposite relationship is seen in the field area, with strain fringe lineations initially developing parallel to the hinge line of the fold and progressively rotating to an orientation perpendicular to the hinge lines, therefore recording the opposite sense of curvature to that required for development of the sheath

fold. Moreover, there is no evidence of steeply dipping strata following the D_1 event to produce extensional folds such as the folds proposed by Froitzheim (1992). The other possibility for the development of the folds during extension is drag folding from the Middle detachment or related normal faults. However, the Middle detachment truncates various structural levels across the field areas and within the folds, thus indicating that the folds developed prior to the Middle detachment. The alternative is that these folds record subhorizontal shortening related to crustal shortening as previously interpreted by Compton (1972) and Wells (1997). The geometry of the folds including hinge lines, and the kinematics are consistent with subhorizontal shortening, and these types of contractional folds are well recognized in the internal parts of most fold-thrust belts. Therefore, it is interpreted that the folds present at Marble Peak, South Hill, and the Rosebud area are related to contraction and produced during crustal thickening within the orogenic wedge.

Relative age of D_2

An absolute age of the D_2 folds and associated fabric was not directly established due to the lack of suitable minerals for isotopic dating. However, a relative age can be established based on overprinting and cross cutting relationships of older and younger deformational fabrics. Moreover, interpreting the folds as recording a contractional event allows relative time constraints to be determined through correlation to dated kinematic sequences elsewhere in the core complex. Age constraints for D_2 are bracketed between 105 Ma and Eocene-Oligocene for the following reasons: (1) D_2 structures deform the 105 Ma D_1 fabric, and thus are younger; and (2) D_2 event predates the development of the

Eocene-Oligocene Middle Mountain shear zone and Middle detachment. Nevertheless, further tightening of the age constraints can be obtained by correlating similar kinematics from other parts of the RAG.

Based on the previously mentioned observations of cross cutting relationships and documented contractional events, two time intervals for D_2 shortening are possible: one at 105-87 Ma, and the other between 68-45 Ma (Figure 38). The kinematic history of the hinterland between 105-87 Ma is unclear with an incomplete and sparse record of Late Cretaceous shortening. An event of ~87 Ma thrust burial of metamorphic rocks from the Basin Creek area, determined by P-T paths derived from growth-zoned garnet, has been interpreted to record burial by thrust-sense motion of the Basin-Elba fault during reactivation (Harris et al., 2007; Uribe-Cruz, unpublished) (Figure 38). Also within the hinterland is the top-to-the-southeast Windermere thrust (153 to 84 Ma), which was responsible for 30 km of crustal thickening and 69 km of shortening, and the Independence thrust responsible for ~5 km of crustal shortening (84 to 75 Ma) (Camilleri and Chamberlain, 1997) (Figure 38). Further east, within the Sevier foreland fold-thrust belt, the Idaho-Wyoming-Utah salient consists of eight major thrust faults with motions younging to the east which span the time between ~153 Ma and ~52 Ma (Armstrong and Oriel, 1965; Royse et al., 1975; Dixon, 1982; Lamerson, 1982; Coogan, 1992; Hudec, 1992; Camilleri and Chamberlain, 1997; Decelles, 2004) and also could be responsible for the D_2 contractional event. These faults include: Paris-Williard (Latest Jurassic-Early Cretaceous); Meade and Crawford (Middle Cretaceous); Absaroka (middle Late Cretaceous); Darby-Hogsback (Paleocene to Early Eocene); and Prospect (Early Eocene). Even though a dynamic relationship in the orogenic wedge exists between the foreland

thrust faults and the hinterland metamorphic rocks, distinguishing which thrust fault is related to the D_2 event is not possible. As a result, timing of the D_2 could not be closely correlated to known motions along foreland thrust faults. Because, there is no direct evidence linking the D_2 structures to an individual thrust fault within the foreland fold thrust belt these thrust faults exposed in the eastern foreland fold-thrust belt can be discarded and attention is focused on the RAG core complex.

Kilometer scale recumbent folds from the Raft River Mountains are bracketed between 68-45 Ma, and are interpreted as recording a contractional event (Figure 38). These recumbent folds deform the Mahogany Peaks fault (bracketed between 60 and 90 Ma by muscovite argon cooling ages) and are overprinted by the Eocene-Oligocene Middle Mountain shear zone (Wells, 1997; Wells et al., 1998) (Figure 38). The Mahogany Peaks fault is exposed within the footwall of the Middle detachment fault at Marble Peak and is deformed by the Oligo-Eocene MMSZ. The time bracket (68-45 Ma) for shortening may be inferred from ages of monazite inclusions in garnet that vary in age from core to rim, and for which the garnets grew during compression, as determined by P-T path modeling (Hoisch et al., 2002). In addition, the recumbent folds are in the upper plate of the Middle detachment and there is no evidence of the detachment being folded. On the other hand, correlating the D_2 event to the ~ 87 Ma Basin-Elba thrust fault could also be a possibility. Therefore, there are two permissive timeframes for the D_2 event, based on our understanding of the ages of shortening in the RAG; one is related to the Basin-Elba thrust (87 Ma) or the waning stages of the Windermere thrust (153-84 Ma) and the Independence thrust (84-75 Ma) during crustal shortening, and the other is related to the D_3 recumbent folding event (68-45 Ma) from the Raft River Mountains and

proposed reactivation of the Basin-Elba fault (Figure 38). Both permissive correlations are significantly older than the time frame of 20-12 Ma as proposed by Compton (1977).

Tectonic implications for D_2

Strain geometry, kinematics, relative age, and vorticity of the D_2 folds and associated fabric all suggest that the D_2 event is of contractional origin, most probably at ~87 Ma or during ~68 to 45 Ma (Figure 38). Evidence of a rotation about the vertical Z axis of finite strain, as evident by lineation curvature within the XY plane (S_2 cleavage) indicates one of two possibilities: (1) counter-clockwise rotation of the paleostress direction; or (2) clockwise rotation of the crustal rocks. Comparing the results to the regional tectonics of the area allows some discrimination between these two hypotheses.

The counter-clockwise curvature recorded by the D_2 fibers could be the result of a rotation of a paleostress direction. In order to test this interpretation, the possibilities of changes in paleostress orientation within the hinterland during the proposed timeframe of the D_2 event will be discussed. Bird (2002) conducted an intensive compilation of 369 paleostress direction indicators from geologic literature of the western United States for the time frame of 85 Ma to present. During the Sevier orogeny at 85 Ma, horizontal compression azimuths of 045°-067° recorded the average tectonic transport of the orogen (Bird, 2002). At the waning stages of the Sevier and the onset of the Laramide orogeny, ~64 Ma, horizontal compression azimuths were ~048°, approximately parallel to the relative direction of the Farallon plate with North America (Engebretson et al., 1985; Bird, 2002). During the Eocene, ~50 Ma, within 50% uncertainty, horizontal compression azimuths were ~083° (Bird, 2002). A reversal from a horizontal

compressional stress to a horizontal tensional stress developed around 33 Ma (Bird, 2002).

As discussed previously, the D_2 event is either ~87 Ma or bracketed between 68-45 Ma, based on two possible correlations to dated contractional events (Figure 38). Extension directions exhibited by the D_2 strain fringes within the XY plane record a counter-clockwise rotation from 215° to 131°. Extension directions recorded by the earlier fibers of the strain fringes are parallel to the horizontal compressional axes, determined by the Bird study (2002). The older parts of the strain fringe fibers at 215° could have resulted from the 87 Ma paleostress direction of 045°-067°. However, the younger parts of the fibers with an orientation of 131° could not have resulted from the 64 Ma paleostress direction of 48°. It is possible that the paleostress directions could have contributed to the vertical axis rotation of the stress field, but with the limited amount of samples collected over a small area; this does not make a compelling argument. In addition, the paleostress directions determined by Bird (2002) record a clockwise rotation not a counter-clockwise rotation as seen by this study. Therefore, the counter-clockwise vertical axis rotation recorded by the strain fringes is unlikely to have resulted from the clockwise rotation of the paleostress direction as documented by Bird (2002).

Alternatively, counter-clockwise curvature of the D_2 fibrous strain fringes within the XY plane could have resulted from a clockwise vertical axis rotation of the crustal rocks. As previously discussed, the D_2 fibrous strain fringes grew synchronously with the development of the D_2 folds and the possible ages for the D_2 event is ~87 Ma or 68-45 Ma. Therefore, the counter-clockwise curvature recorded by the strain fringes will be

discussed in the context a crustal rocks undergoing vertical axis rotation within the tectonic setting. Because the progression in stretching direction is from parallel to perpendicular to hinge lines, the opposite relationship to that predicted by the sheath fold model (as discussed above), rotation during sheath fold development is discounted.

Vertical axis rotation is a common and important component of crustal deformation. A well known example of vertical axis rotation is the Western Transverse Ranges of California, where vertical axis rotation is associated with wrench tectonics (McKenzie and Jackson, 1983; Lamb, 1994; Onderdonk, 2007). The Western Transverse Range has rotated 90° clockwise since 18 Ma, indicated by paleomagnetic data and geologic evidence (Onderdonk, 2007). However, this vertical axis rotation occurred within a transform boundary between the North American and Pacific plates, whereas the vertical axis rotation discussed in this study is within a fold-thrust belt. Several studies document vertical axis of rotation within thrust sheets from salients of the Sevier fold-thrust belt (Apotria, 1995; Conder et al., 2003; Kwon and Mitra, 2004). The primary control for the development of the arcuate shape of a salient during vertical axis rotation has been attributed to the basin geometry (Apotria, 1995; Conder et al., 2003; Kwon and Mitra, 2004). In particular, a study by Conder et al. (2003) analyzed vertical axis rotation from paleomagnetic data within the Charleston-Nebo salient in Utah and attributed it divergent flow. The divergent flow model for thrust-salient development characterizes the overall stress distribution along the salient and predicts opposite sense of rotation along both lateral margins of the salient (Laubscher, 1972). Results from Conder et al. (2003), in conjunction with the divergent flow model (Laubscher, 1972; Marshak et al., 1992), indicate counter-clockwise rotation in the northern parts and clockwise rotation in

the southern parts of the salient. If the kinematic modeling of this salient is correct, and the divergent model is valid, then clockwise rotation would be predicted in northwest Utah.

The Grouse Creek Mountains lie west of the central to southern portion of the Idaho-Wyoming-Utah-Salient. During the time interval of ~93 Ma and ~89 Ma, the Paris-Mead-Willard thrust system was active at the latitude of the RAG and initial development of the salient is suggested (Decelles, 2004). The overall trend of fold axes at Marble Peak and South Hill is north-south, and in the Rosebud area is north-east. If the trend of the fold axes at Marble Peak and South Hill represents the frontal straight margin of the divergent flow model, and the fold trend at Rosebud represents the southern portion, then the counter-clockwise curvature observed by the D_2 strain fringes is consistent with clockwise rotation and the divergent flow model. Therefore, the development and forward movement of the Idaho-Wyoming-Utah salient could have influenced the development of the D_2 event, causing clockwise vertical axis rotation, as recorded by the strain fringes, of the folds during eastward-directed thrusting.

CHAPTER 6

CONCLUSIONS

The earliest ductile fabric (D_1) in the Grouse Creek Mountains of northwest Utah affects Archean to Permian rocks and records an episode of mid-Cretaceous synconvergent orogen-parallel extension in the hinterland of the Sevier orogen. Fibrous strain fringes from the Oquirrh Formation within the Middle allochthon provide a rare opportunity to establish the kinematics and vorticity of this top-to-the-north extensional flow. In addition, a second deformational event (D_2), also recorded by fibrous strain fringe growth, shows kinematics of top-to-the-southeast shearing and is interpreted as a contractional event.

The following conclusions are drawn for D_1:

(1) Kinematic and vorticity studies within the D_1 shear zone consistently demonstrate top-to-the-north noncoaxial extensional flow with a significant component of vertical shortening.

(2) S_1 in the study areas is a flat-lying foliation parallel to bedding with a north-northeast trending elongation lineation.

(3) Finite strain magnitudes are heterogeneous and range from 28% to 634%, increasing vertically and laterally towards the southern extent of the field areas within the Oquirrh Formation.

(4) Rosebud D_1 strain fringes exhibit a clockwise curvature within the S_1 plane.

(5) The D_1 fabric records an extensional event, as opposed to earlier interpretations of D_1 as recording contraction.

(6) D_1 fabric records an episode of mid-Cretaceous synconvergent orogen-parallel extension related to gravitational collapse, within the hinterland of the Sevier orogen.

The following conclusions are drawn for D_2:

(1) D_2 fabric and structures (folds) record a contractional event and overprint the ~105 Ma D_1 event.

(2) The D_2 folds at Marble Peak and South Hill trend north, whereas the folds at the furthest extent of the field area from Rosebud trend north-northeast.

(3) Kinematic and vorticity studies of D_2 demonstrate top-to-the-south noncoaxial flow with a component of horizontal shortening.

(4) D_2 fibrous strain fringes evolved in a changing displacement field from top-to-the-southwest during early D_2 to top-to-the-southeast during late D_2.

(5) S_2 in the study areas is an axial planar cleavage associated with recumbent folds that developed by pressure solution, and is most pronounced at the Rosebud area.

(6) The absolute timing for D_2, based on correlation to other shortening events in the RAG, permits D_2 to be either ~87 Ma or between 68-45 Ma.

(7) Finite strain magnitudes ranging from 17% to 511% increase laterally and vertically towards the southern extent of the field areas within the Oquirrh Formation.

Figure 1. Generalized geologic map of Raft River-Albion-Grouse Creek Mountains (RAG) showing distribution of the L_1 stretching lineation. Field areas (in boxes) are at Marble Peak, North and South Hill, and Rosebud area. Stereoplots showing L_1 from Compton (1972, 1975), Miller (1980), Todd (1980), Sheely (2002), and Wells (1997). Inset, shows location map of Raft River-Albion-Grouse Creek metamorphic core complex, within the hinterland of the Sevier fold-thrust belt (Decelles, 2004). Lower grade metamorphic rocks shown in stippled pattern include: BP, Black Pine; PM, Pequop; higher grade metamorphic rocks shown in wavy line pattern include: R, Ruby; WH, Wood Hills; SR, Snake Range, and RAG. Traces of major thrusts of the fold-thrust belt include: W, Willard; P, Paris; M, Meade; C, Crawford; A, Absaroka; H, Hogsback. WC, Wasatch basement culmination. Arrows indicate estimates for thrust transport direction from Royse (1993) and Yonkee (1997). Inferred positions of Precambrian crustal boundary shown by light grey dashed line modified Lush et al. (1988), and by grey solid line after Nelson et al. (2002), modified from Zartman (1974). Early Paleozoic shelf-slope break from Miller et al. (1991).

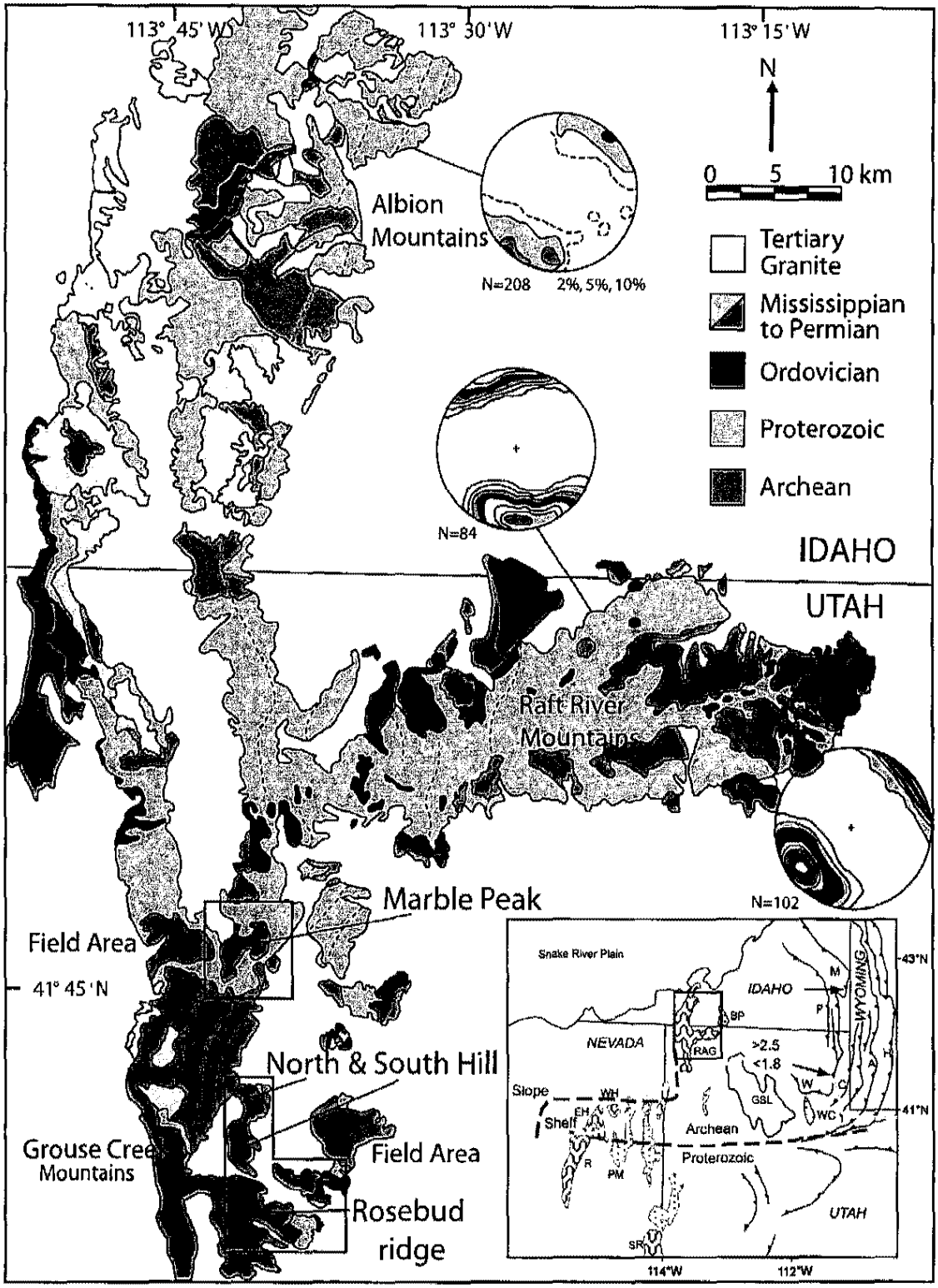
113° 45' W
113° 30' W
113° 15' W
N
0 5 10 km
Albion Mountains
N=208 2%, 5%, 10%
Tertiary Granite
Mississippian to Permian
Ordovician
Proterozoic
Archean
N=84
IDAHO
UTAH
Raft River Mountains
N=102
Marble Peak
Field Area
41° 45' N
North & South Hill
Grouse Creek Mountains
Field Area
Rosebud ridge
Snake River Plain
IDAHO
WYOMING
NEVADA
RAG
BP
>2.5
<1.8
Slope
Shelf
WH
EH
GSL
Archean
Proterozoic
UTAH
43°N
41°N
114°W
112°W

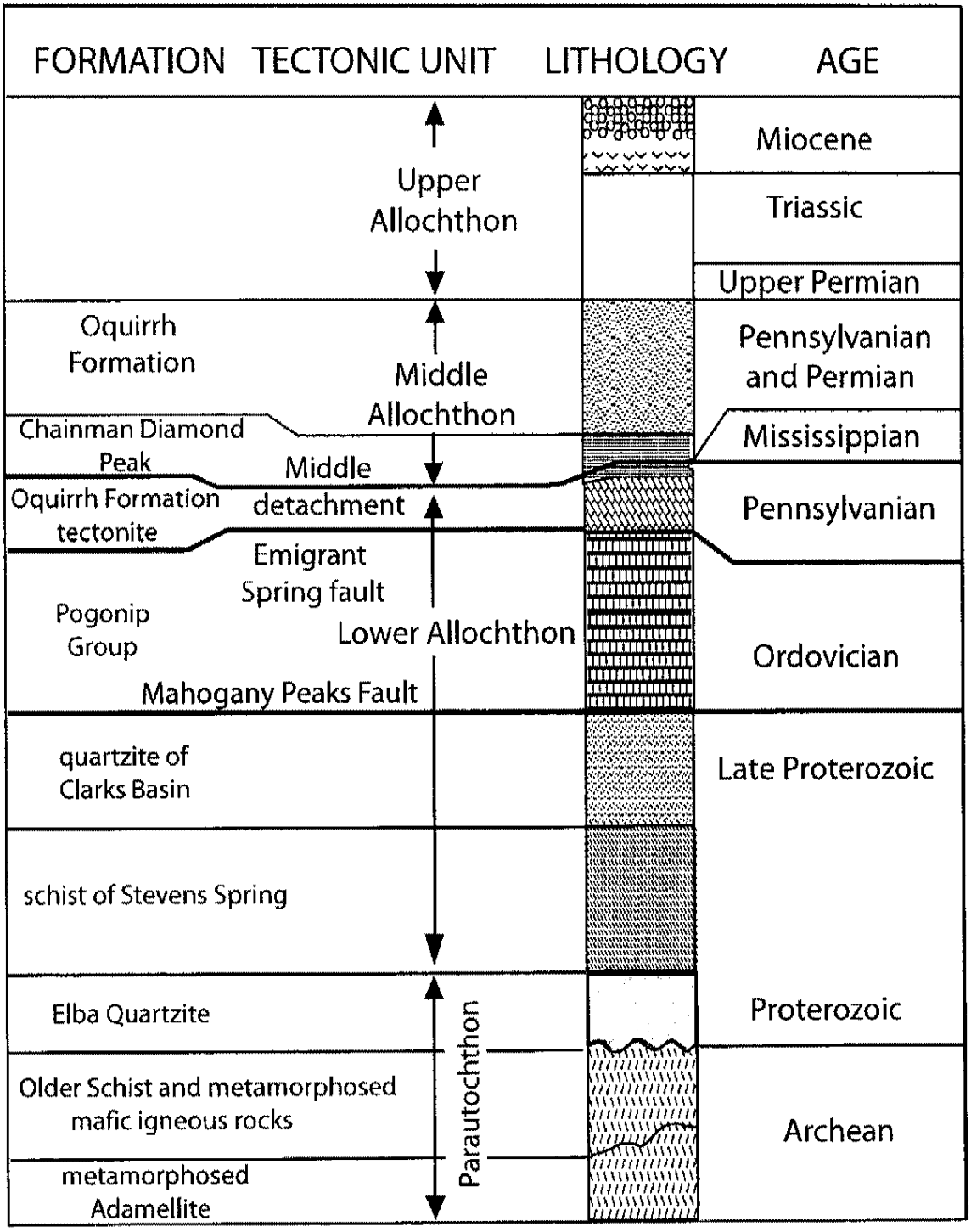

Figure 2. Tectonostratigraphic column of Archean to Miocene rocks in the Grouse Creek Mountains. Archean to Pennsylvanian-Permian rocks are present within the three field areas. The primary focus of this study was the Pennsylvanian-Permian Oquirrh Formation within the Middle allochthon. Modified from Wells et al. (1998).

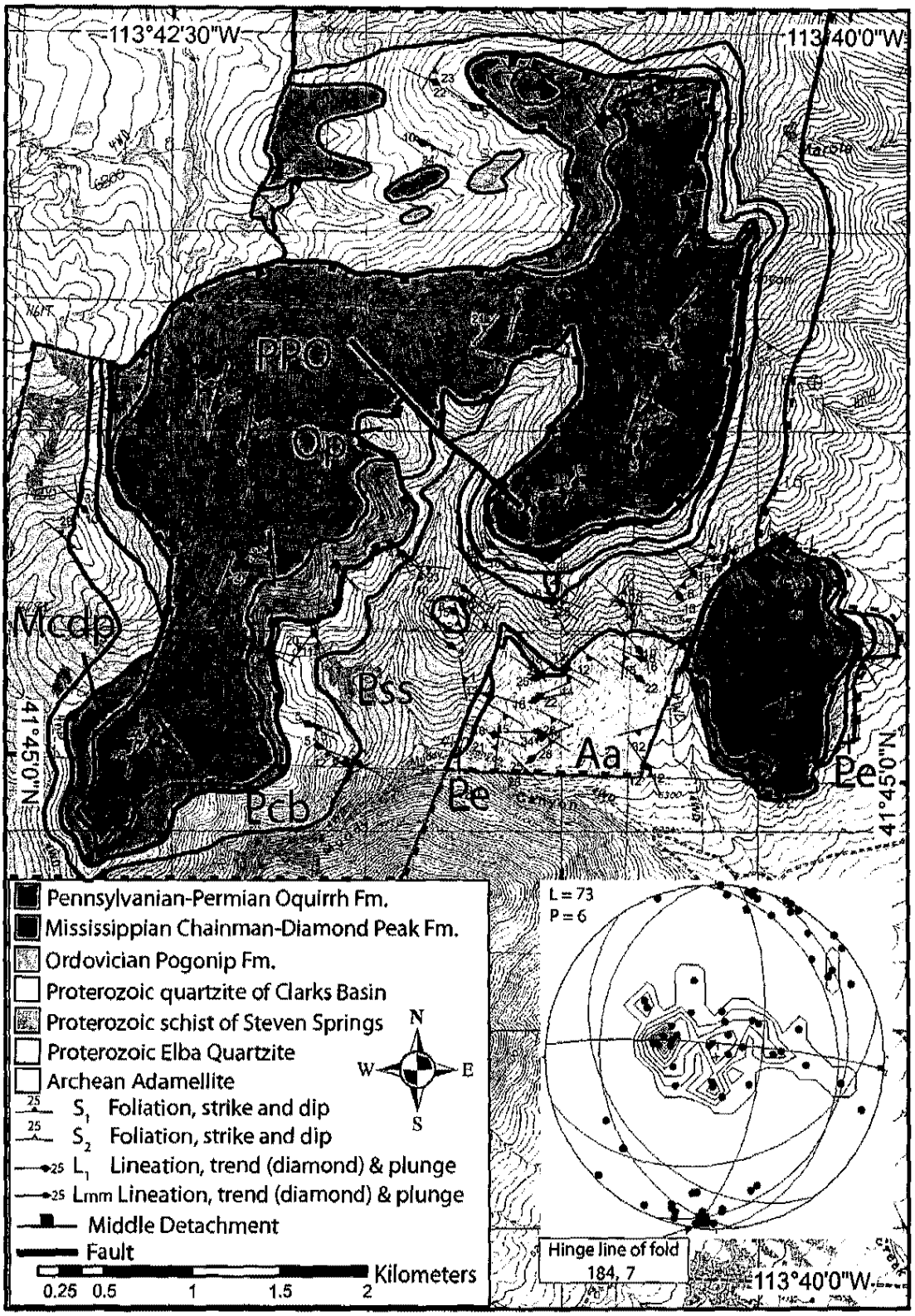

Figure 3. Geologic map of the Marble Peak klippe, showing the distribution and orientation of S_1, S_2, L_1, L_{mm}. Archean to Mississippian rocks show overprint of MMSZ; Pennsylvanian-Permian rocks preserve D_1. Stereoplot shows lineations in red, poles to S_1 (black dots), S_2 axial cleavages (blue lines), and hinge line of fold (red box with black outline). Dashed grey line marks outline of map area. Contour intervals are 40 feet.

Figure 4. Photographs A-E showing L_1 elongation lineation in Oquirrh Formation. A, strain fringe elongation lineation at Rosebud. B and C, stretched crinoids at Rosebud. D, stretched brachiopods at Marble Peak. E, mineral stretching lineation at Marble Peak. F, relationship between S_1 and S_2 at Marble Peak, facing east. Pencil and hammer for scale.

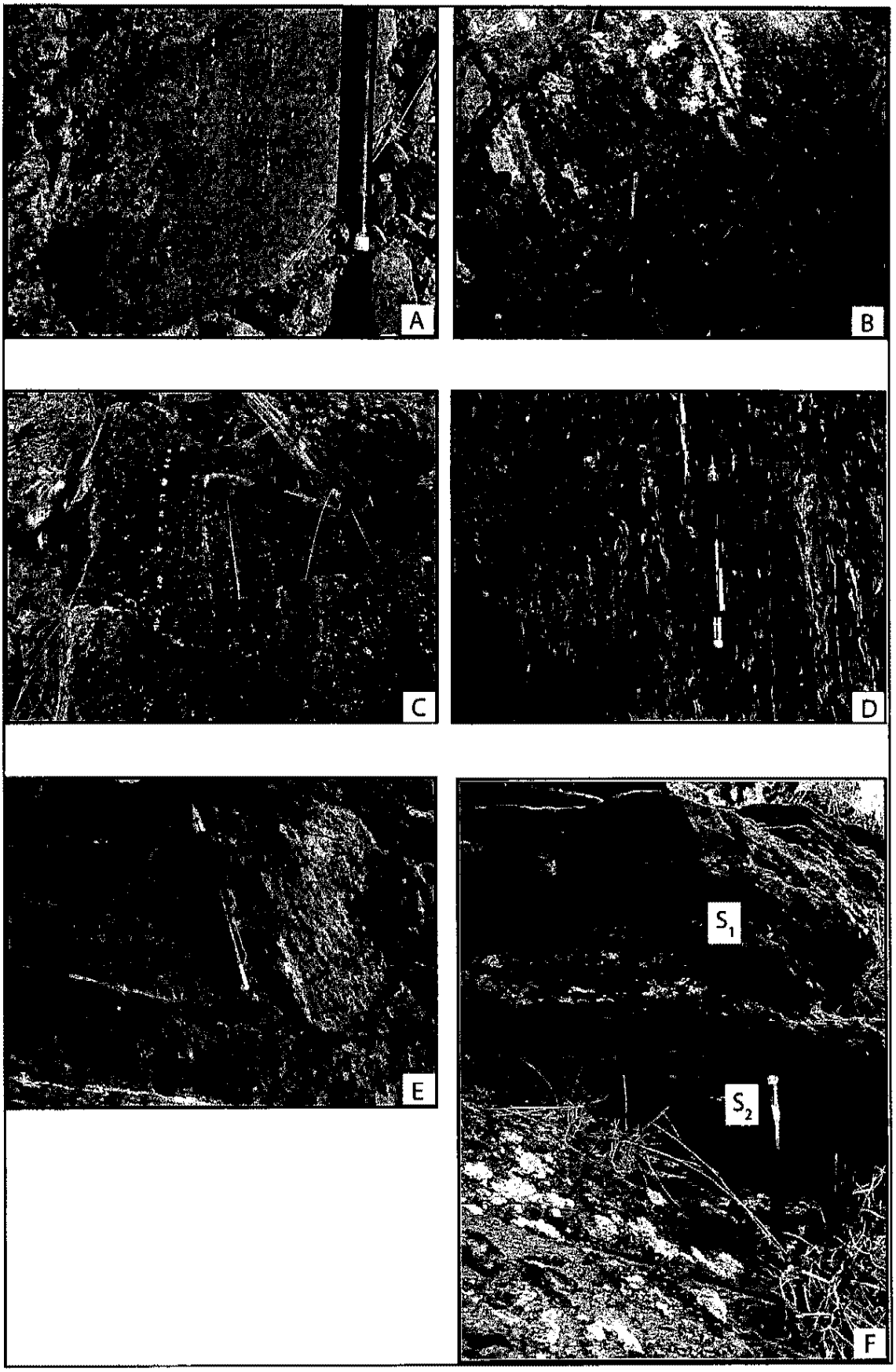
A
B
C
D
E
S_1
S_2
F

Figure 5. Geologic map of North and South Hill, showing distribution and orientation of S_1, S_2, L_1, L_{mm}. Pennsylvanian-Permian rocks preserve D_1 at South Hill, overprinted by Cenozoic deformation at North Hill. A, stereoplot of North Hill showing lineations in red, poles to S_1 in black dots and S_2 axial planar cleavages with blue lines. B, stereoplot of South Hill showing lineations in red, poles to S_1 in black dots and S_2 axial planar cleavages with blue lines, and hinge line of overturned anticline. Contour intervals are 20 feet.

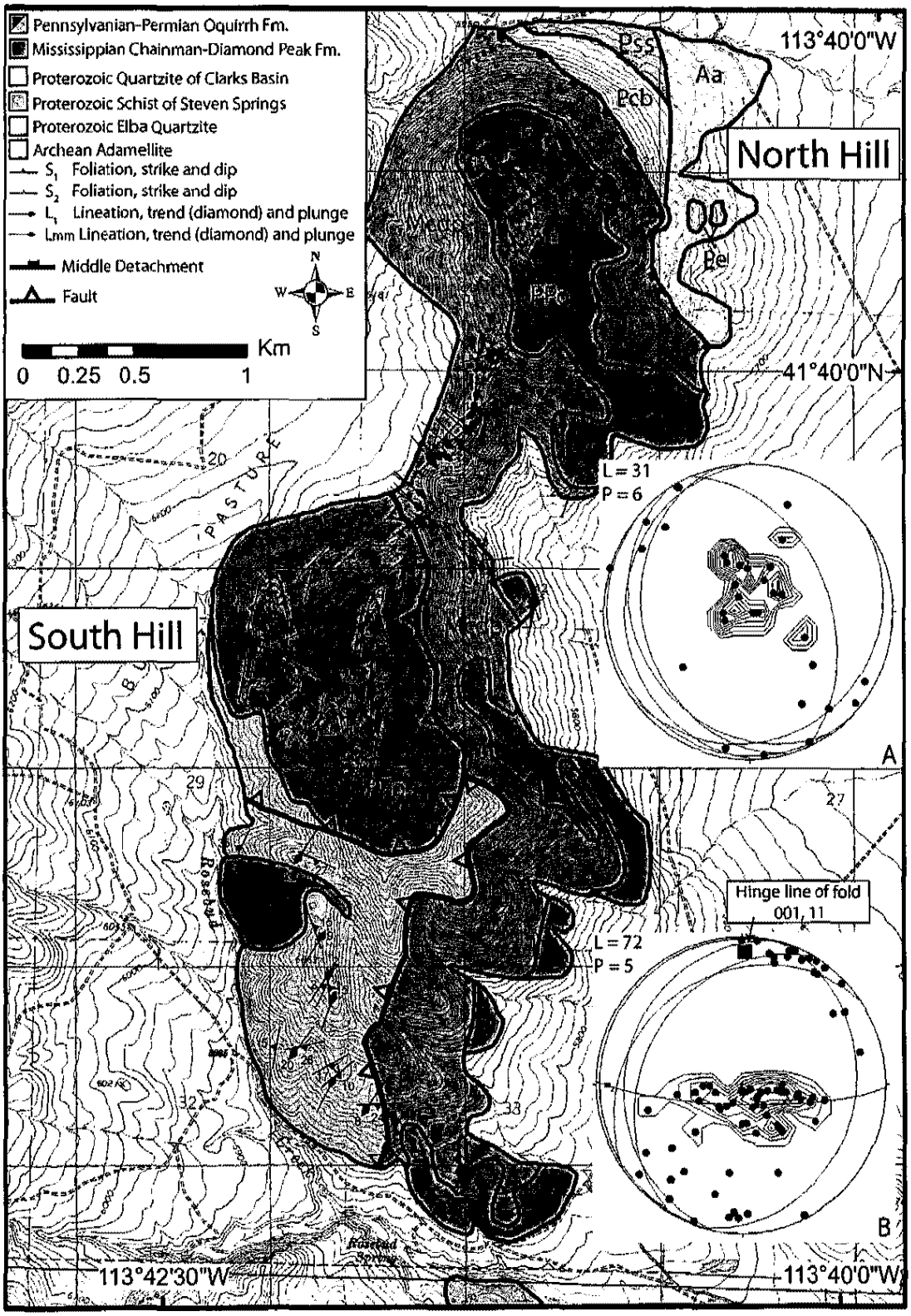
Pennsylvanian-Permian Oquirrh Fm.
Mississippian Chainman-Diamond Peak Fm.
Proterozoic Quartzite of Clarks Basin
Proterozoic Schist of Steven Springs
Proterozoic Elba Quartzite
Archean Adamellite
S1 Foliation, strike and dip
S2 Foliation, strike and dip
L1 Lineation, trend (diamond) and plunge
Lmm Lineation, trend (diamond) and plunge
Middle Detachment
Fault
N
W
E
S
Km
0 0.25 0.5 1
113°40'0"W
Pss
Aa
Pcb
North Hill
Pe
41°40'0"N
L = 31
P = 6
A
PASTURE
South Hill
Hinge line of fold
001, 11
L = 72
P = 5
B
113°42'30"W
113°40'0"W

Figure 6. Geologic map of Rosebud area, showing the distribution and orientation of S_1, S_2, L_1, L_{mm}. Pennsylvanian-Permian rocks preserve D_1. Stereoplot separated into North and South Hill showing lineations in red, poles to S_1 in black dots, and S_2 axial planar cleavages with blue lines, and hinge line of fold (red box with black outline). Contour intervals are 20 feet.

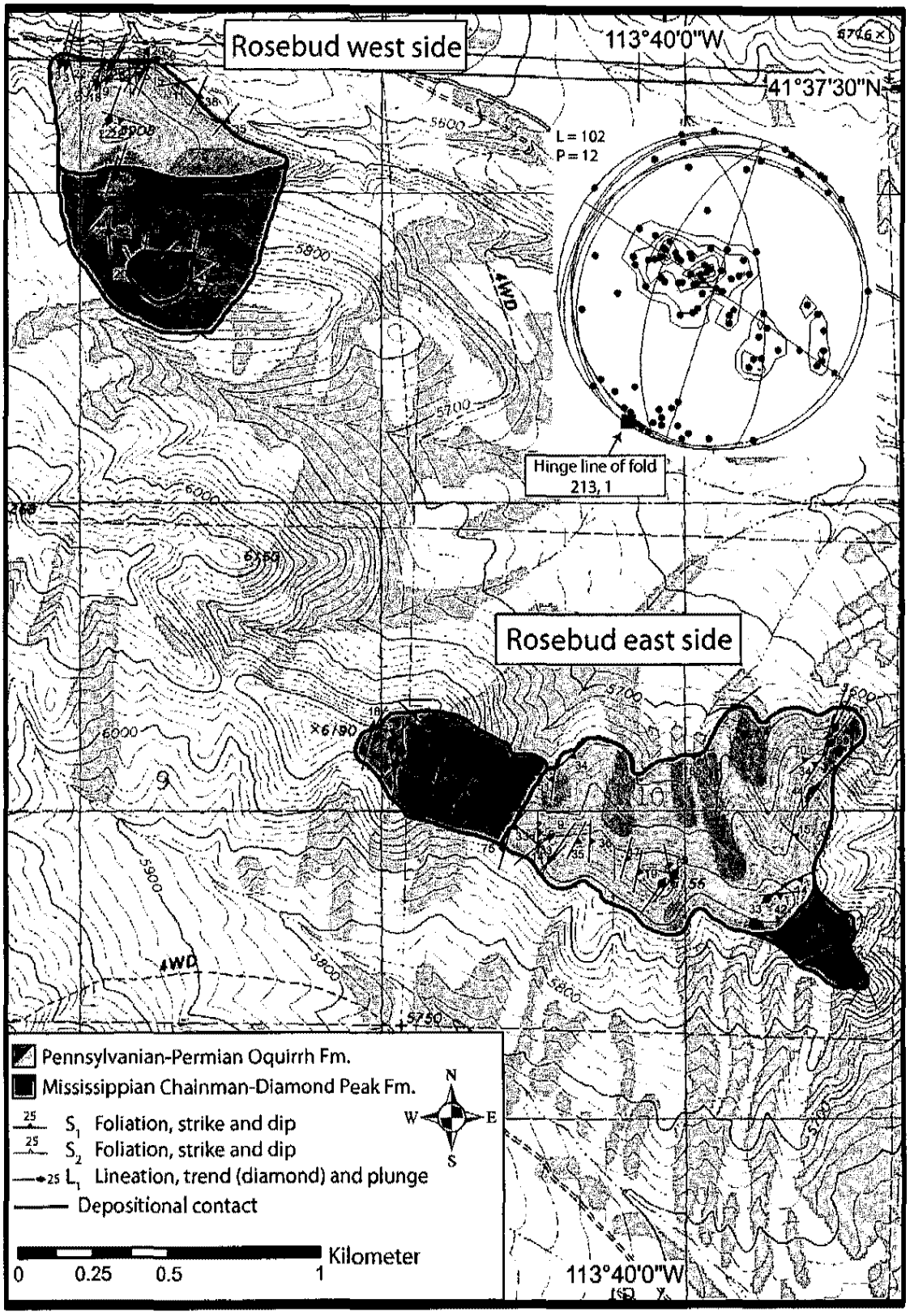
Rosebud west side
113°40'0"W
41°37'30"N
L = 102
P = 12
Hinge line of fold
213, 1
Rosebud east side
4WD
5800
5700
6000
6150
5900
5750
Pennsylvanian-Permian Oquirrh Fm.
Mississippian Chainman-Diamond Peak Fm.
S1 Foliation, strike and dip
S2 Foliation, strike and dip
L1 Lineation, trend (diamond) and plunge
Depositional contact
N
W
E
S
Kilometer
0
0.25
0.5
1
113°40'0"W

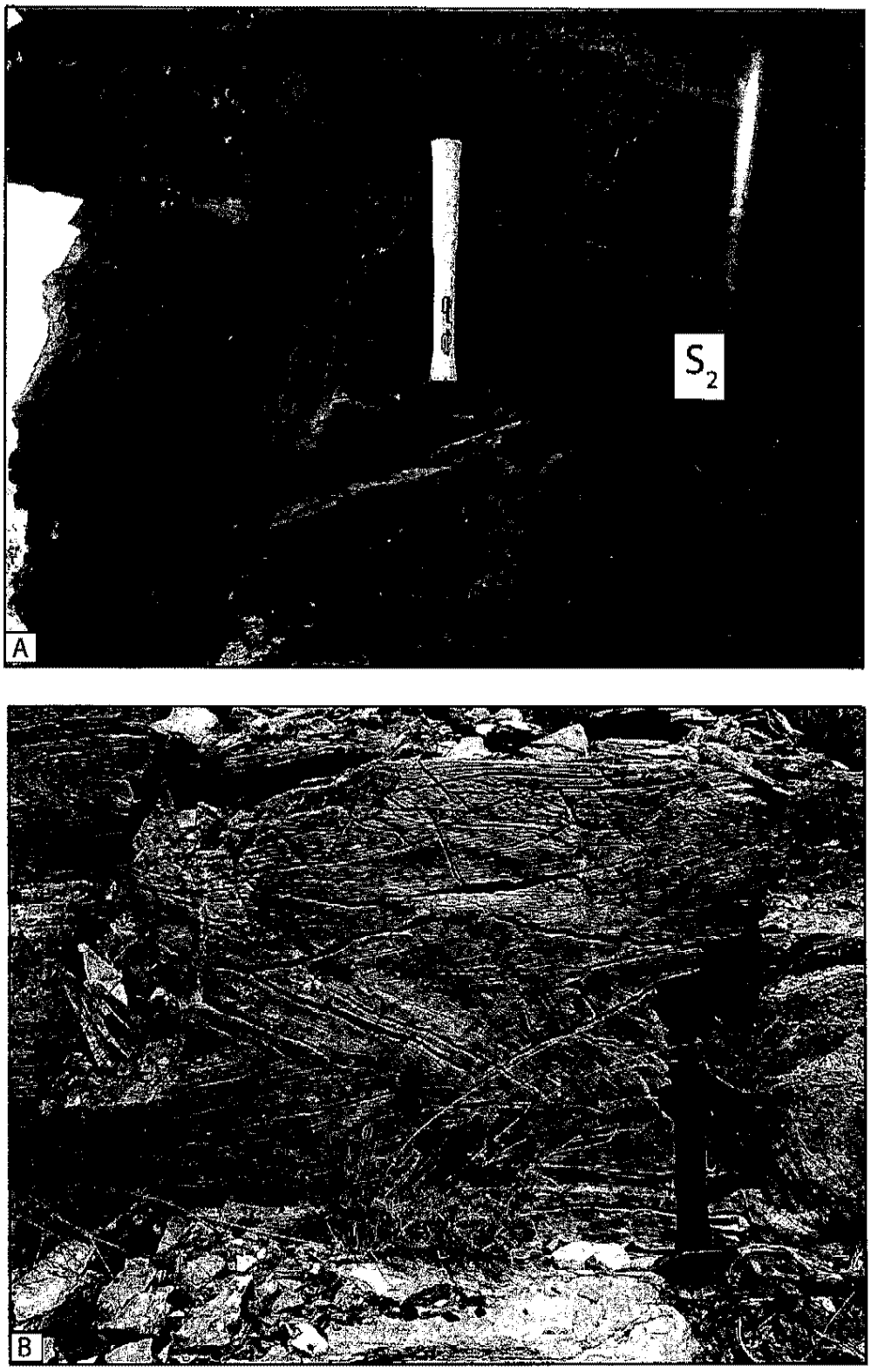

Figure 7. A, axial planar cleavage S_2, at low angle with respect to compositional layering at Marble Peak; view looking south. S_1 and S_2 relationship is indicative of a lower limb of an east verging fold present at Marble Peak. Hammer for scale. B, "S" shaped parasitic fold at Marble Peak indicating the lower limb of an overturned east verging fold. Picture facing north. Hammer for scale.

Figure 8. A, geologic map of South Hill. B, photo of recumbent anticline in the Oquirrh Formation at South Hill, facing south from location 1 of A. C, close-up of the relationship between S_1 and S_2 in the upper limb of the overturned fold, facing south.

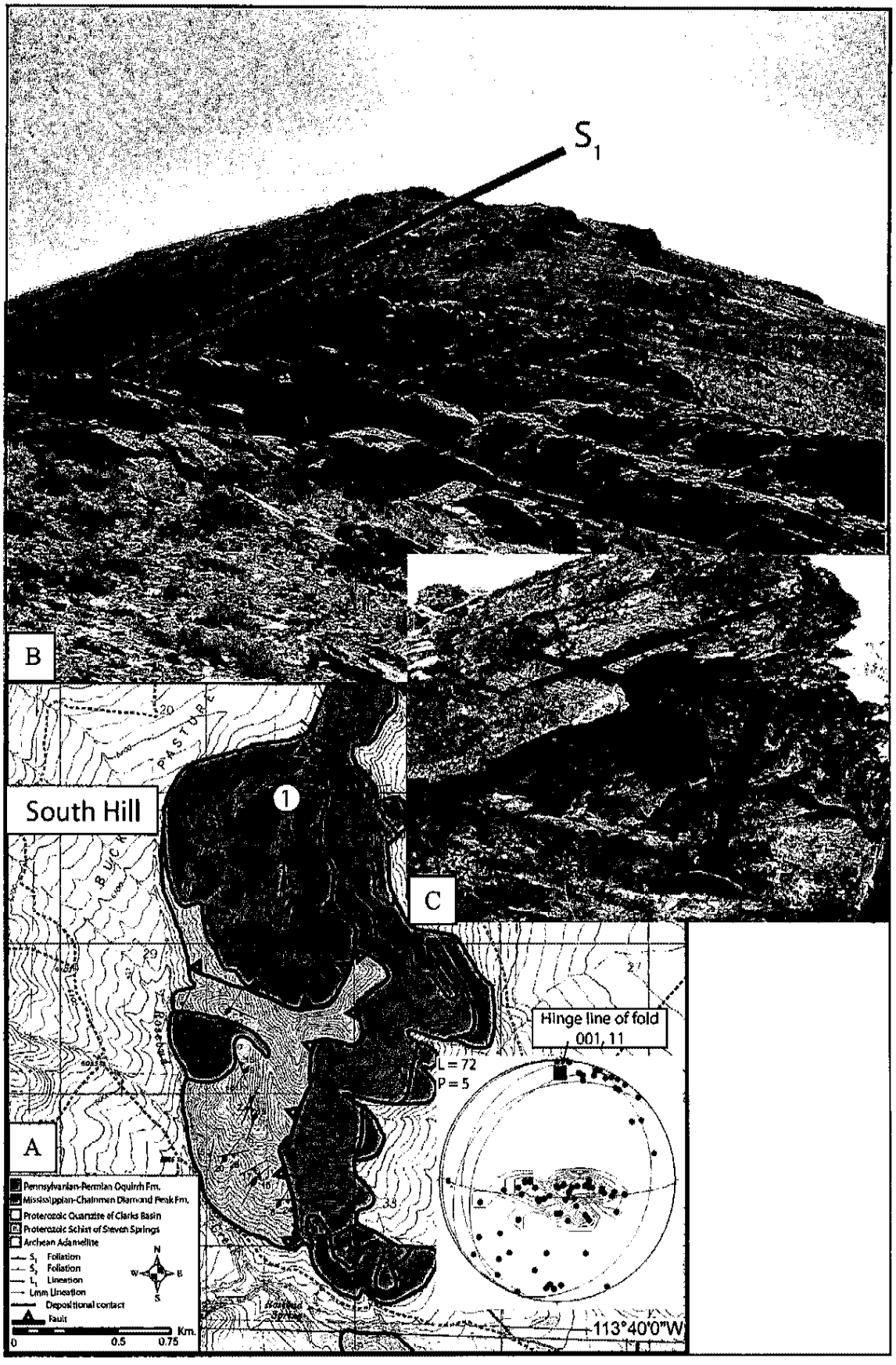
S_1
B
C
South Hill
1
A
PASTURE
BUCK
Hinge line of fold
001, 11
L = 72
P = 5
113°40'0"W
Pennsylvanian-Permian Oquirrh Fm.
Mississippian-Chainman Diamond Peak Fm.
Proterozoic Quartzite of Clarks Basin
Proterozoic Schist of Steven Springs
Archean Adamellite
S_1 Foliation
S_2 Foliation
L_1 Lineation
Lmm Lineation
Depositional contact
Fault
N
W
E
S
Km.
0
0.5
0.75

Figure 9. Photomosaics and GoogleEarth images of South Hill recumbent fold. A, aerial view of North and South Hill. B, GoogleEarth image of fold viewing east. C, photomosaic of fold viewing east. D, GoogleEarth image of fold viewing west. E, photomosaic of fold viewing west. Black lines trace S_1 foliation of the fold, and blue line traces the axial surface of the recumbent fold.

A
B
C
D
E
©Google
©Google

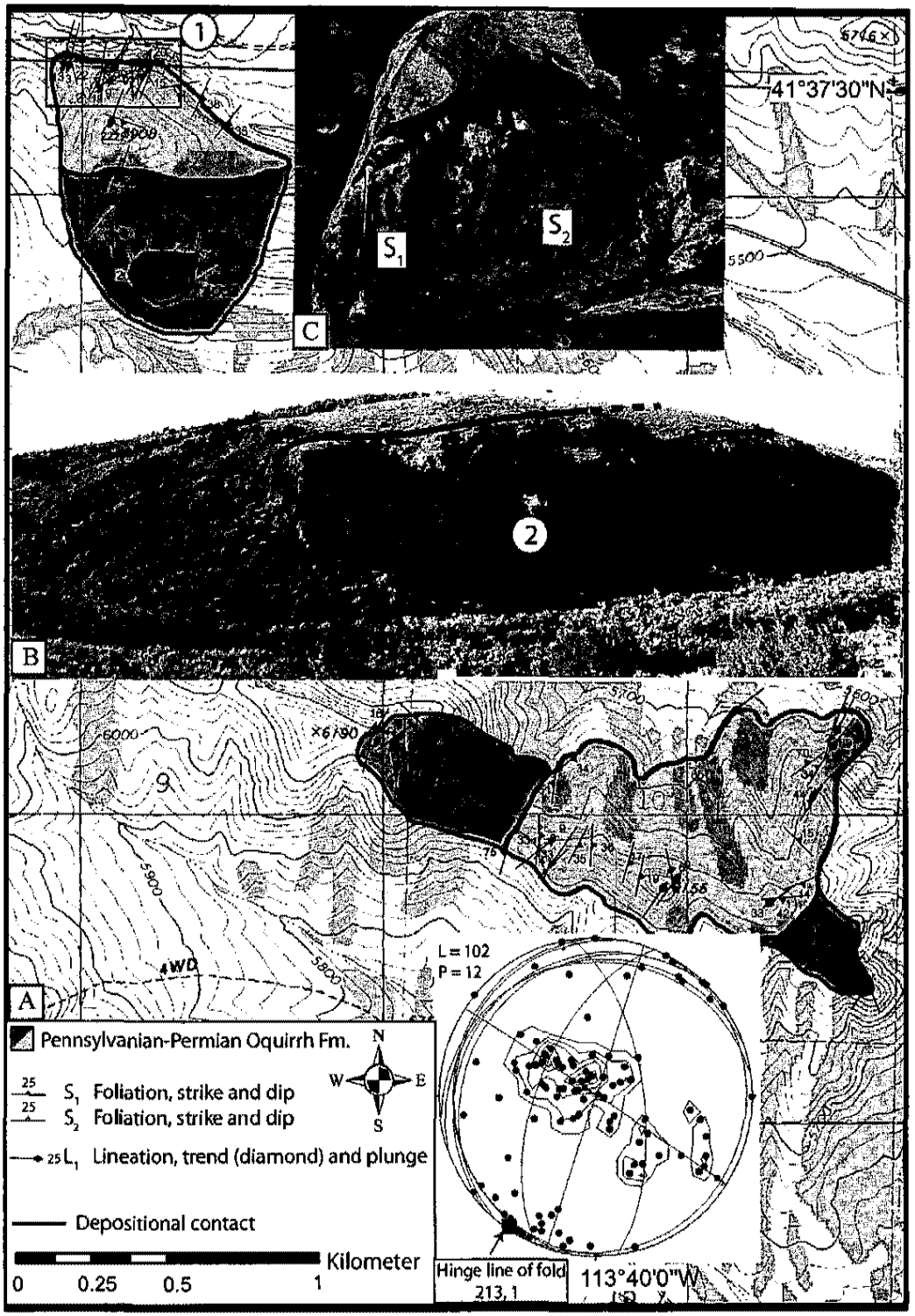

Figure 10. A, geologic map of Rosebud area with stereoplot data showing L_1 elongation lineation in red dots, poles to the S_1 planes in black dots, and S_2 axial planar cleavage in blue lines. B, south-facing picture of the Rosebud fold exposed on a cliff face (box around area); red lines represent a form line, view to the south from circle 1. Dashed where interpretative. C, S_1 and S_2 relationship in a parasitic fold on the western limb, looking south at circle 2.

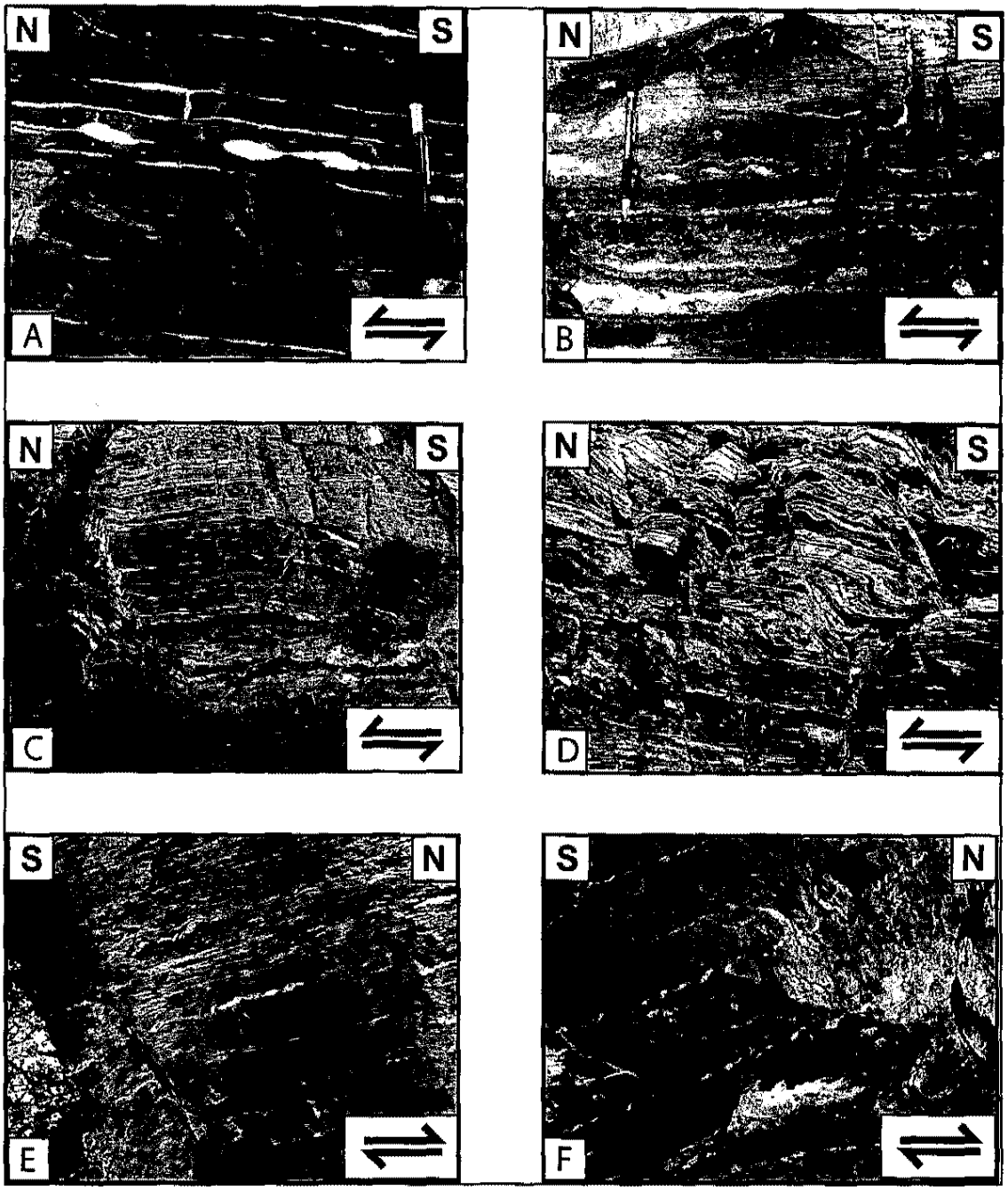

Figure 11. Shear sense indicators for D_1 deformation. A, asymmetric boudins in the tectonite at South Hill. B and C, asymmetric boudins in the Rosebud area. D, asymmetric chert stringers in the Rosebud area. E-F, asymmetic boudins at the cliff face of the Rosebud fold on the upright limb of the fold. Arrows on the pictures show the shear sense relative to north-south at the top of each picture. All show top-to-the-north sense of shear.

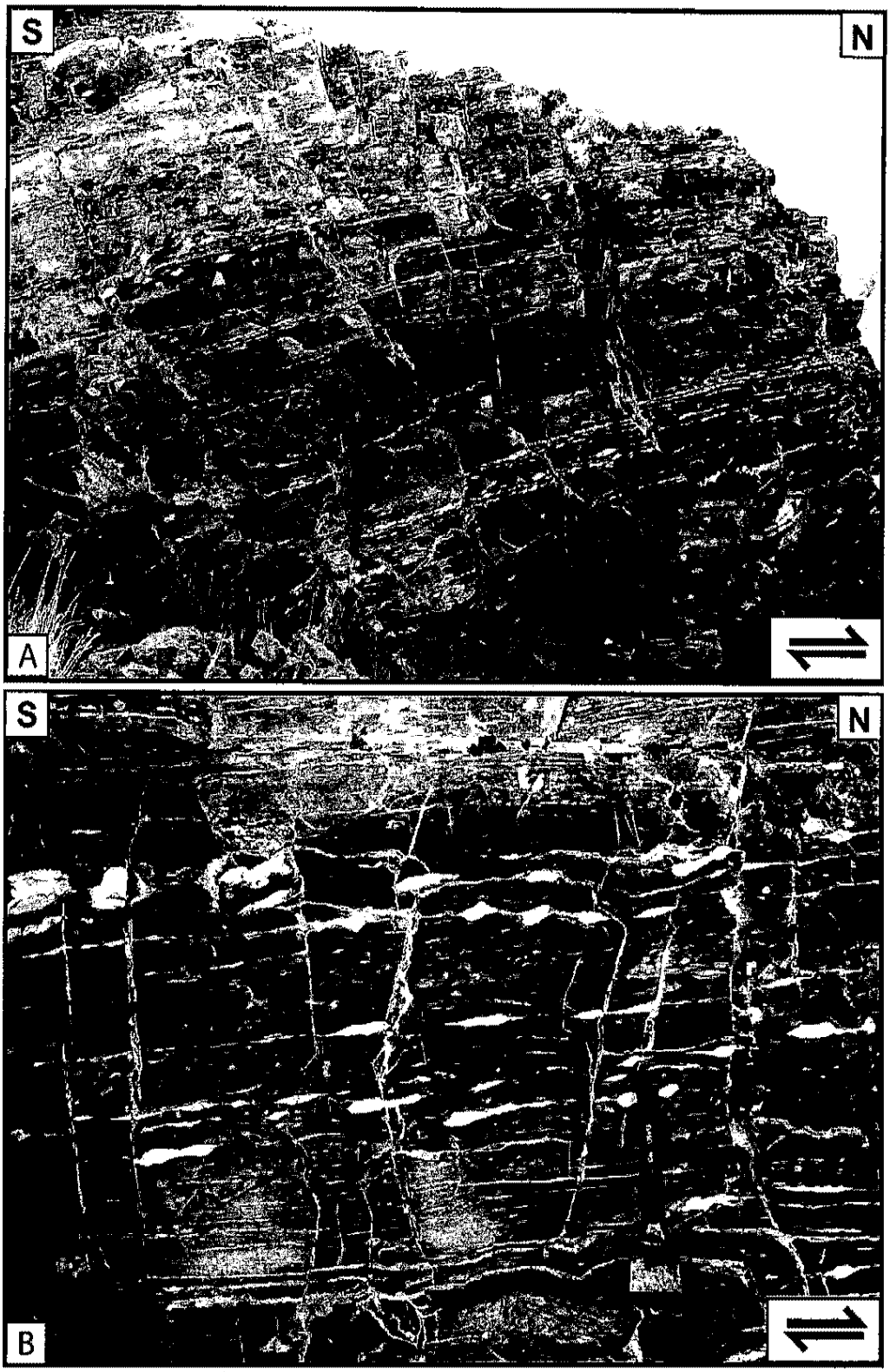

Figure 12. Shear sense indicators for D_2 deformation. A and B, top-to-the-north D_2 fabric shear indicators within the Oquirrh Formation tectonite. A and B, asymmetric boudins in the tectonite at South Hill. The tectonite at South Hill is in the overturned limb of the east-vergent recumbent fold; shear sense is reversed recording a top-to-the-south shear sense for the D_2 fabric.

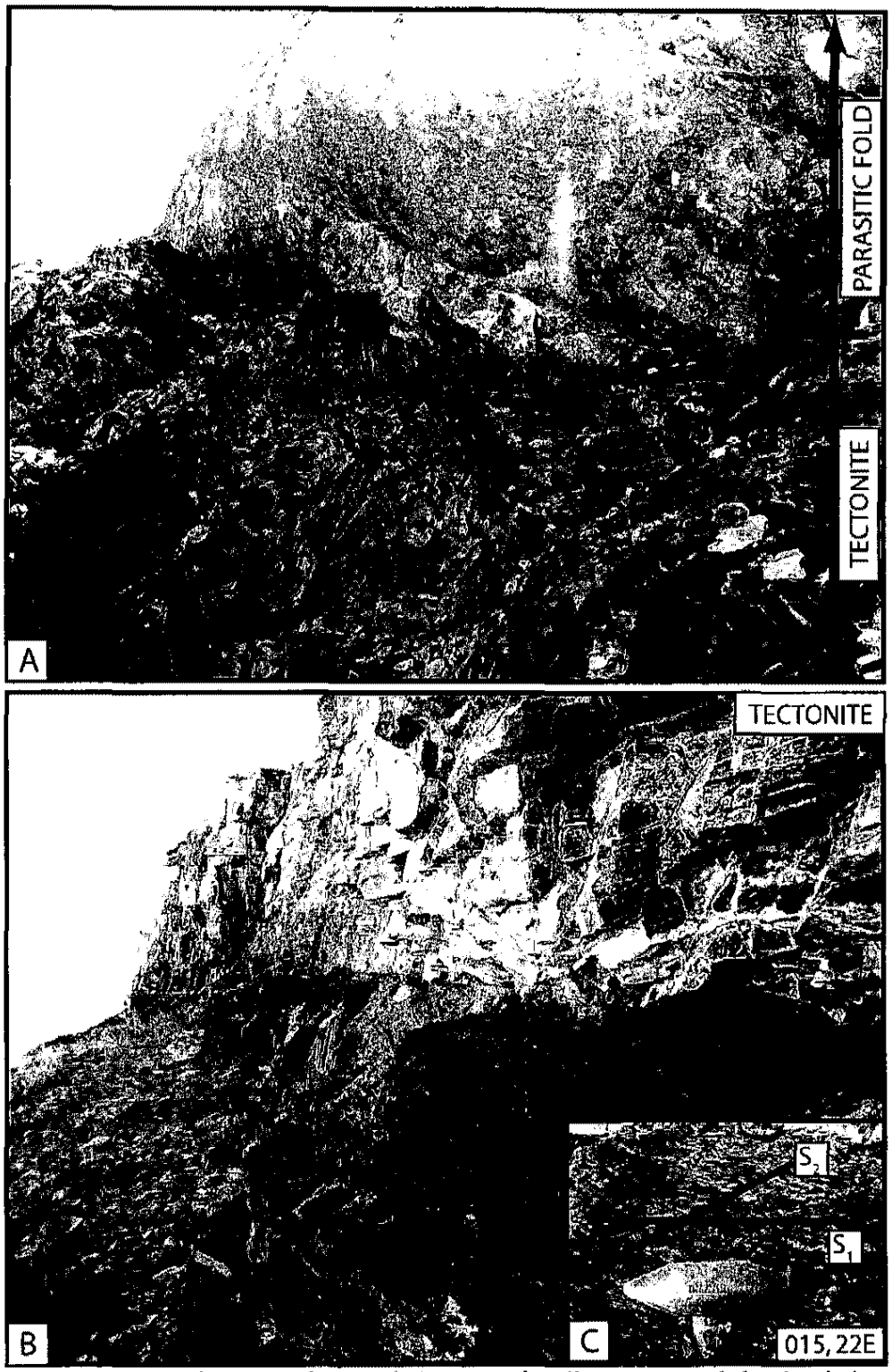

Figure 13. A, contact between the Oquirrh Formation limestone and the Oquirrh Tectonite in a parasitic fold in the South Hill fold. B, quartz rich section below the tectonite. C, relationship between the axial planar S_2 cleavage and the flat-lying S_1 foliation. This relationship along with orientation data indicates that the tectonite at South Hill is in the overturned limb of the east-vergent recumbent fold. Hammer for scale. Photograph facing southwest.

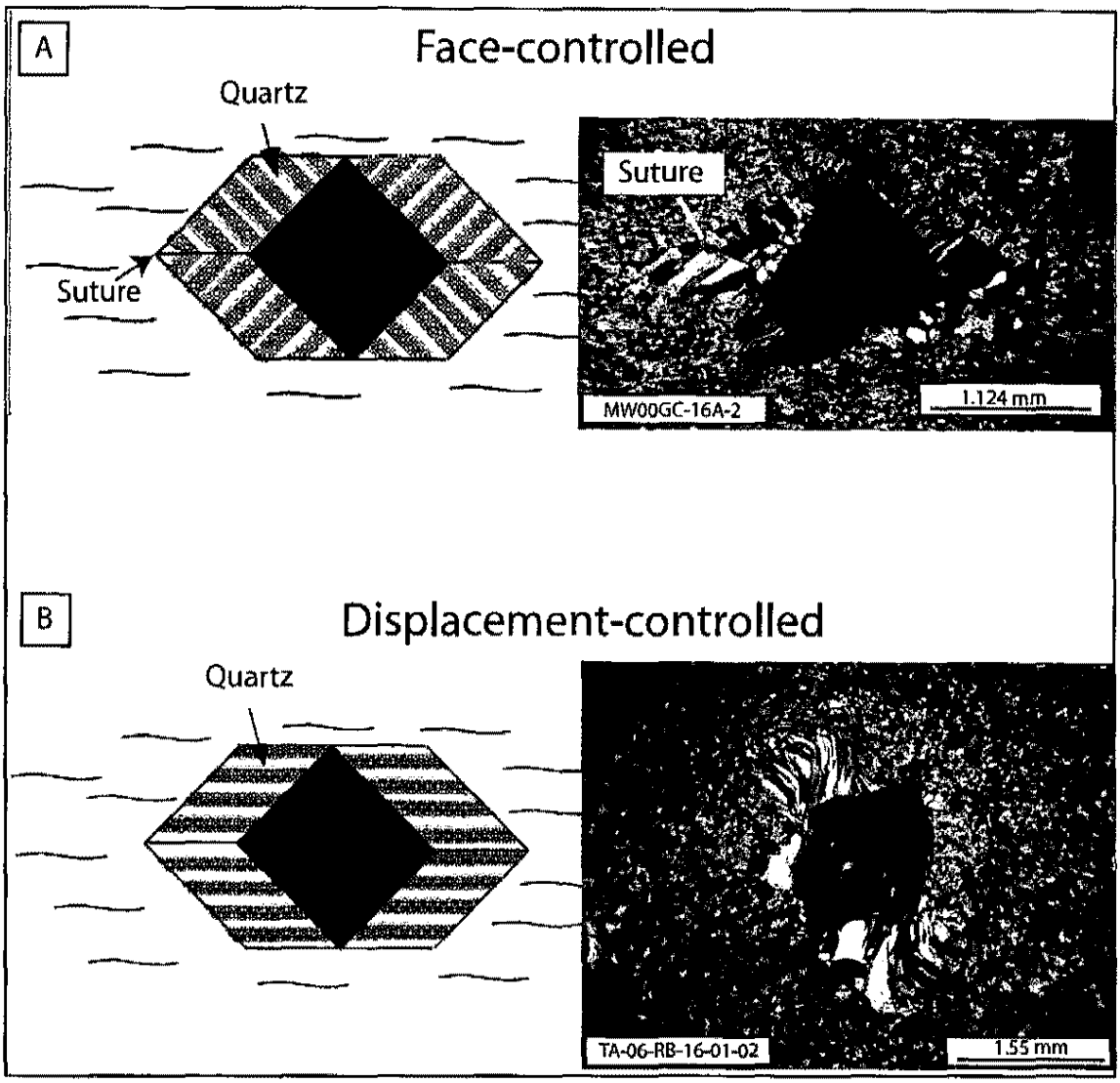

Figure 14. Photomicrographs for face-controlled fibers versus displacement-controlled fibers, showing geometric difference between the two types. A, face-controlled fibers form perpendicular to the face of the core object. Strain history cannot be determined by direction but can be determined from the suture, which records the progressive displacement history. B, displacement-controlled fibers grow parallel to the relative displacement between the matrix and the core object and are thought to record the incremental and finite strain history.

Figure 15. Figure showing the three principal planes of finite strain in relation to the strain fringes for Marble Peak and the Rosebud Creek ridge. Block diagrams represent the geometry and orientation of the strain fringes in this study. Curvatures for both D_1 and D_2 strain fringes within respective XY planes are shown with respect to L_1 elongation lineations.

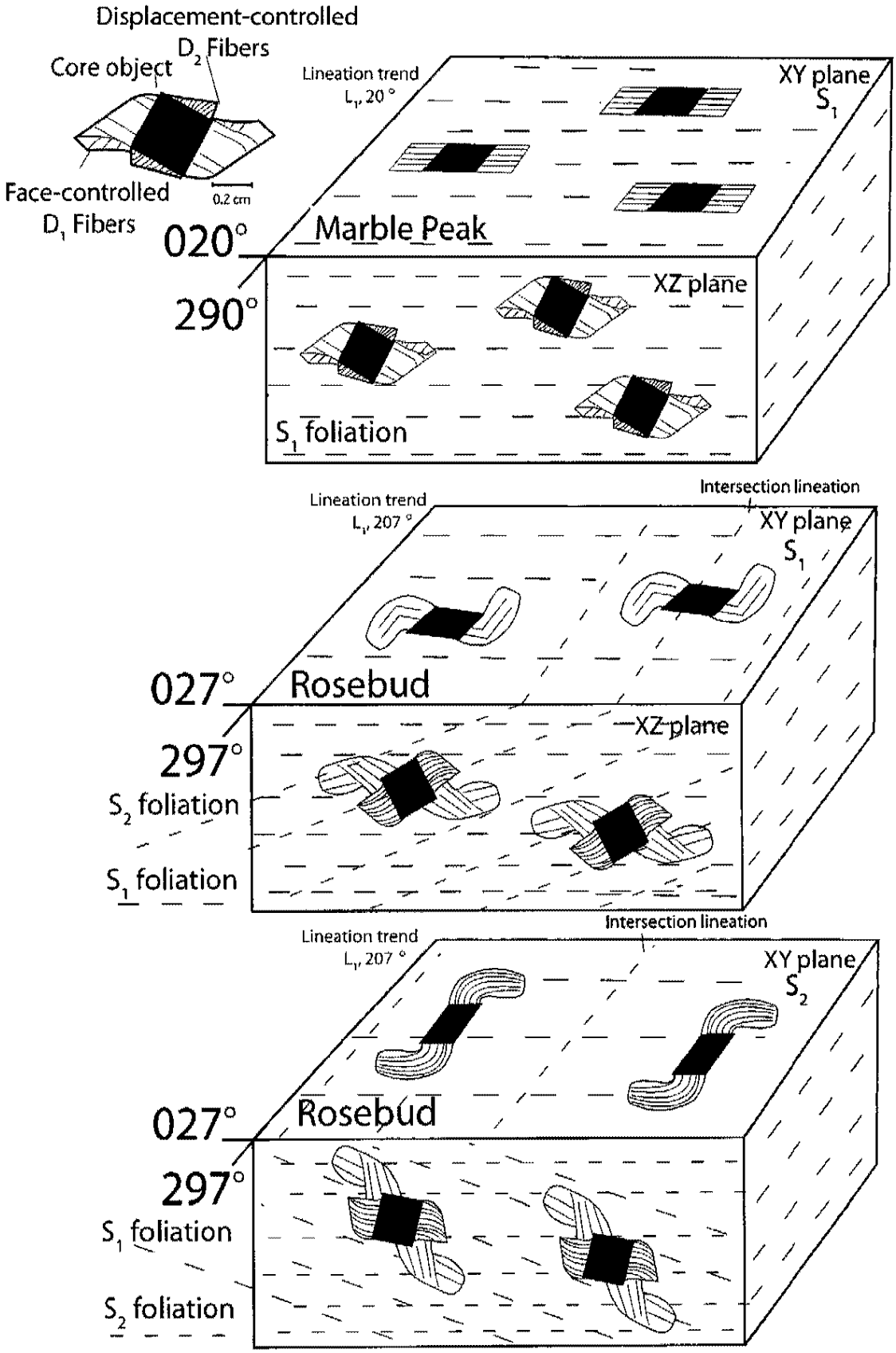
Displacement-controlled
D2 Fibers
Core object
Face-controlled
D1 Fibers
0.2 cm
Lineation trend
L1, 20 °
XY plane
S1
020°
Marble Peak
290°
XZ plane
S1 foliation
Intersection lineation
Lineation trend
L1, 207 °
XY plane
S1
027°
Rosebud
297°
XZ plane
S2 foliation
S1 foliation
Intersection lineation
Lineation trend
L1, 207 °
XY plane
S2
027°
Rosebud
297°
S1 foliation
S2 foliation

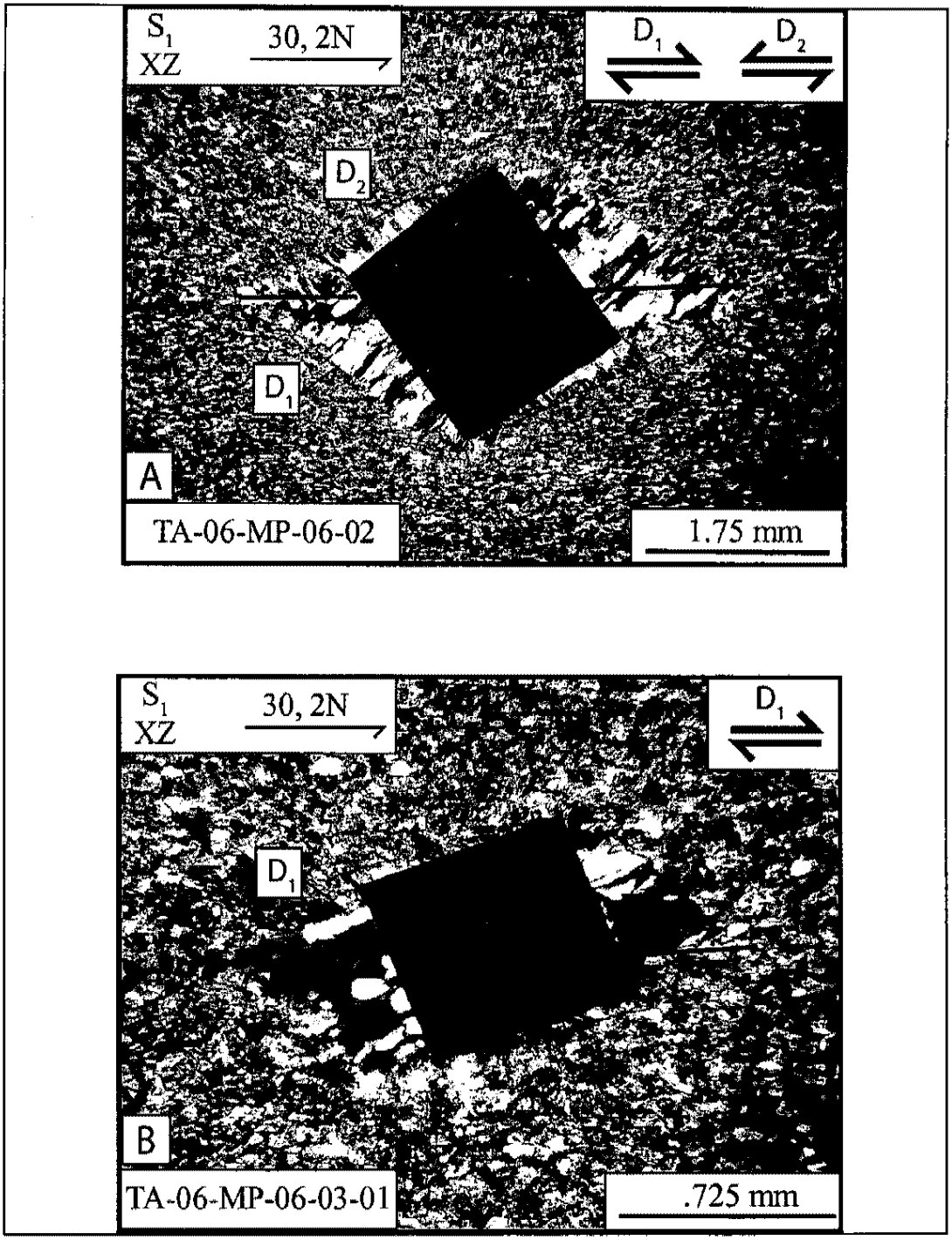

Figure 16. Photomicrograph A is showing both D_1 and D_2 strain fringes within the XZ plane of S_1 at Marble Peak. D_1 displays face-controlled fibers and D_2 exhibits displacement-controlled fibers. D_1 records top-to-the-north and D_2 records top-to-the-south shear sense. Photomicrograph B shows D_1 face-controlled fibers within the XZ plane of S_1 at Marble Peak. D_1 shear sense records top-to-the-north shear sense.

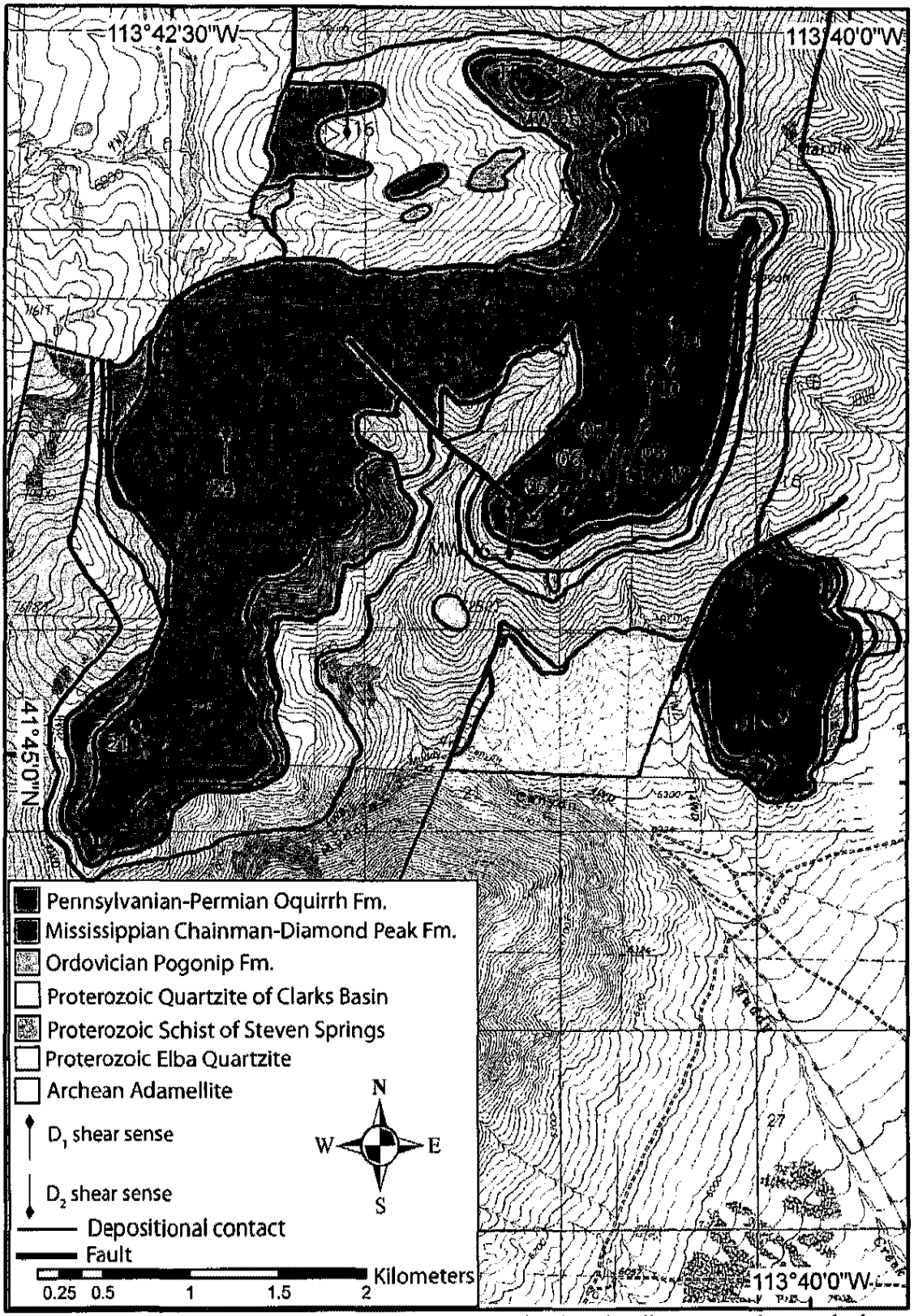

Figure 17. Simplified geologic map of Marble Peak, showing D_1 top-to-the-north shear sense and D_2 top-to-the-south shear sense. Southward shear sense from D_1 fibers was recorded within the Chainman-Diamond Peak Formation in the northern part of the map, overprinted by the D_2 deformation. Sample numbers are next to each arrow.

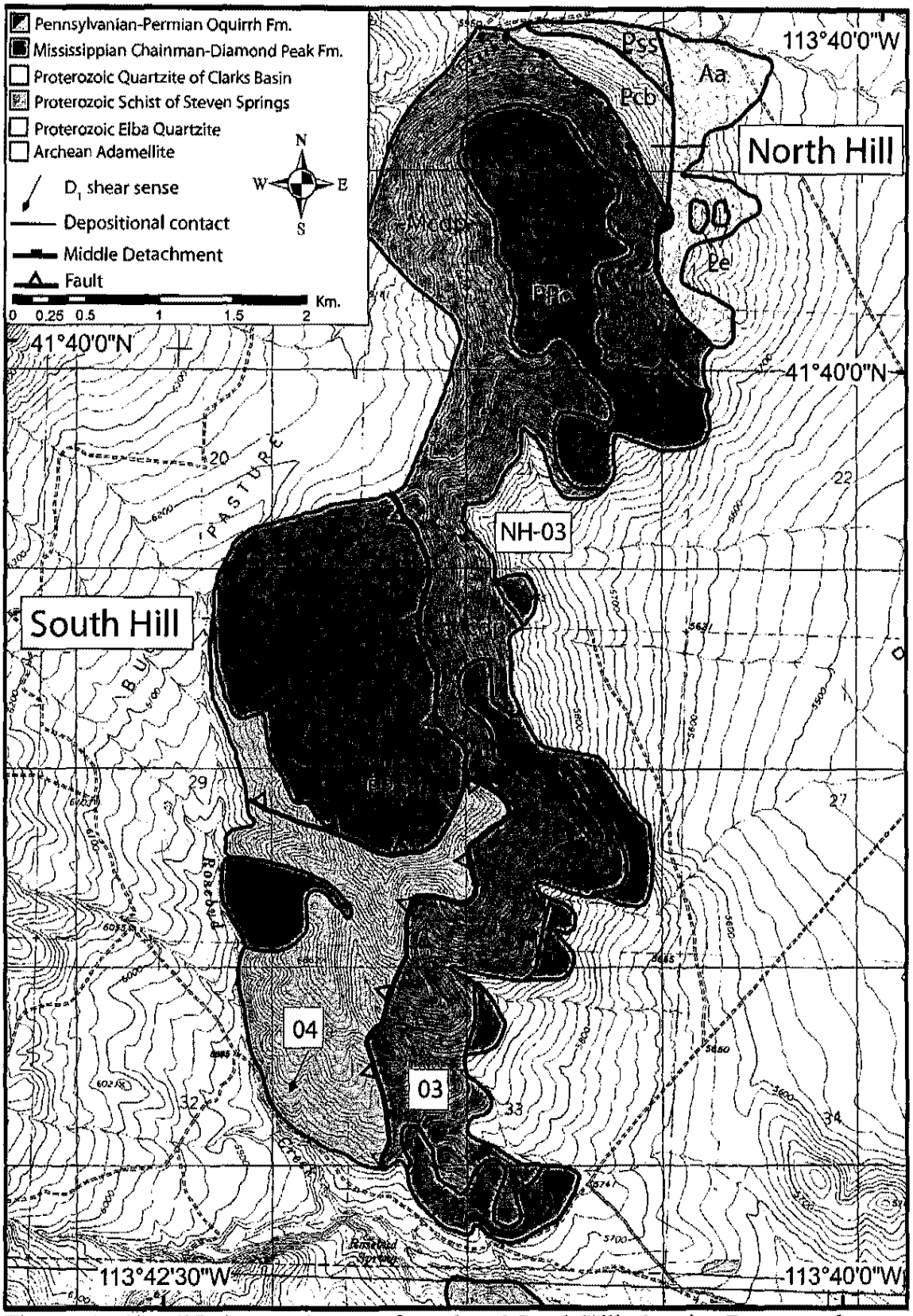

Figure 18. Simplified geologic map of North and South Hill, showing D_1 top-to-the-south shear sense. Shear sense is to the south in the overturned limb of the recumbent fold. Sample numbers are next to each arrow.

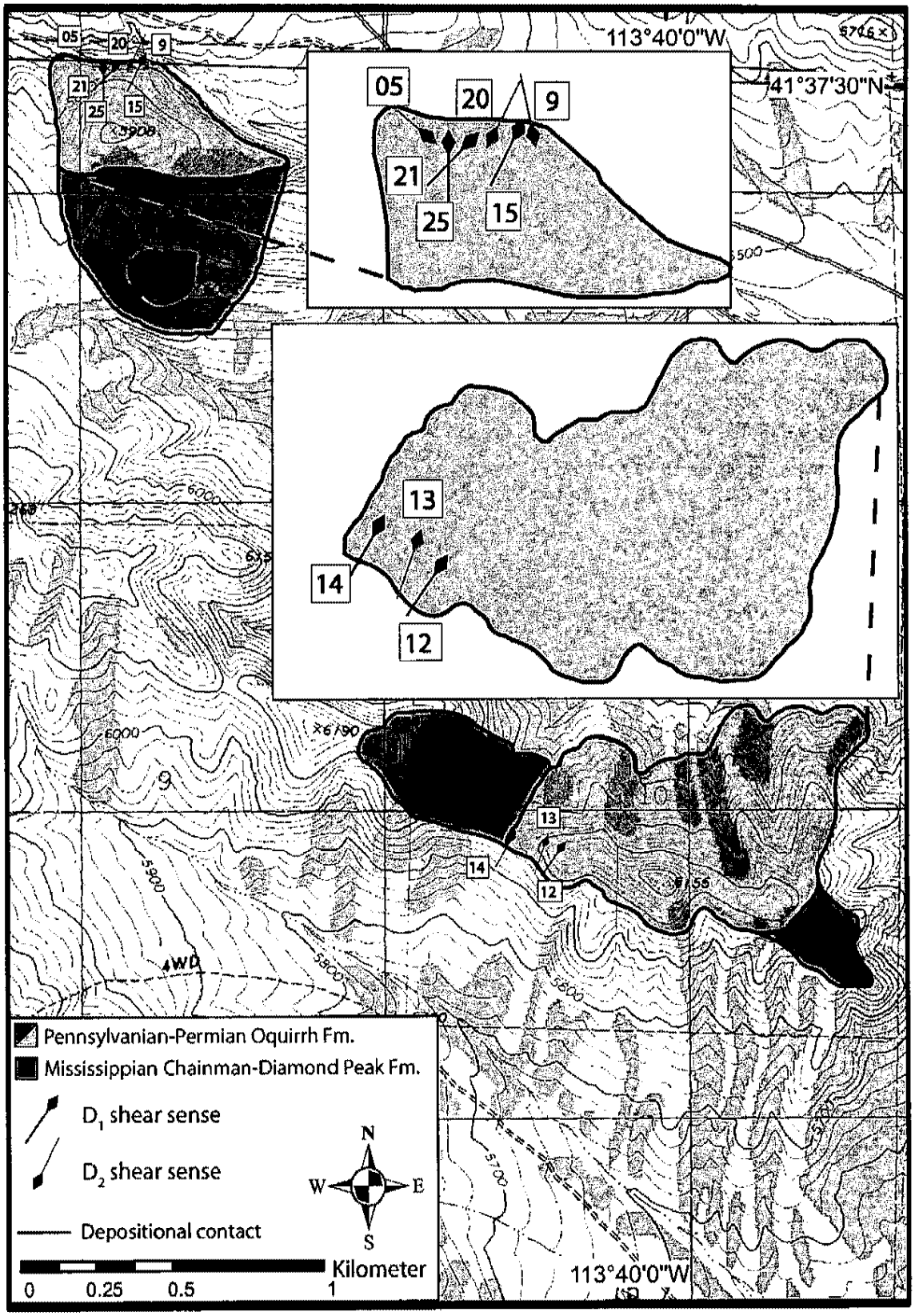

Figure 19. Simplified geologic map of Rosebud, showing D_1 top-to-the-north shear sense and D_2 top-to-the-south shear sense. Sample numbers are next to each arrow.

Figure 20. Photomicrographs illustrating the Rigid Fiber Model for incremental coaxial and object-center path method for non-coaxial strain fringes. A, showing how measurements for finite strain were made for the Rigid Fiber Model from photomicrographs. Total finite extension is derived by dividing the total length of the strain fringe (l_{sf}) structure by the diameter of the pyrite core object (D_{co}), multiplied by 100 to gain an extension percent. B and C, show how measurements were made for the object-center path method. The object-center path is determined by rotating a traced rigid core object along marginal points reproducing the natural fiber pattern from a photomicrograph. The center of the core object is plotted on each increment tracing the displacement path and showing the translation between the core object and the fringes. This method allows incremental and finite strains to be determined. See text for details.

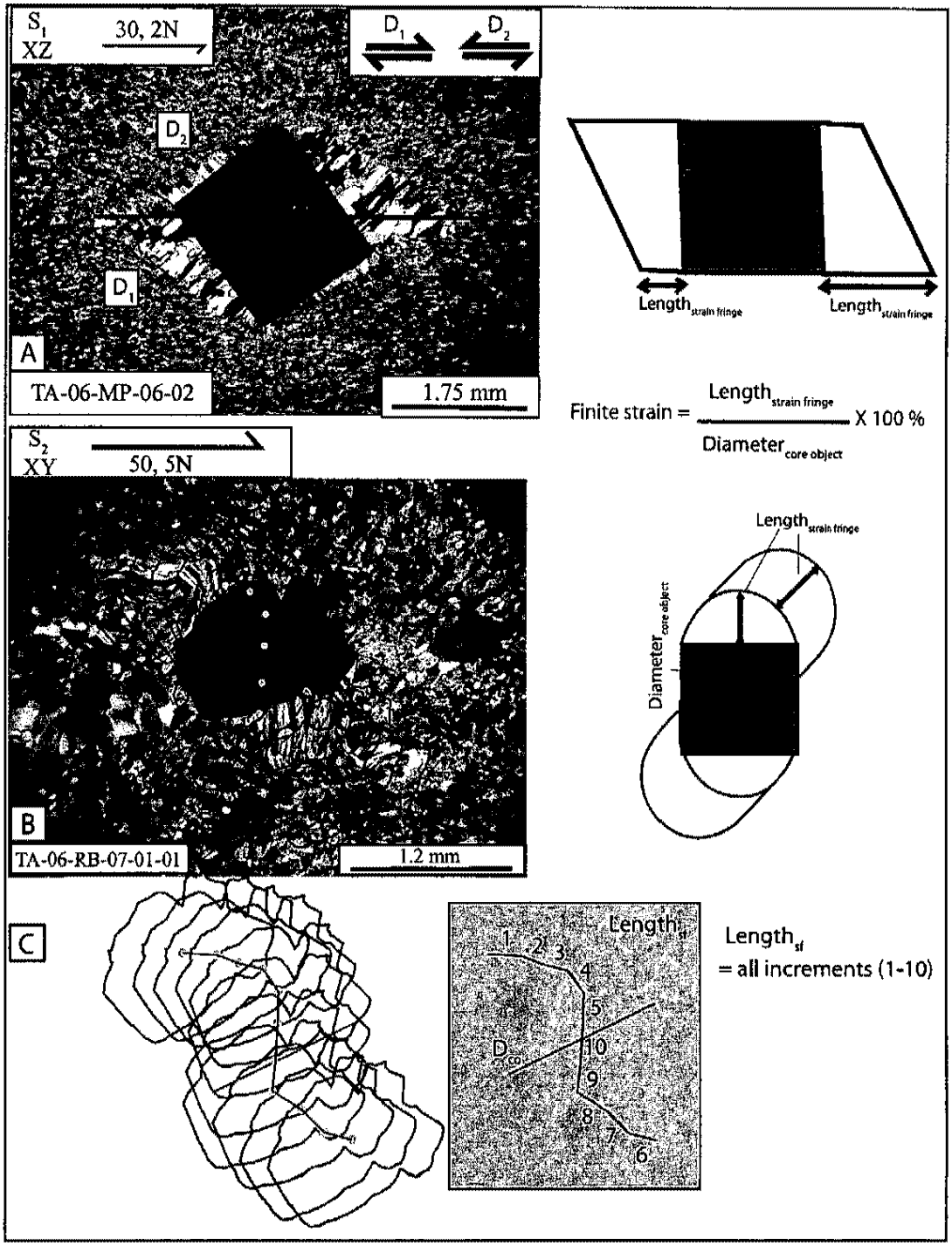
S1
XZ
30, 2N
D1
D2
D2
D1
A
TA-06-MP-06-02
1.75 mm
Length strain fringe
Length strain fringe
Finite strain = Length strain fringe / Diameter core object X 100 %
S2
XY
50, 5N
B
TA-06-RB-07-01-01
1.2 mm
Length strain fringe
Diameter core object
C
Length sf
1
2
3
4
5
6
7
8
9
10
D co
Length sf
= all increments (1-10)

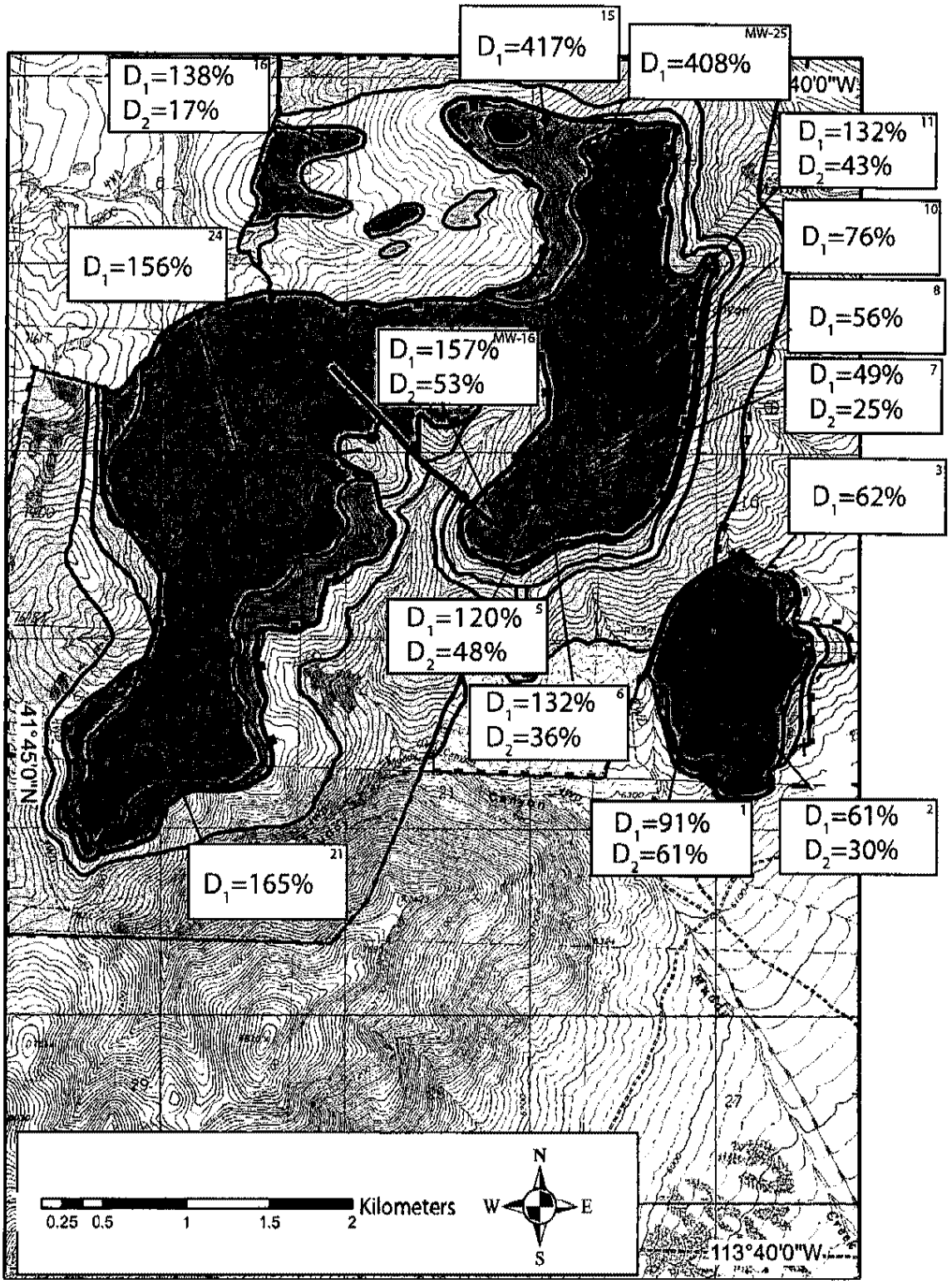

Figure 21. Finite strain map of D_1 and D_2 deformation for Marble Peak. Sample numbers are in the upper right hand corner of each rectangle.

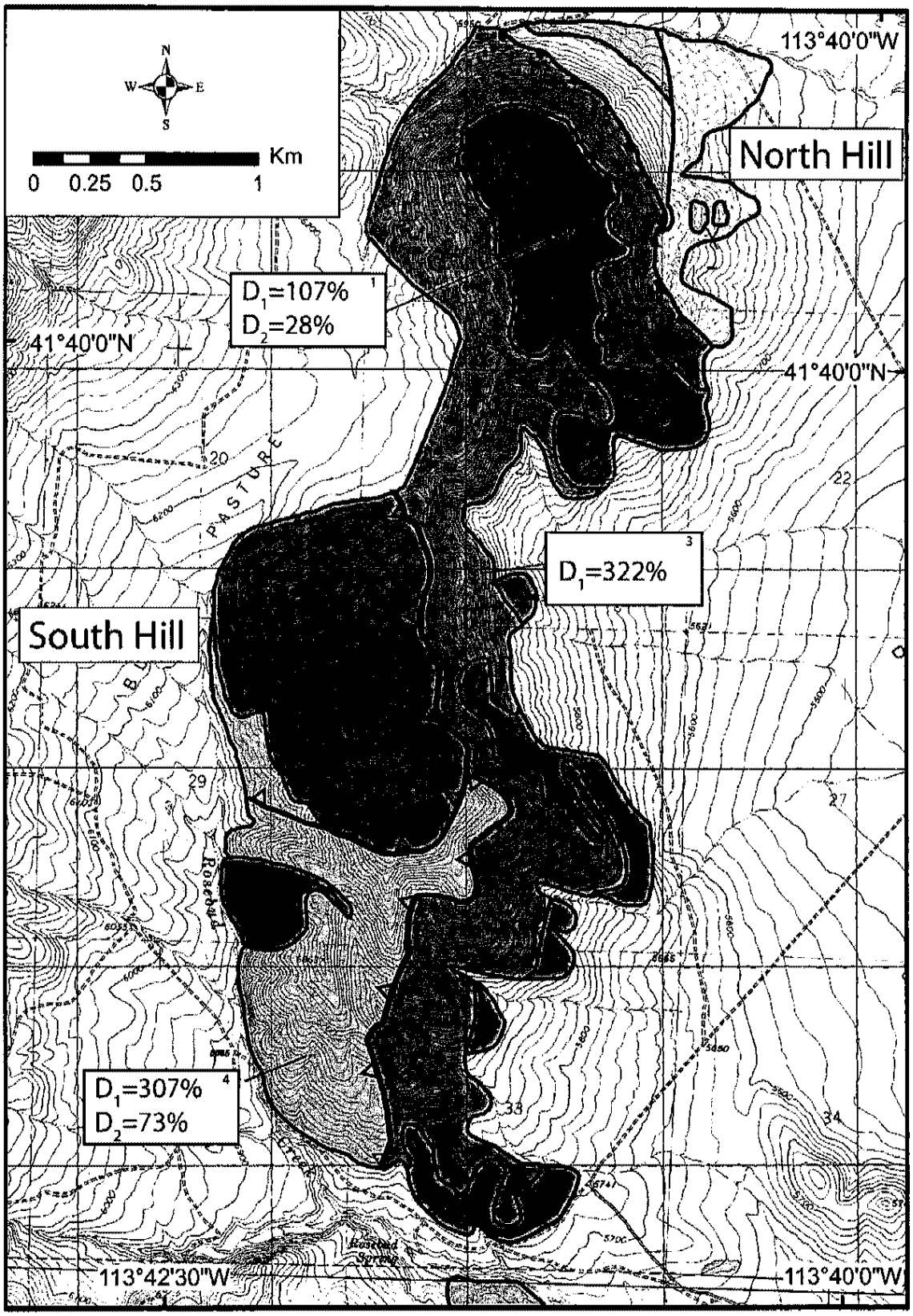

Figure 22. Finite strain map for D_1 and D_2 deformation for North and South Hill. Sample numbers are in the upper right hand corner of each rectangle.

Figure 23. Finite strain map of D_1 and D_2 deformation for the Rosebud area. Sample numbers are in the upper right hand corner of each rectangle. Dashed box indicates enlarged area.

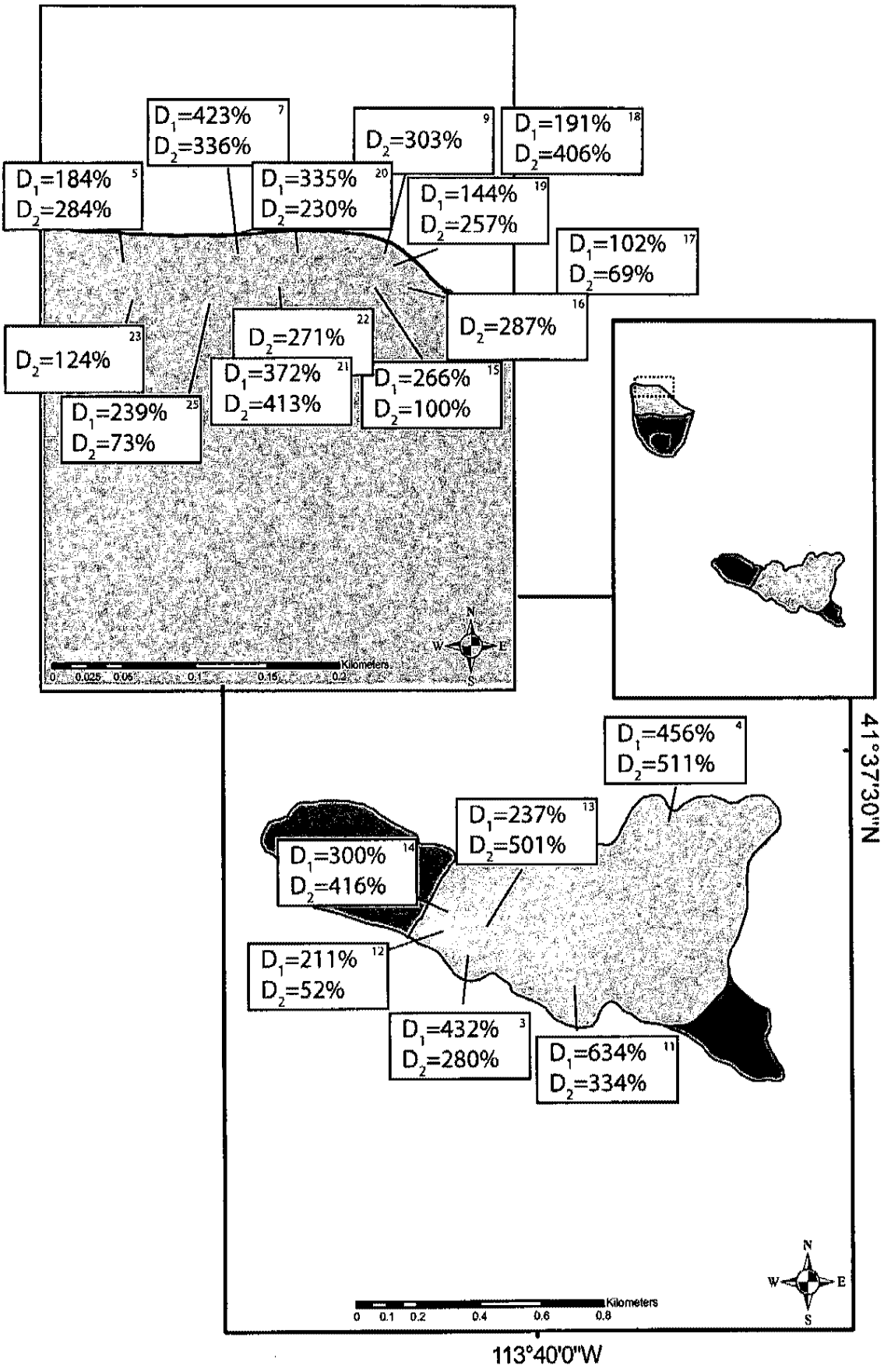
D1=423% 7
D2=336%
D2=303% 9
D1=191% 18
D2=406%
D1=184% 5
D2=284%
D1=335% 20
D2=230%
D1=144% 19
D2=257%
D1=102% 17
D2=69%
D2=287% 16
D2=124% 23
D2=271% 22
D1=372% 21
D2=413%
D1=266% 15
D2=100%
D1=239% 25
D2=73%
N
W
E
S
0 0.025 0.05 0.1 0.15 0.2 Kilometers
D1=456% 4
D2=511%
D1=237% 13
D2=501%
D1=300% 14
D2=416%
D1=211% 12
D2=52%
D1=432% 3
D2=280%
D1=634% 11
D2=334%
0 0.1 0.2 0.4 0.6 0.8 Kilometers
41°37'30"N
113°40'0"W

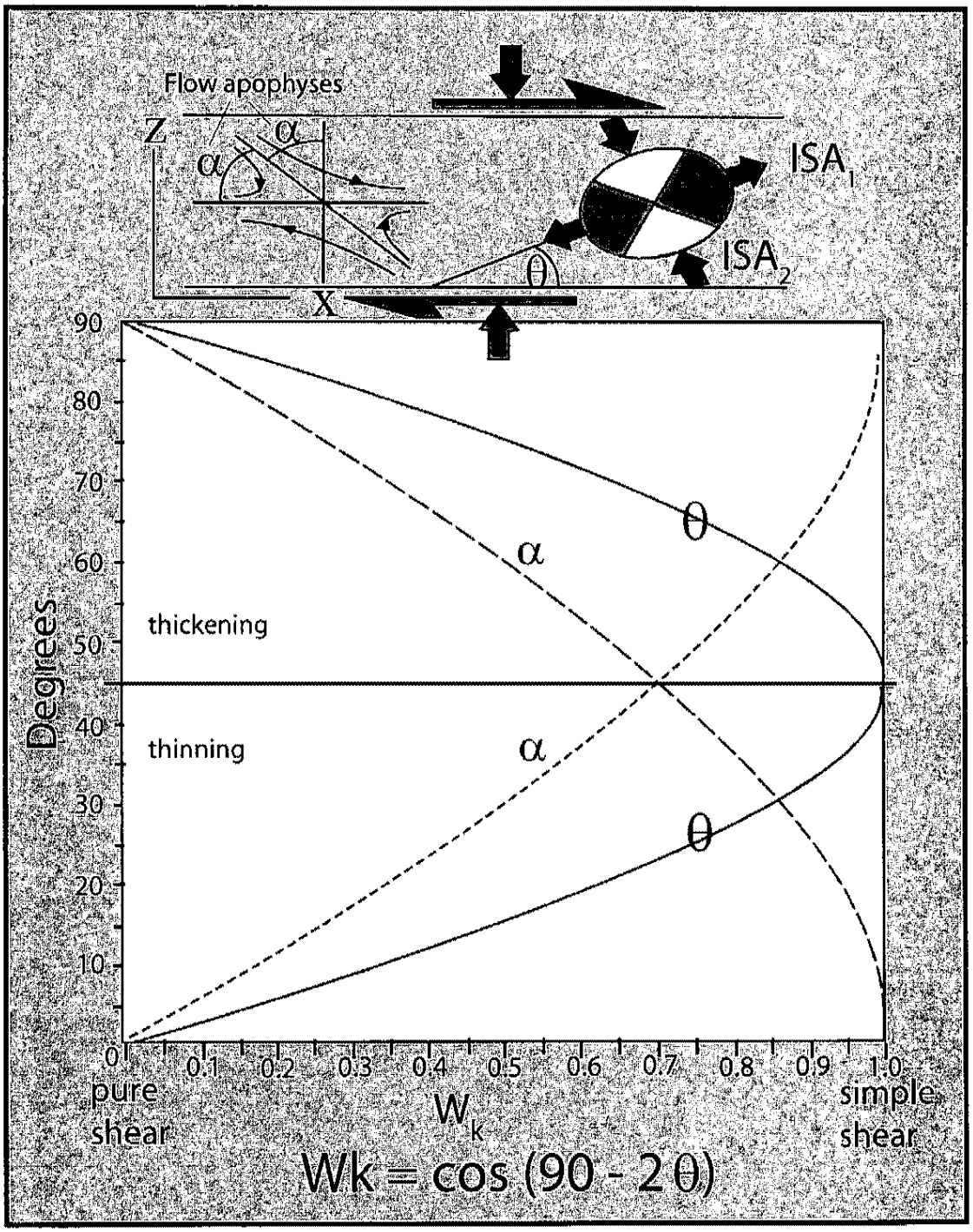

Figure 24. Diagram illustrating the relationship between W_k with the flow apophyses and the orientation of the instantaneous stretching axes. Theta defines the angle between the deformation zone boundary and the instantaneous stretching axis. Theta angles between 0° and 45° record a thinning shear zone, and angles greater than 45° record a thickening shear zone. Alpha is the acute angle between the flow apophyses and the shear plane. Modified from Tikoff and Fossen, 2001.

Figure 25a-b. Photomicrographs illustrating measurements used for vorticity analysis for the D_1 face-controlled strain fringes. Theta measurements, determined as the angle between the sutures (red line) and S_1, reflect the displacement path with respect to S_1 foliation (blue line). Last increment of suture records the approximate orientation of the maximum instantaneous stretching axis. Kinematic vorticity number is determined by $W_k = \cos(90\text{-}2\text{theta})$.

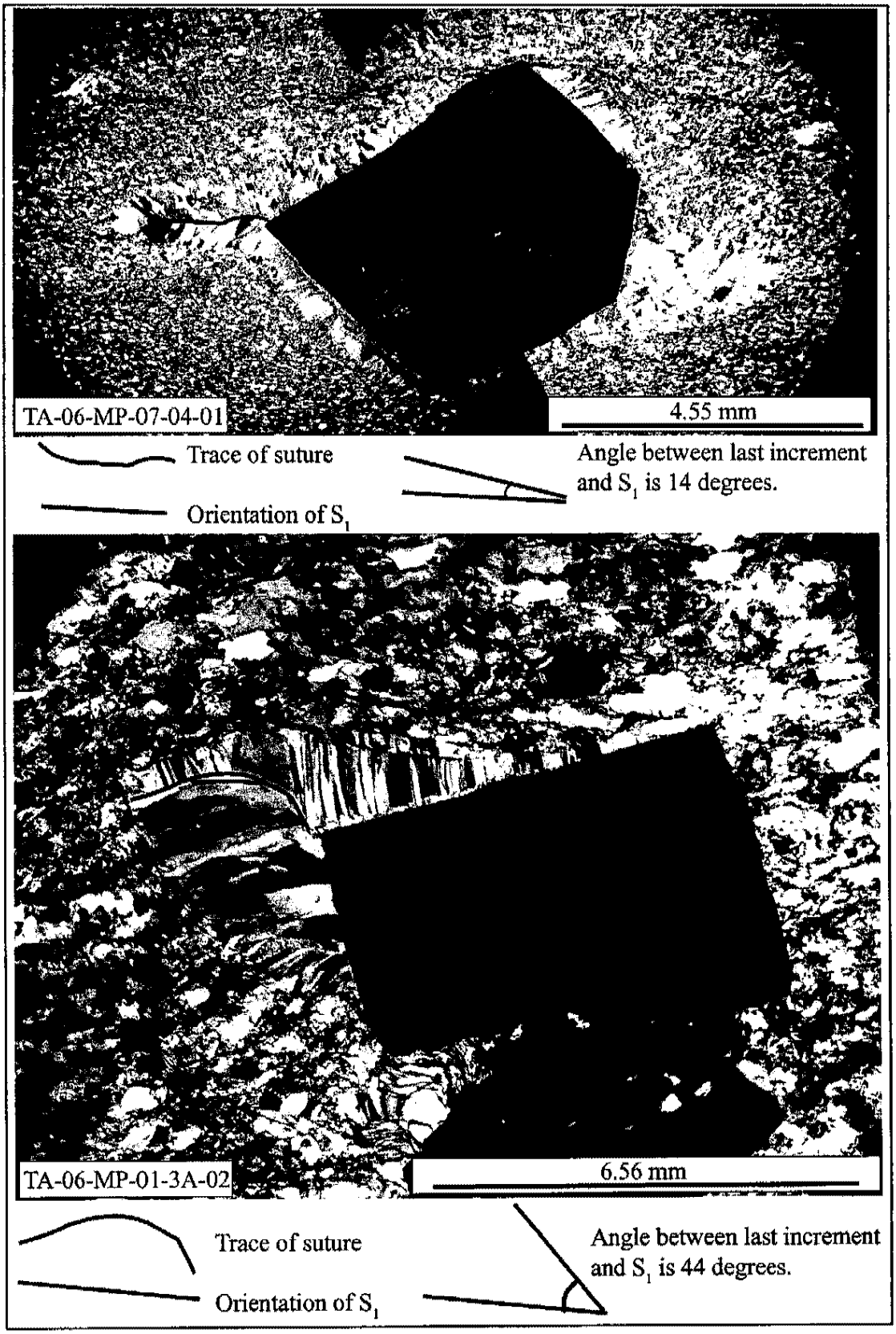
TA-06-MP-07-04-01
4.55 mm
Trace of suture
Angle between last increment and S_1 is 14 degrees.
Orientation of S_1
TA-06-MP-01-3A-02
6.56 mm
Trace of suture
Angle between last increment and S_1 is 44 degrees.
Orientation of S_1

Figure 25a.

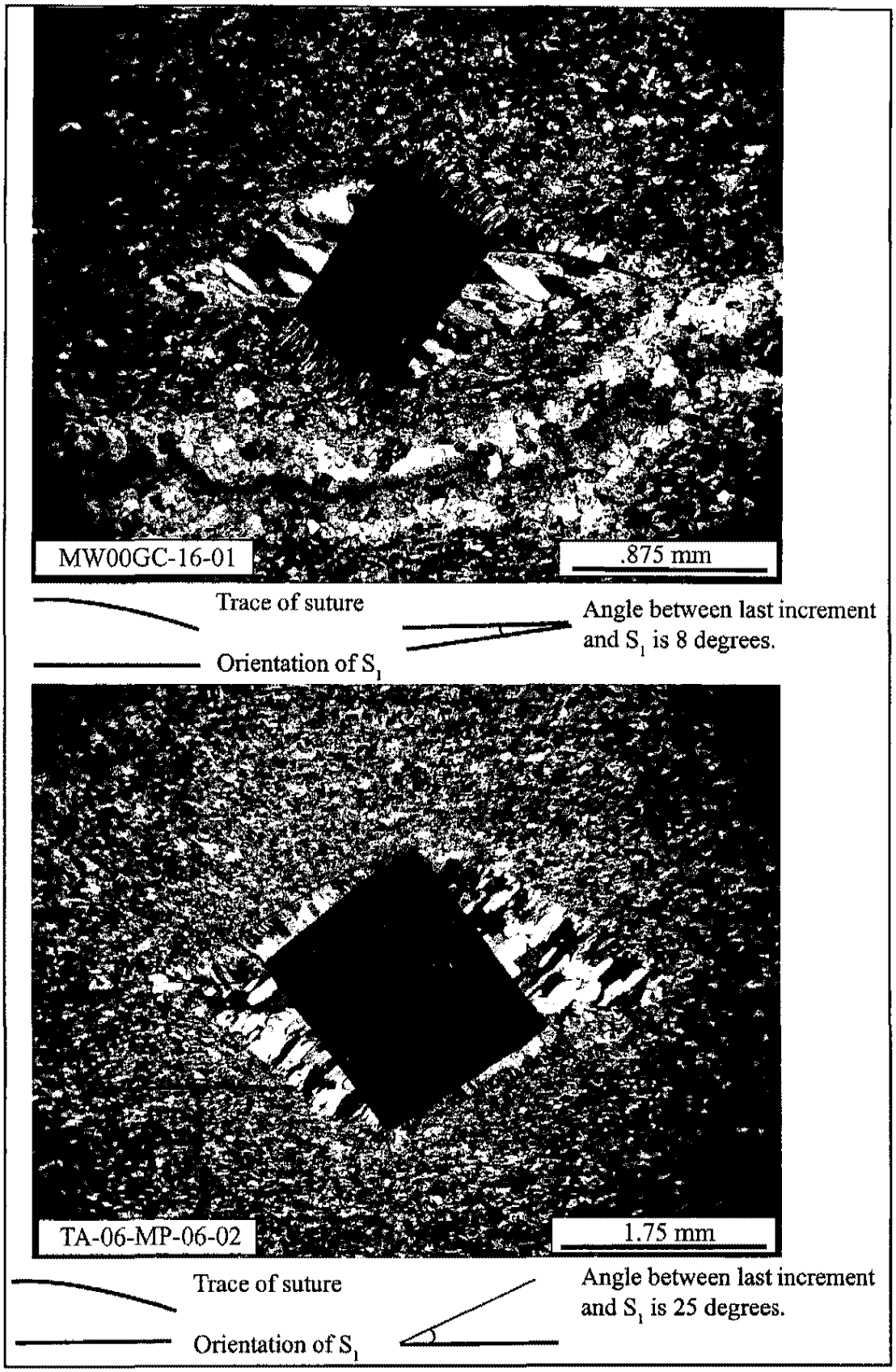
MW00GC-16-01
.875 mm
Trace of suture
Orientation of S_1
Angle between last increment and S_1 is 8 degrees.
TA-06-MP-06-02
1.75 mm
Trace of suture
Orientation of S_1
Angle between last increment and S_1 is 25 degrees.

Figure 25b.

Figure 26. Photomicrographs of D_1 strain fringes within the XY plane at Rosebud area. Red lines represent the proximal parts (younger) and green lines represent the distal parts (older) of the D_1 strain fringes. A, distal parts (older) of the strain fringe record an orientation of 326 and the proximal parts (younger) record an orientation of 047, recording a clockwise orientation of infinitesimal strain. B, distal parts (older) record an orientation of 311 and 024, recording a clockwise orientation of infinitesimal strain. C, distal parts (older) record an orientation of 326 and 027, recording a clockwise orientation of infinitesimal strain. The scale is in the right hand corner of each sample, and the sample number is in the lower left hand corner.

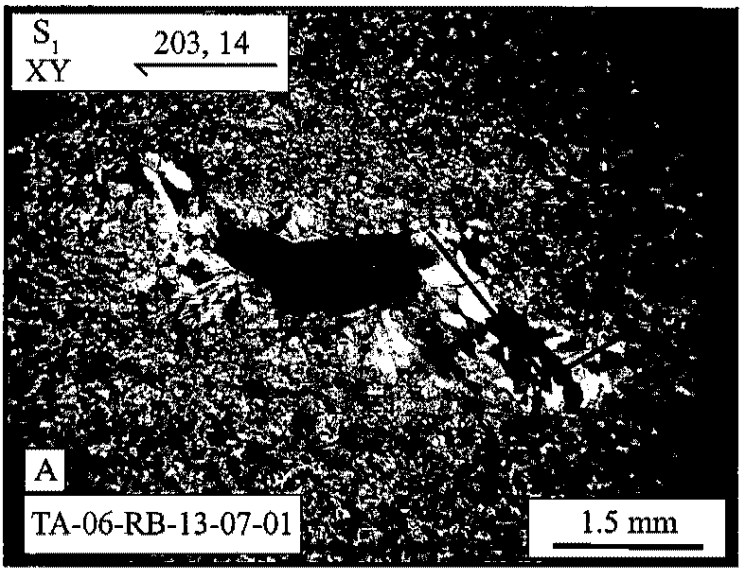
S1
XY
203, 14
A
TA-06-RB-13-07-01
1.5 mm

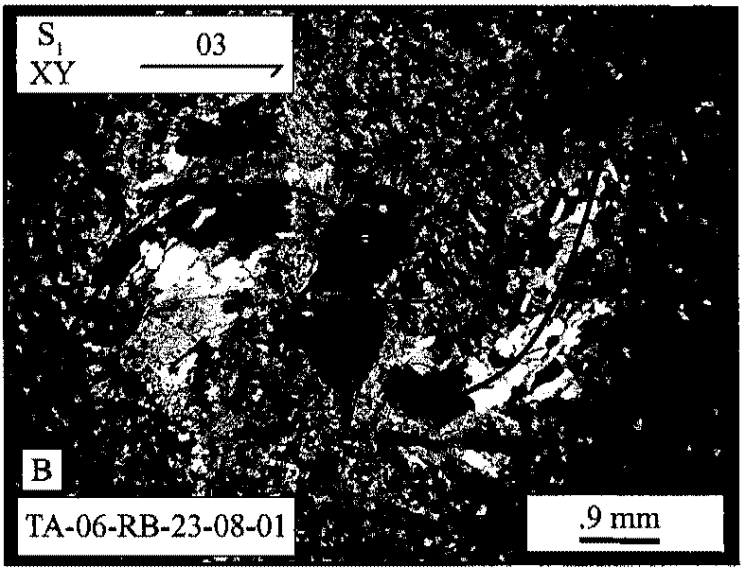
S1
XY
03
B
TA-06-RB-23-08-01
.9 mm

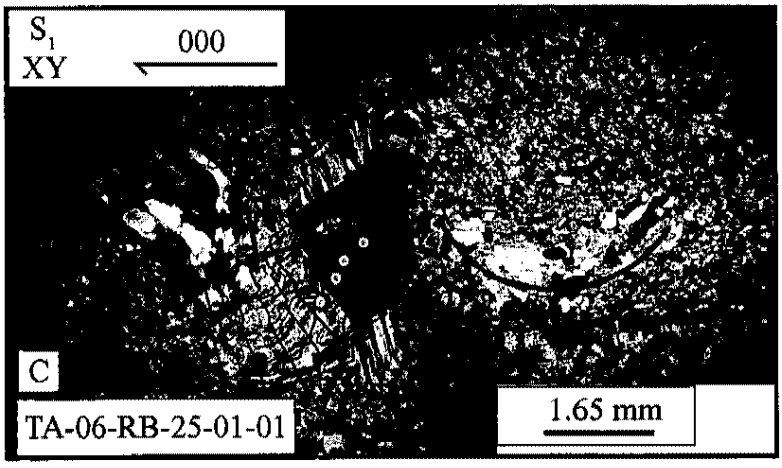
S1
XY
000
C
TA-06-RB-25-01-01
1.65 mm

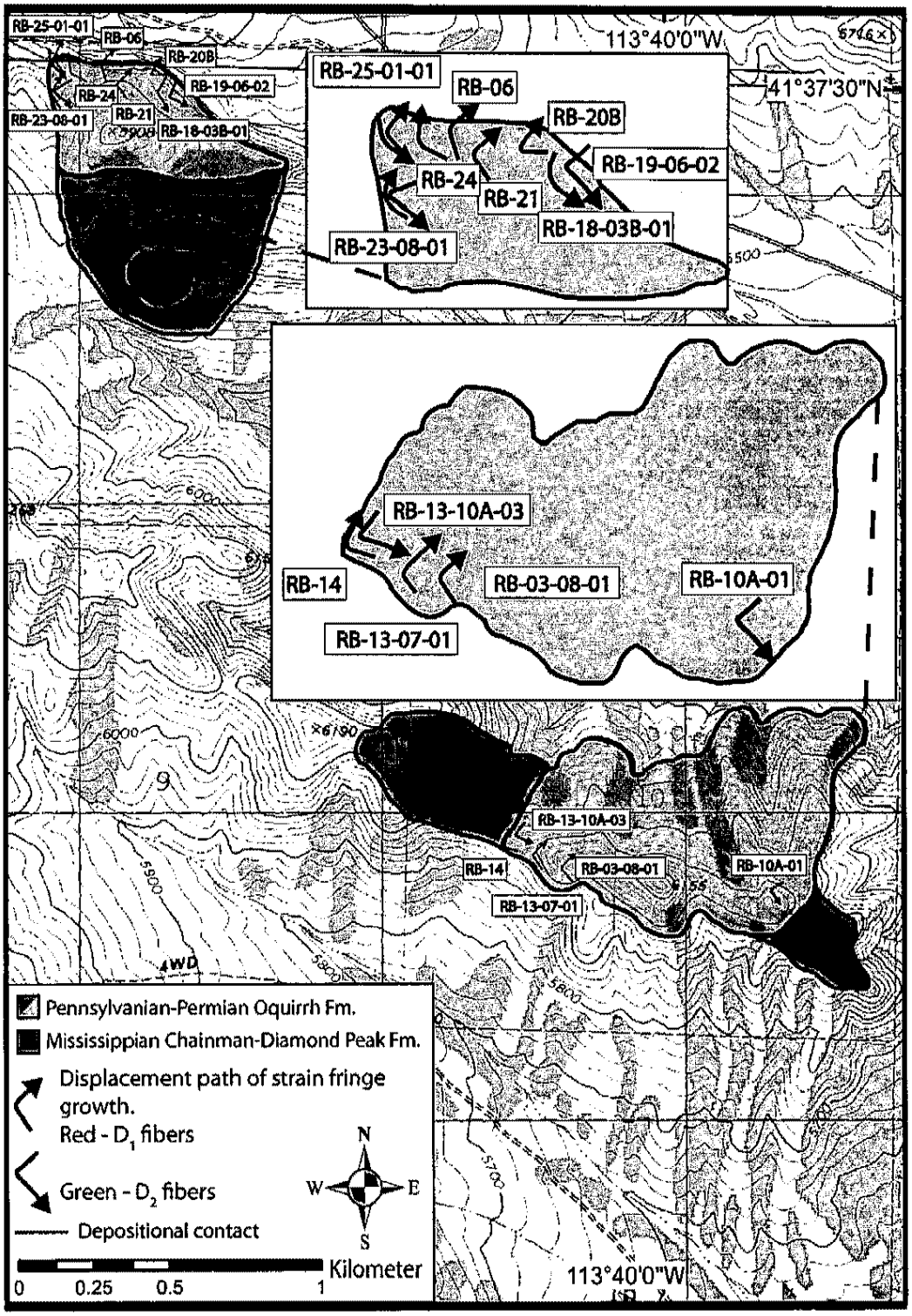

Figure 27. Geologic map of Rosebud area showing displacement paths for D_1 and D_2 strain fringes within the XY plane of S_1 and S_2 respectively. The displacement path for D_1, in red, records a clockwise change in the maximum stretch direction through time. The displacement path for D_2, in green, records a counter-clockwise rotation.

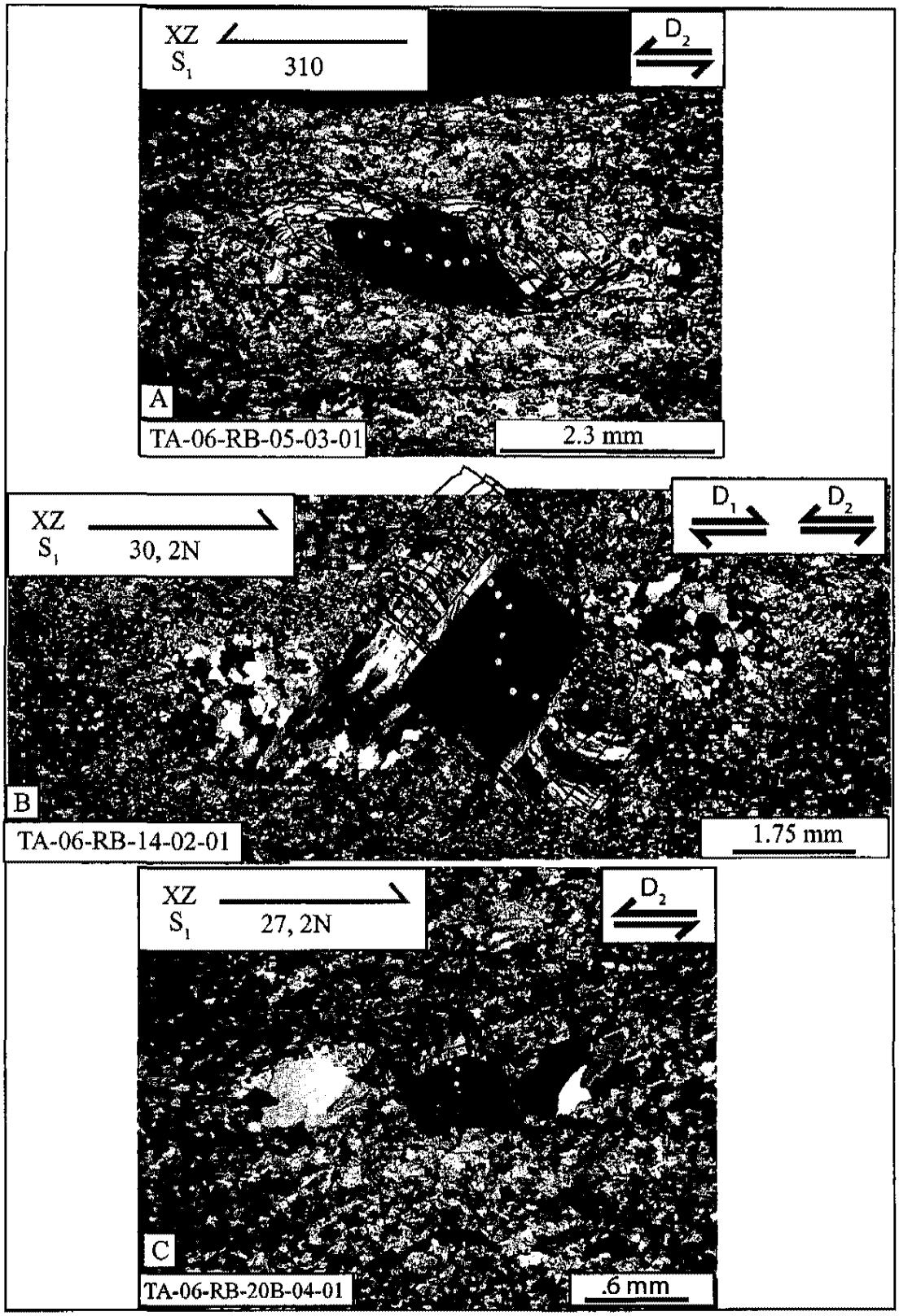

Figure 28. Photomicrographs showing how the object-center path method was used to determine the finite and incremental strain. Yellow dots represent the center of the core object and trace the translation and rotational paths used for measuring the incremental and finite strain. See text for details.

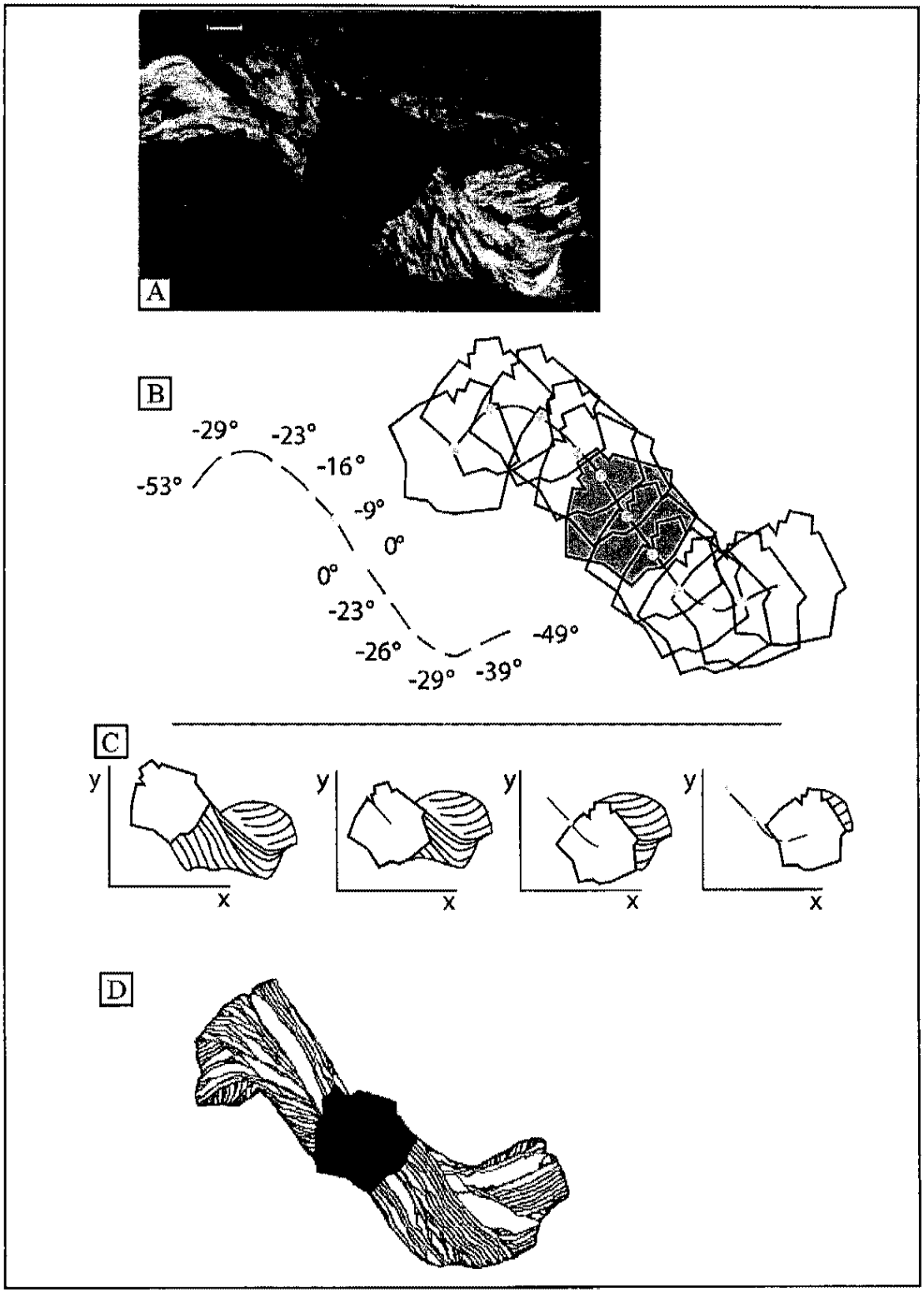

Figure 29. Figure from Koehn et al. (2000) showing how increments of translation and rotation were measured from photomicrograph A and figure B and inputted into the "Fringe Growth" program shown in C. D represents the final outcome of the modeling to reproduce the strain fringe in A, using the object-center path method. See text for details.

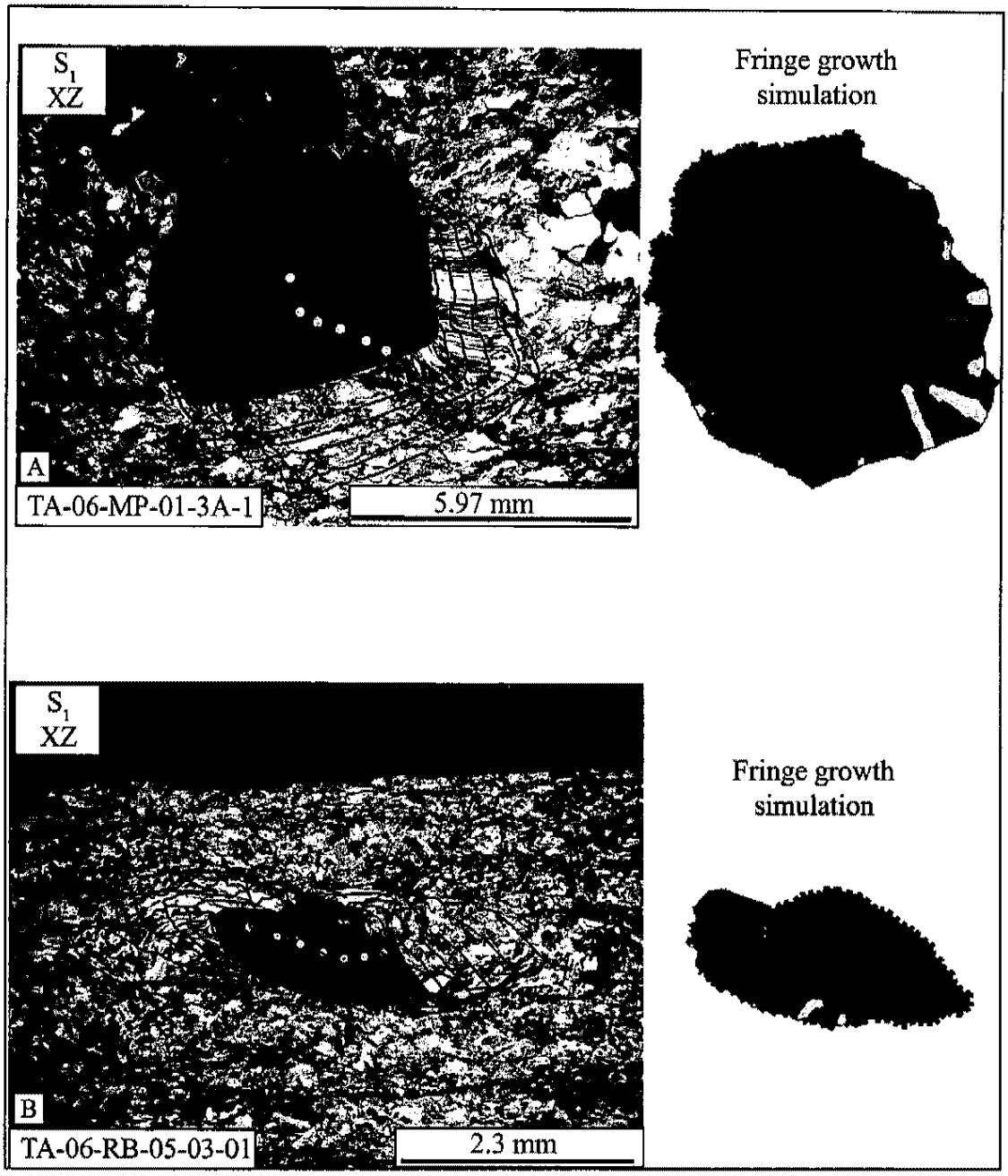

Figure 30a-c. Simulations of fibrous strain fringes conducted using the "Fringe Growth" program to substantiate the object-center path method, which was used to measure the incremental and finite strain. Translations and rotations were measured from photomicrographs in ImageJ and inputted into "Fringe Growth". Pre-defined shapes were used in the program. Principal planes are in upper left corner of each photomicrograph.

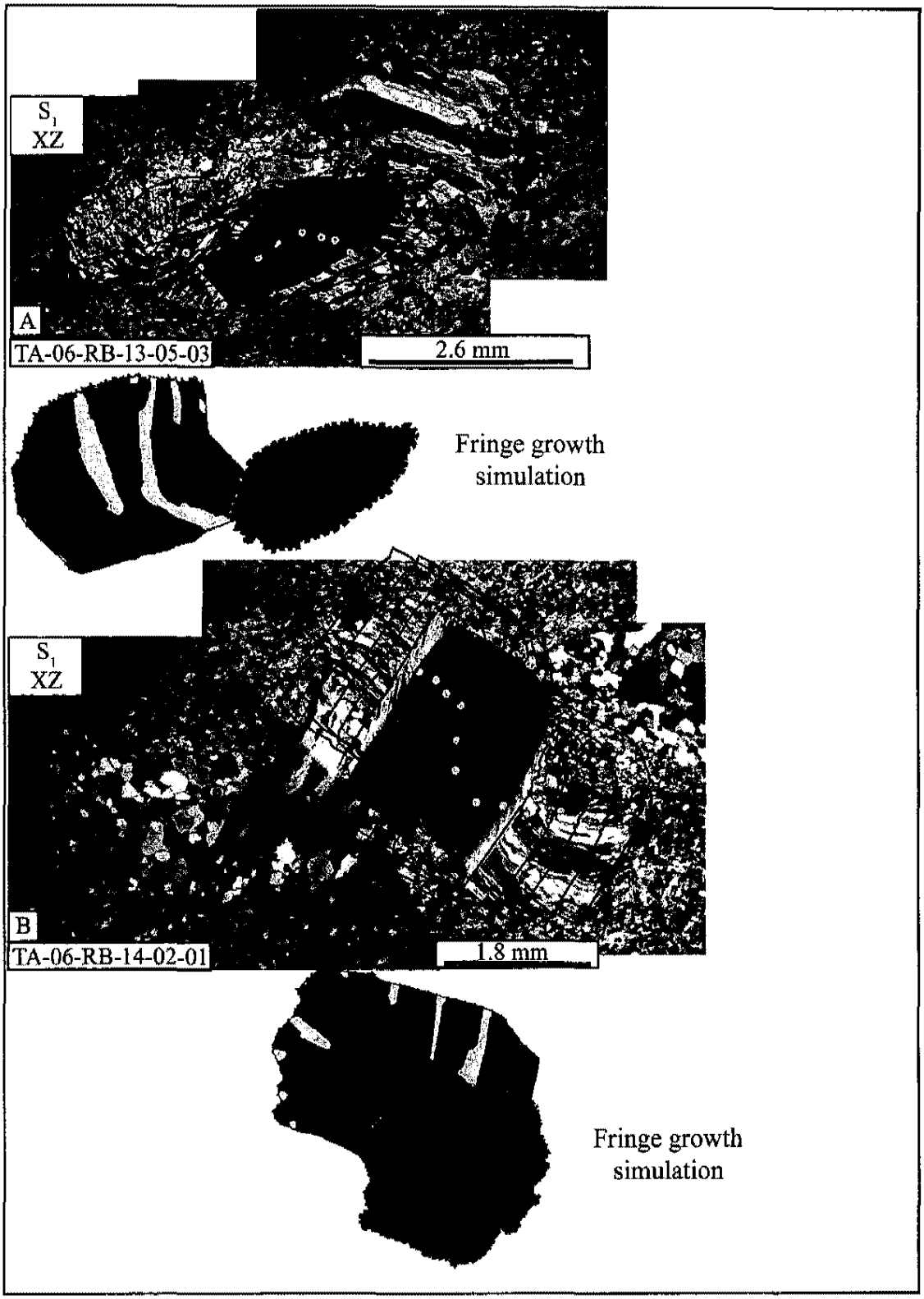
S1
XZ
A
TA-06-RB-13-05-03
2.6 mm
Fringe growth
simulation
S1
XZ
B
TA-06-RB-14-02-01
1.8 mm
Fringe growth
simulation

Figure 30b.

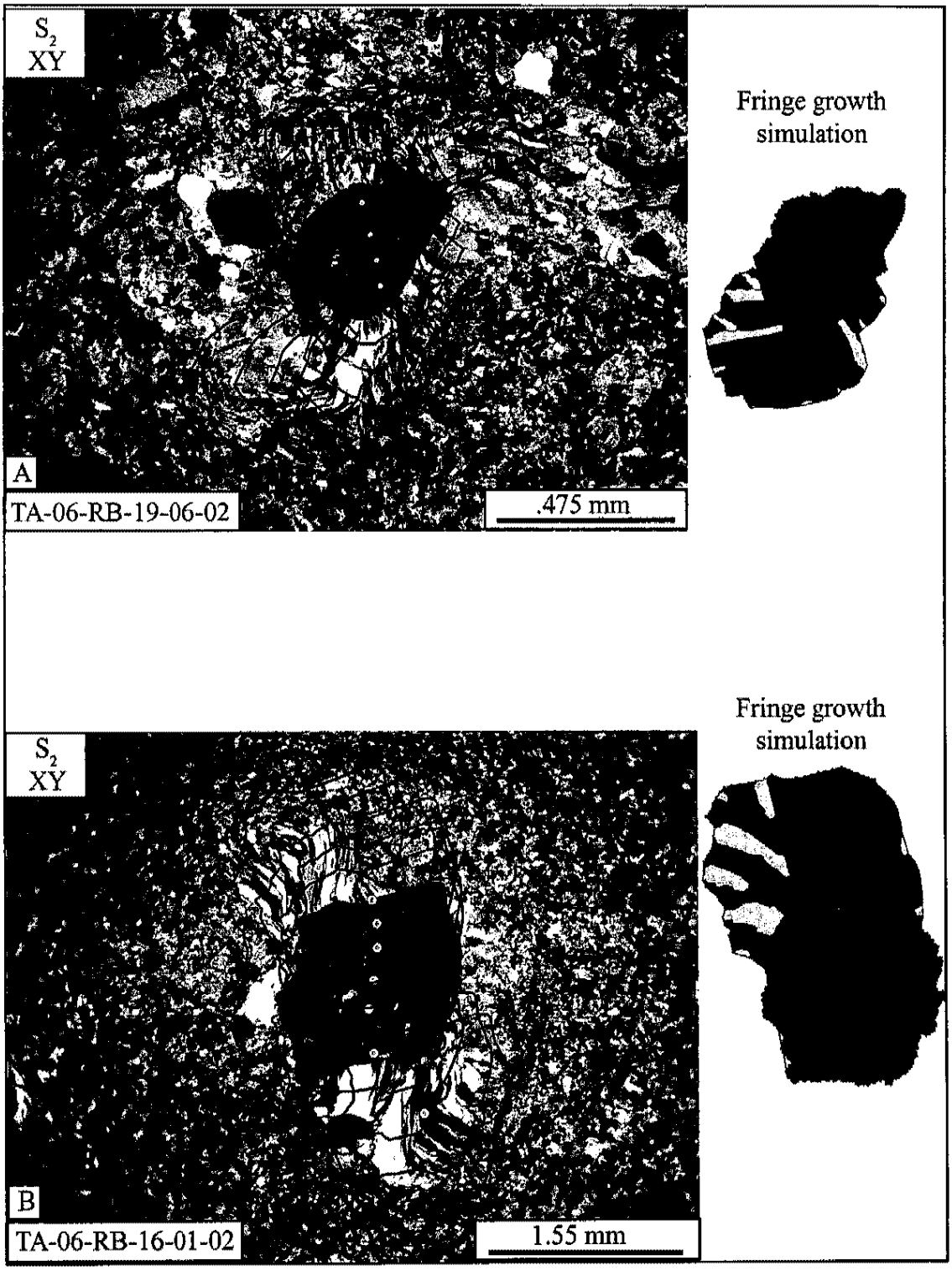
S2
XY
A
TA-06-RB-19-06-02
.475 mm
Fringe growth
simulation
S2
XY
B
TA-06-RB-16-01-02
1.55 mm
Fringe growth
simulation

Figure 30c

Figure 31. Cumulative incremental strain history diagrams for D_2 within the XZ plane of S_1 for the folds at the northwest section of the map at Rosebud area. CISH diagrams illustrate strain (y axis) relative to the changes of the orientation of the incremental extension direction from the horizontal reference frame (x axis). Graphs depict the extension versus orientation with respect to a horizontal reference frame (S_2). Reference frame for all measurements is a view looking west with north to the right. Therefore, clockwise rotation on the graphs are positive and counter-clockwise are negative. Slope represents the amount of external vorticity. Vertical paths represent coaxial deformation, and horizontal paths represent non-coaxial deformation.

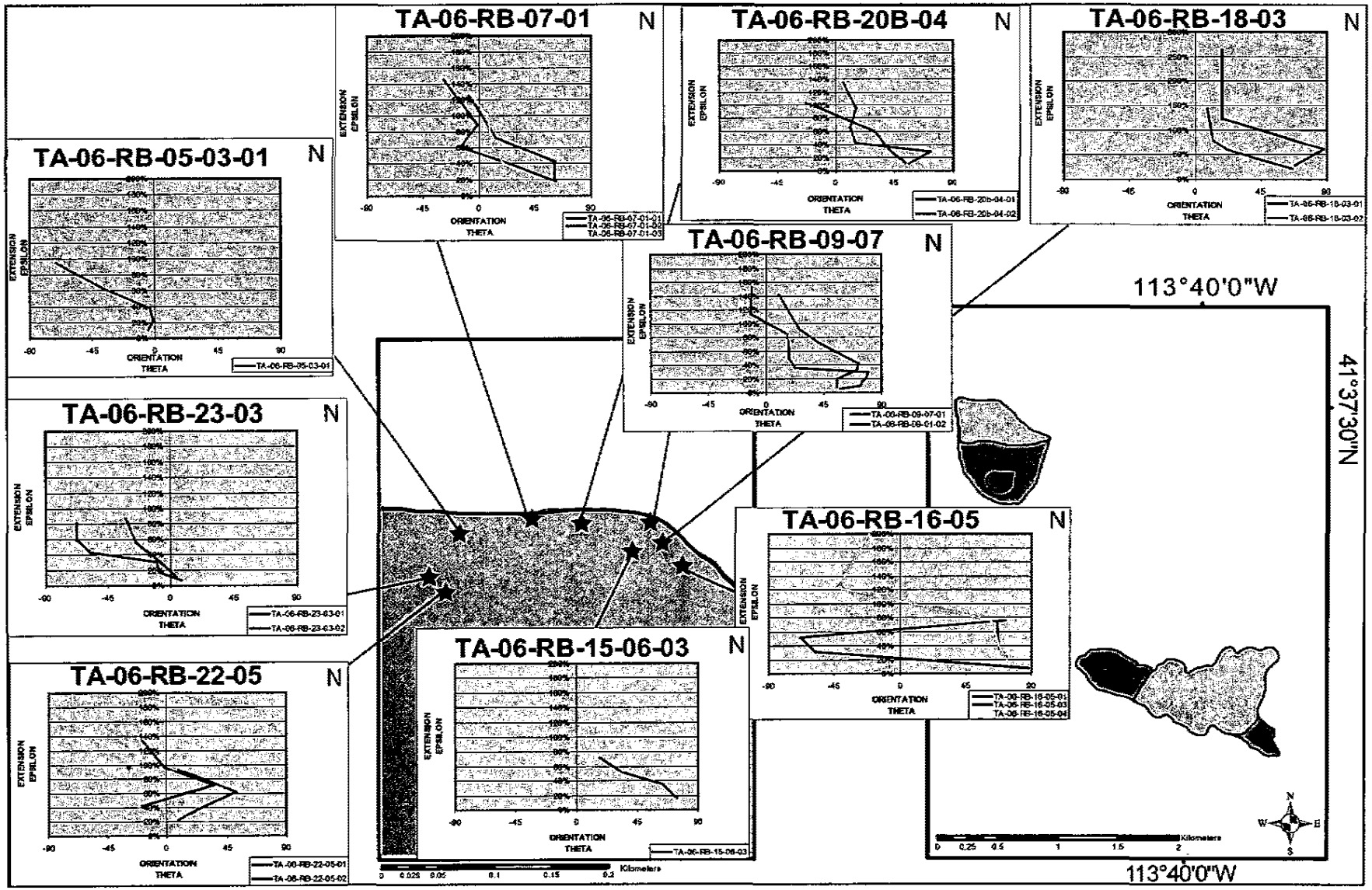
TA-06-RB-07-01
N
TA-06-RB-20B-04
N
TA-06-RB-18-03
N
TA-06-RB-05-03-01
N
TA-06-RB-09-07
N
113°40'0"W
41°37'30"N
TA-06-RB-23-03
N
TA-06-RB-16-05
N
TA-06-RB-15-06-03
N
TA-06-RB-22-05
N
EXTENSION EPSILON
ORIENTATION THETA
Kilometers
113°40'0"W

Figure 31. Cumulative incremental strain history diagrams for D_2 within the XZ plane of S_1 for the folds at the northwest section of the map at Rosebud area. CISH diagrams illustrate strain (y axis) relative to the changes of the orientation of the incremental extension direction from the horizontal reference frame (x axis). Graphs depict the extension versus orientation with respect to a horizontal reference frame (S_2). Reference frame for all measurements is a view looking west with north to the right. Therefore, clockwise rotation on the graphs are positive and counter-clockwise are negative. Slope represents the amount of external vorticity. Vertical paths represent coaxial deformation, and horizontal paths represent non-coaxial deformation.

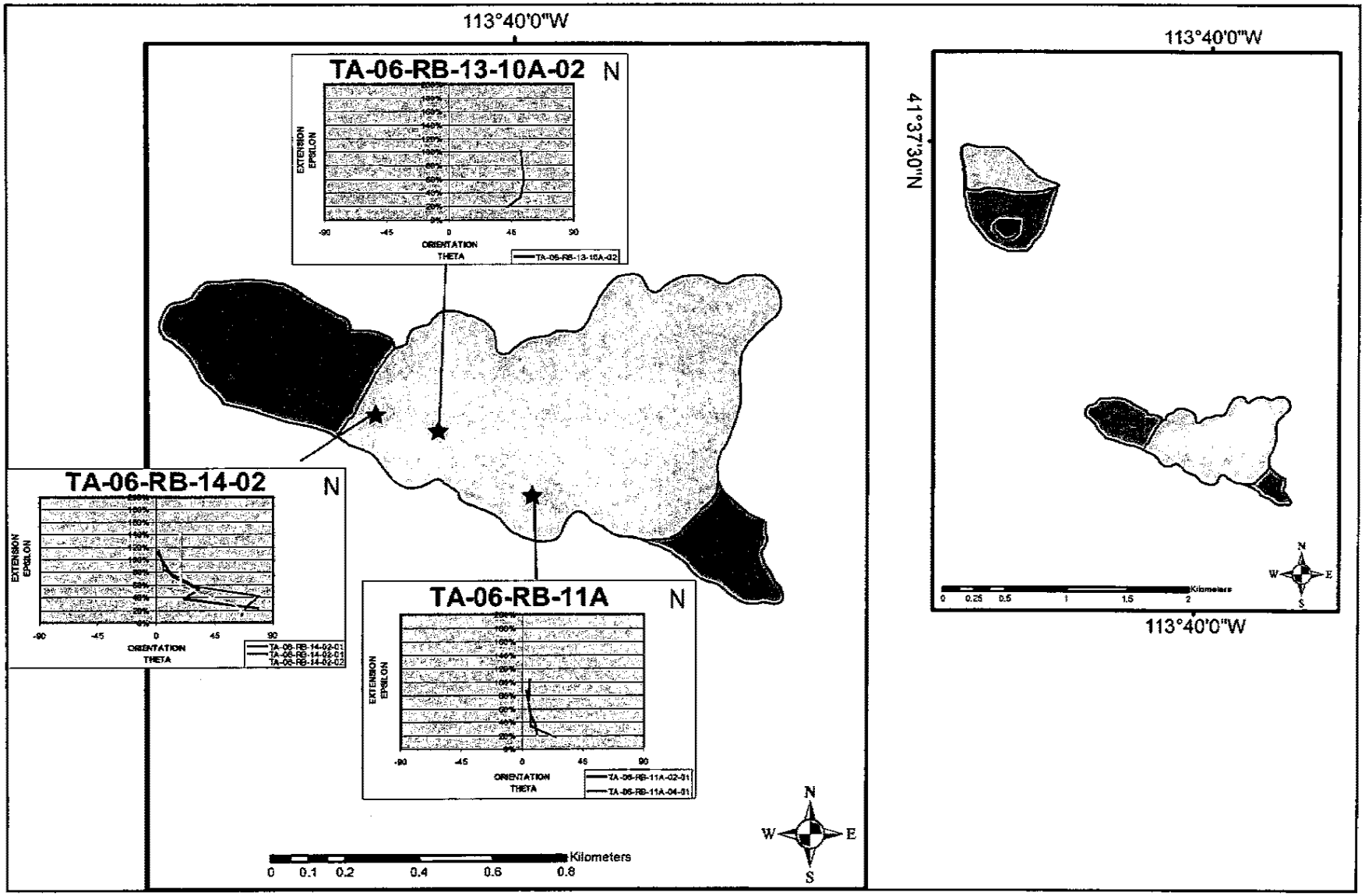
113°40'0"W
TA-06-RB-13-10A-02
N
EXTENSION EPSILON
ORIENTATION THETA
TA-06-RB-13-10A-02
TA-06-RB-14-02
N
TA-06-RB-11A
N
Kilometers
0 0.1 0.2 0.4 0.6 0.8
N
W
E
S
113°40'0"W
41°37'30"N
113°40'0"W
Kilometers
0 0.25 0.5 1 1.5 2

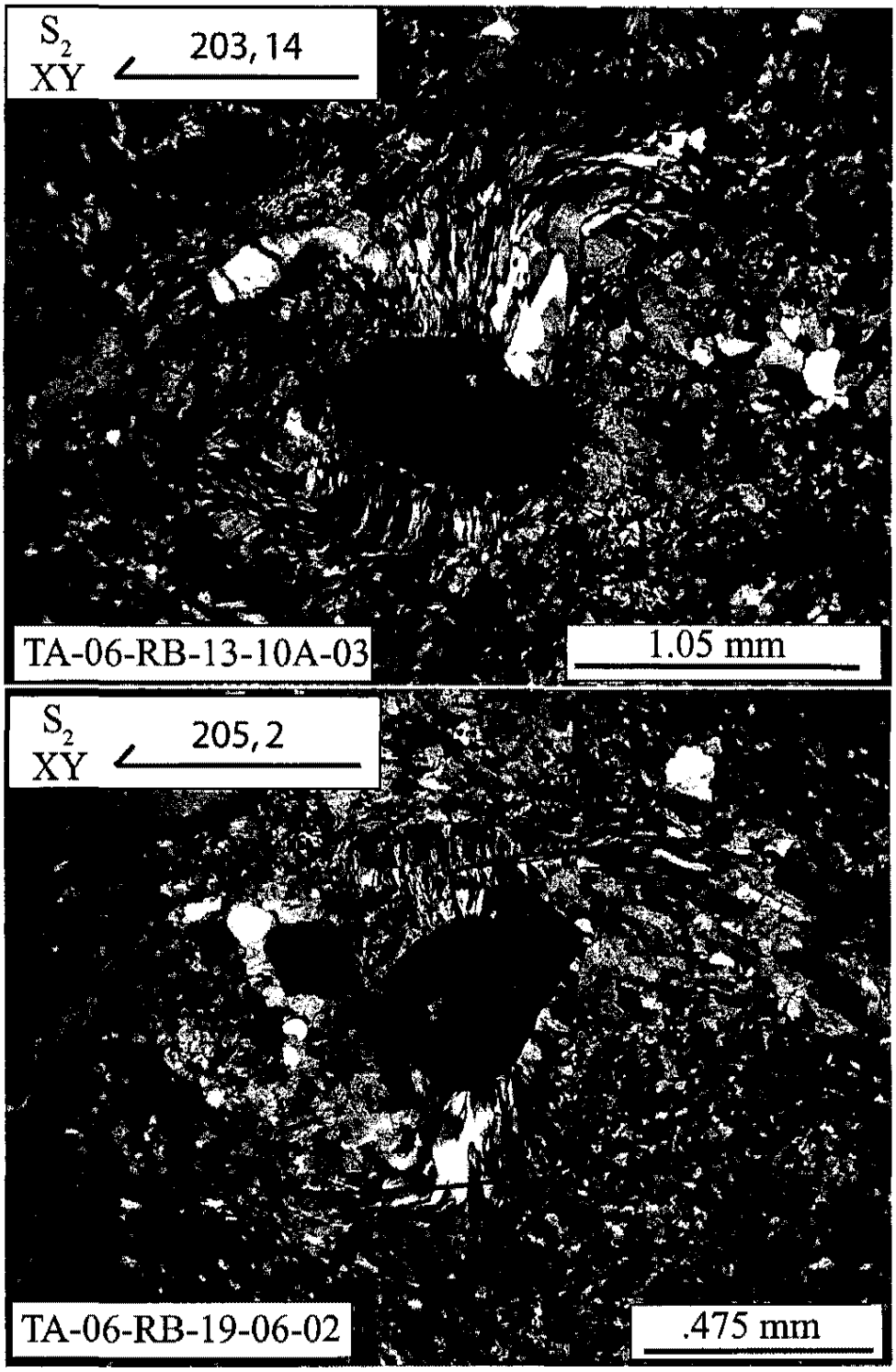

Figure 33. Photomicrographs of D_2 displacement-controlled strain fringes within the XY plane of the S_2 axial planar cleavage at Rosebud area. A, distal parts (older) of the strain fringe record an orientation of 218 and the proximal parts (younger) record an orientation of 113, recording a counter-clockwise orientation of infinitesimal strain. B, distal parts (older) record an orientation of 204 and the proximal parts (younger) record an orientation of 115, recording a counter-clockwise rotation. The scale is in the right hand corner of each sample, and the sample number is in the lower left hand corner.

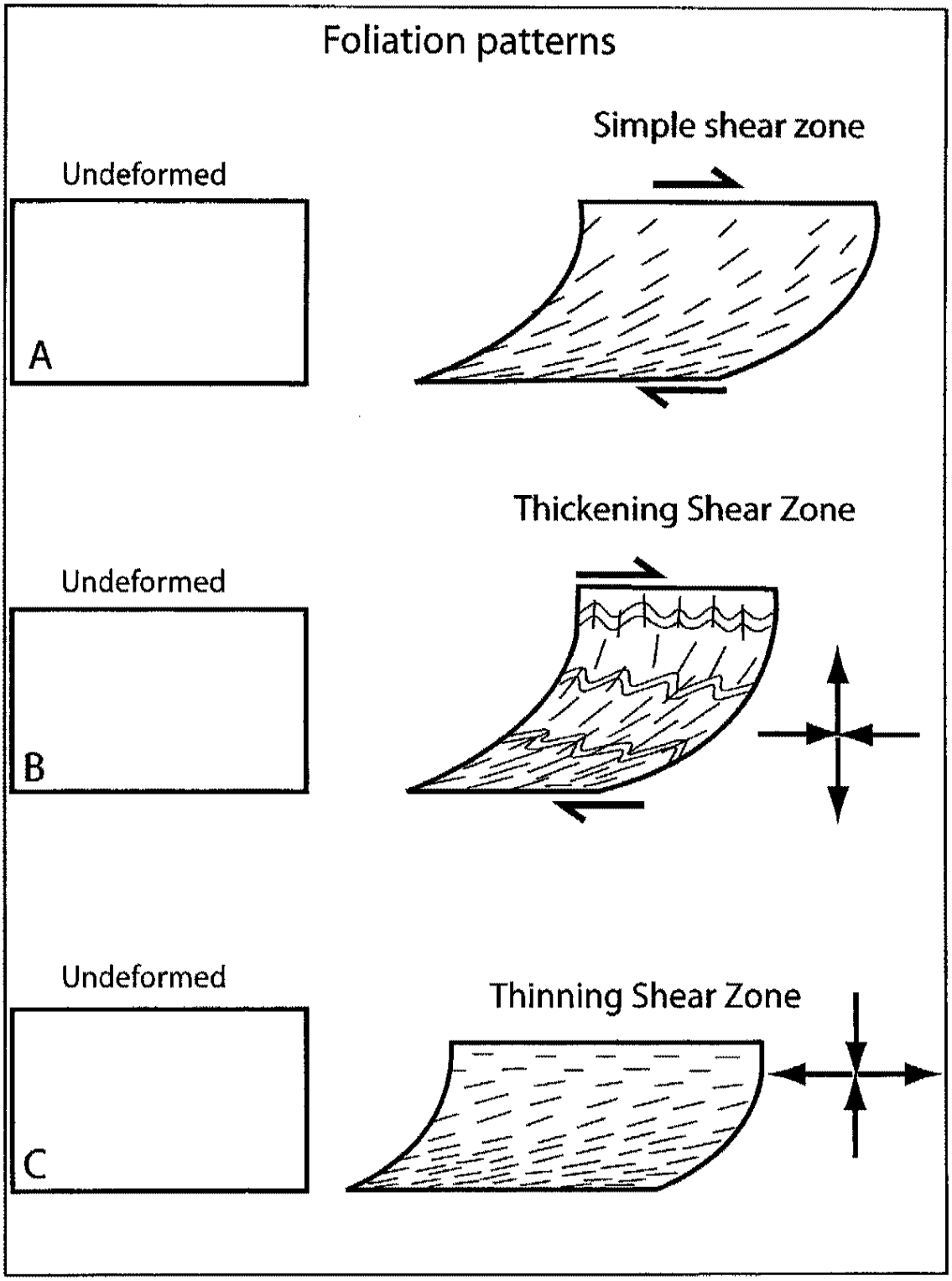

Figure 34. Patterns of foliation trajectories. A, heterogeneous simple shear zone increasing towards the base. B, thickening shear zone related to horizontal shortening (layer parallel) and vertical thickening. C, thinning shear zone related to horizontal thinning (layer parallel) and vertical thinning. Modified from Sanderson (1982).

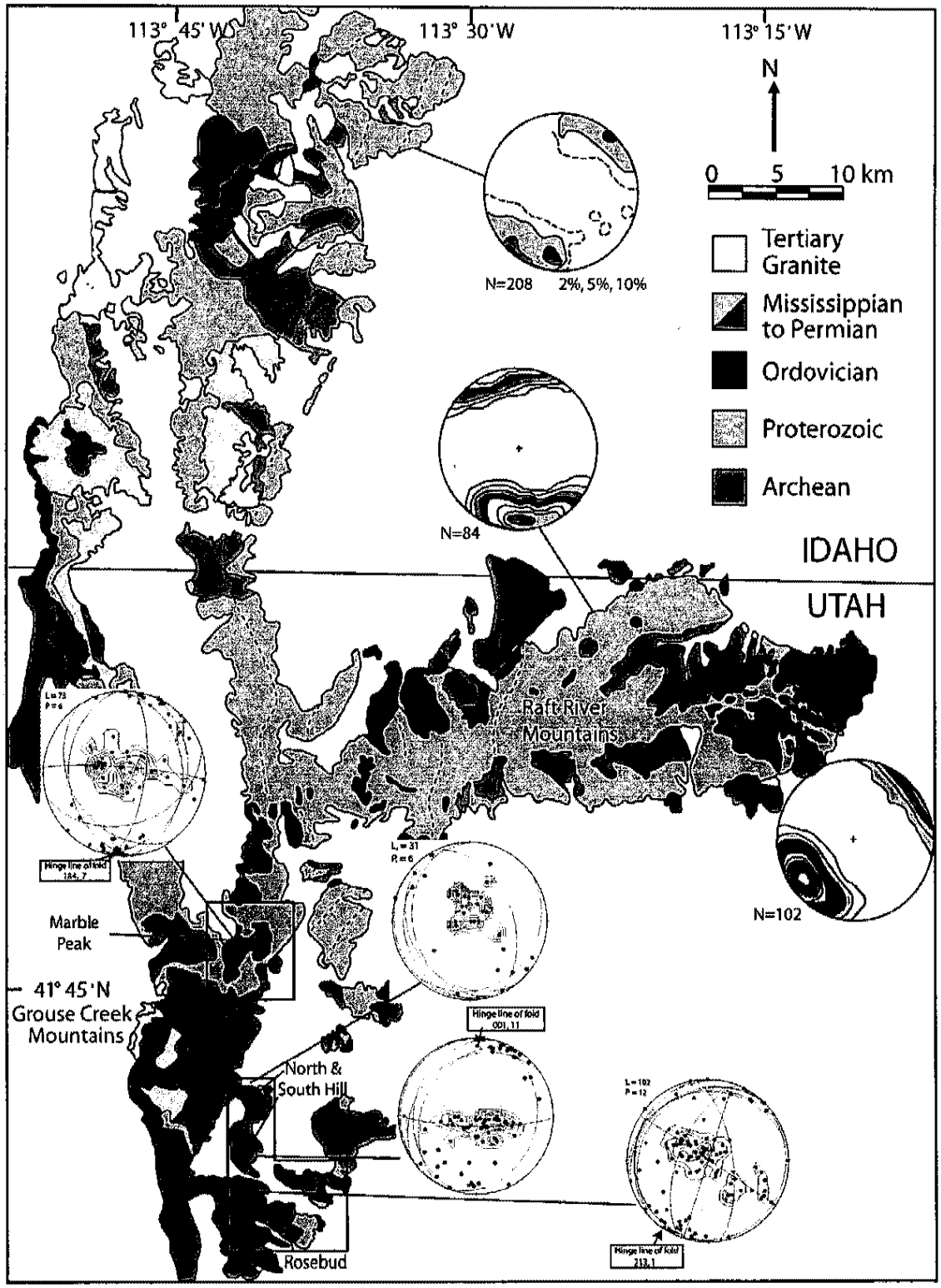

Figure 35. Generalized geologic map of Raft River-Albion-Grouse Creek Mountains (RAG) showing distribution of the L_1 stretching lineation. Field areas (in boxes) are at Marble Peak, North and South Hill and Rosebud area. Stereoplots showing L_1 from Compton (1972, 1975), Miller (1980), Todd (1980), Sheely (2002), Wells (1997), and this study. Modified from Wells et al. (2008).

Figure 36. Vertical strain gradient for D_1 and D_2 at Marble Peak within the Oquirrh Formation in relation to the Middle detachment. View looking east at Marble Peak from GoogleEarth. Finite strain magnitudes and approximate sample locations vertically within the allochthon are represented by triangles.

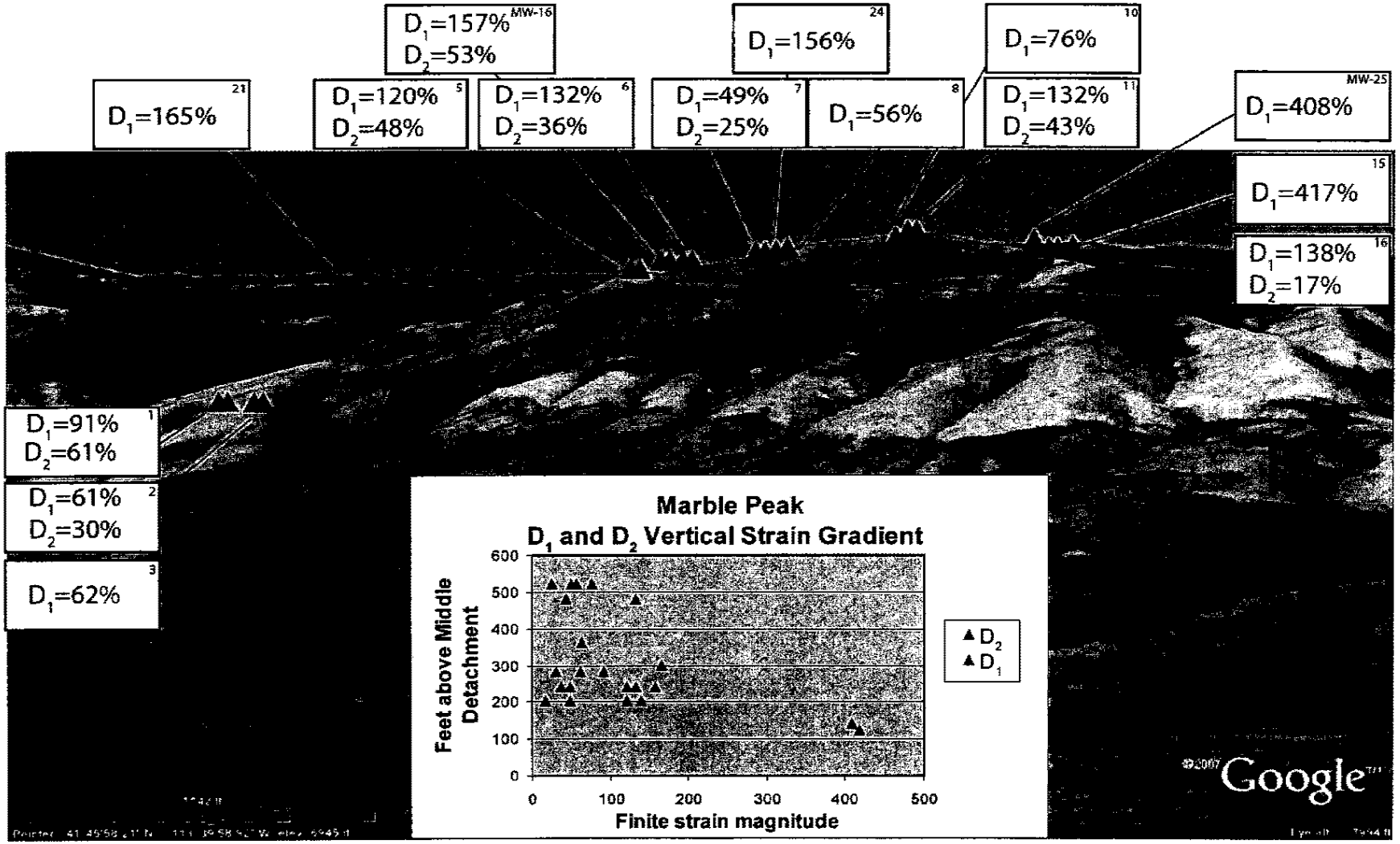
D1=157% MW-16
D2=53%
D1=156% 24
D1=76% 10
D1=165% 21
D1=120% 5
D2=48%
D1=132% 6
D2=36%
D1=49% 7
D2=25%
D1=56% 8
D1=132% 11
D2=43%
MW-25
D1=408%
15
D1=417%
16
D1=138%
D2=17%
1
D1=91%
D2=61%
2
D1=61%
D2=30%
3
D1=62%
Marble Peak
D1 and D2 Vertical Strain Gradient
Feet above Middle Detachment
600
500
400
300
200
100
0
0
100
200
300
400
500
Finite strain magnitude
D2
D1
©2007 Google

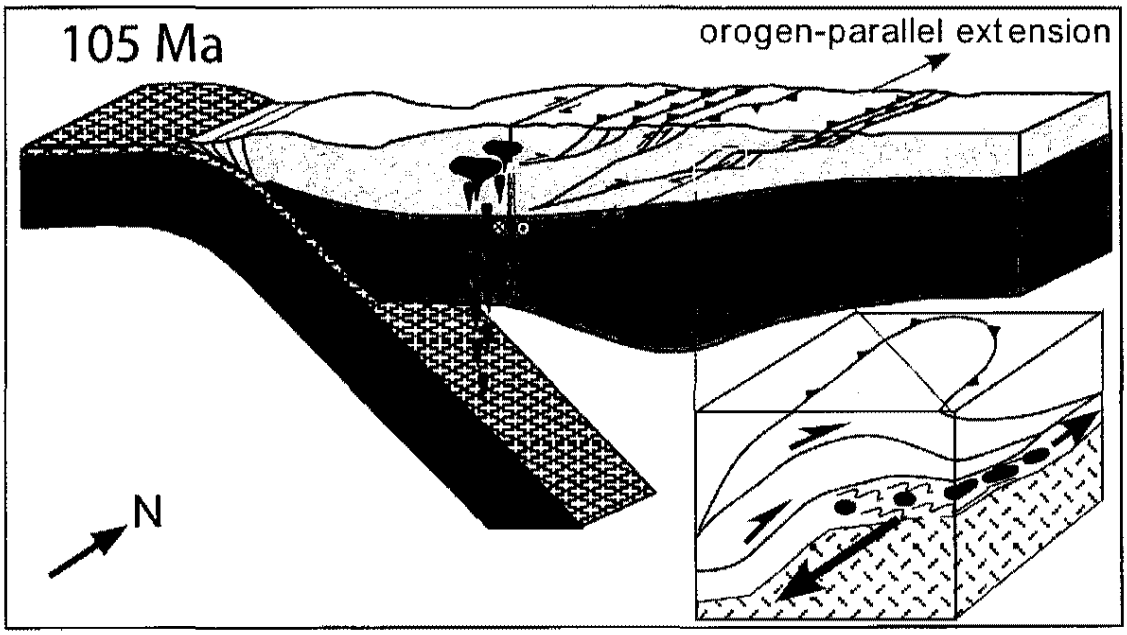

Figure 37. Simplified tectonic model for development of orogen-parallel extension at mid-crustal levels in the interior of the Sevier orogen around ~105 Ma. Inset shows a structural culmination with lineations oriented parallel to the fold hinge lines. (From Wells et al., 2008).

Figure 38. Sequence of Mesozoic to early Cenozoic deformation proposed for relative constraints on timing for the "D_2" event. (Malavieille, 1998; Hoisch et al., 2002; Hoisch and Wells; 2004; Wells et al., 1998; Wells et al., 2000; Wells et al., 2008).

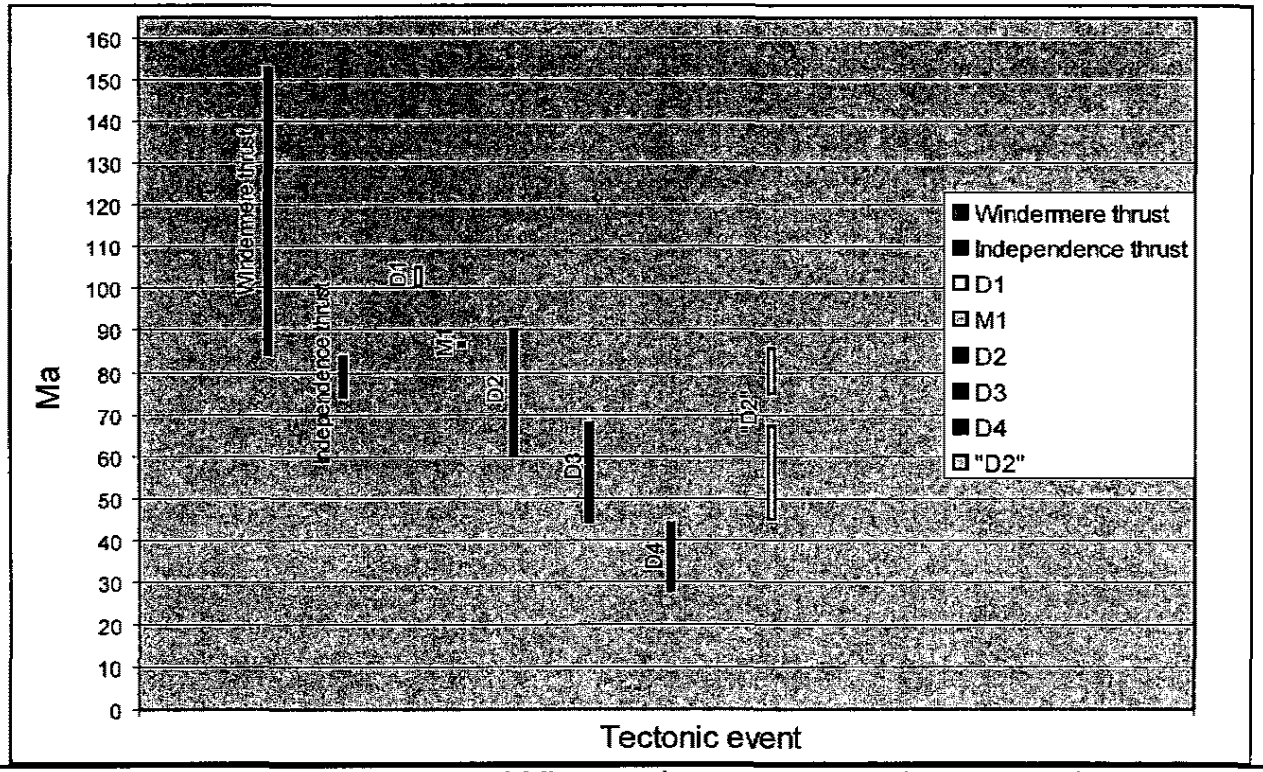

Tectonic event	Structure and Kinematics	Interpretation	Timing (Ma)
Windermere thrust	Top-to-the-southeast	Contraction	153-84
Independence thrust	Top-to-the-southeast	Contraction	84-75
D1 "this study"	Top-to-the-north shearing	Extension	105
M1	Isothermal compression, Basin-Elba fault (?)	Contraction	87
D2	Emigrant Spring and Mahogany Peaks faults	Extension	90-60
D3	Recumbent folding and thrust burial	Contraction	68-45
D4	Top-to-WNW shearing of MMSZ	Extension	45-38
"D2" this study	Top-to-the-southeast	Contraction	87-75 and 68-45

REFERENCES

Aerden, D.G., 1996, The pyrite-type strain fringes from Lourdes (France): indicators of Alpine thrust kinematics in the Pyrenees: Journal of Structural Geology, v. 18, p. 75-91.

Alsop, G.I., and Holdsworth, R.E., 2002, The geometry and kinematics of flow perturbation folds: Tectonophysics, v. 350, p. 99-125.

Alsop, G.I., and Holdsworth, R.E., 2004, The geometry and topology of natural sheath folds: a new tool for structural analysis: Journal of Structural Geology, v. 26, p. 1561-1589.

Alsop, G.I., and Holdsworth, R.E., 2006, Sheath folds as discriminators of bulk strain type: Journal of Structural Geology, v. 28, p. 1588-1606.

Anastasio, D.J., Fisher, D.M., Messina, T.A., and Holl, J.E., 1997, Kinematics of decollement folding in the Lost River Range, Idaho: Journal of Structural Geology, v. 19, p. 355-368.

Apotria, T.G., 1995, Thrust sheet rotation and out-of-plane strains associated with oblique ramps: an example from the Wyoming salient, U.S.A.: Journal of Structural Geology, v. 17, p. 647-662.

Armstrong, F.C., and Oriel, S.S., 1965, Tectonic development of the Idaho-Wyoming thrust belt: American Association of Petroleum Geologists Bulletin, v. 49, p. 1847-1866.

Armstrong, R.L., 1968, Sevier Orogenic Belt in Nevada and Utah: Geological Society of America Bulletin, v. 79, p. 429-458.

Beutner, E.C., and Diegel, F.A., 1985, Determination of fold kinematics from syntectonic fibers in pressure shadows, Martinsburg Slate, New Jersey: American Journal of Science: v. 285, p. 16-50.

Bird, P., 2002, Stress direction history of the western United States and Mexico since 85 Ma: Tectonics, v. 21, p. 1-12.

Burchfiel, B.C., Cowan, D.S., and Davis, G.A., 1992, Tectonic overview of the Cordilleran orogen in the western United States, *in* Burchfiel, B.C., Lipman, P.W.,

and Zoback, M.L., eds, The Cordilleran Orogen: Conterminous U. S.: Geological Society of America, The Geology of North America, v. G-3, p. 407–480.

Butler, R.W., and Freeman, S., 1996, Can crustal extension be distinguished from thrusting in the internal parts of mountain belts? A case history of the Entrelor shear zone, western Alps: Journal of Structural Geology, v. 18, p. 909-923.

Camilleri, P.A., 1998, Prograde metamorphism, strain evolution, and collapse of footwalls of thick thrust sheets: a case study from the Mesozoic Sevier hinterland U.S.A.: Journal of Structural Geology, v. 20, p. 1023-1042.

Camilleri, P.A., and Chamberlain, K.R., 1997, Mesozoic tectonics and metamorphism in the Pequop Mountains and Wood Hills region, northeast Nevada: implications for the architecture and evolution of the Sevier orogen: Geological Society of America Bulletin, v. 109, p. 74–94.

Clark, M.B., Fisher, D.M., and Chia-yu, 1993, Kinematic analysis of the Hfueshan Range: A large-scale pop-up structure: Tectonics, v. 12, p. 205-217.

Cobbold, P.R., and Quinquis, H., 1980, Development of sheath folds in shear regimes: Journal of Structural Geology, v. 2, p. 119-126.

Coleman, M.E., 1996, Orogen-parallel and orogen perpendicular extension in the central Nepalese Himalayas: Geological Society of America Bulletin, v. 108, p. 1594-1607.

Compton, R. R., 1972, Geologic map of Yost quadrangle, Box Elder County, Utah, and Cassia County, Idaho: U.S. Geological Survey Miscellaneous Geologic Investigations Map, I-672, 1 p.

Compton, R. R., 1975, Geologic map of Park Valley quadrangle, Box Elder County, Utah, and Cassia County, Idaho: U.S. Geological Survey Miscellaneous Geologic Investigations Map, I-873, 1 p.

Compton, R. R., 1980, Fabrics and strains in quartzites of a metamorphic core complex, Raft River Mountains,

Compton, R.R., Todd, V.R., Zartman, R.E., and Naeser, C.W., 1977, Oligocene and Miocene metamorphism, folding, and low-angle faulting in northwestern Utah: Geological Society of America Bulletin, v. 88, p. 1237-1250.

Compton, R.R., 1983, Displaced Miocene rocks on the west flank of the Raft River-Grouse Creek core complex, Utah *in* Miller, D.M., Todd, V.R., and Howard, K.A., eds., Tectonic and stratigraphic studies in the eastern Great Basin: Geological Society of America Memoir, v. 157, p. 271-279.

Conder, J., Butler, R.F., DeCelles, P.G., and Constenius, K., 2003, Paleomagnetic determination of vertical-axis rotations within the Charleston-Nebo salient, Utah: Geology, v. 31, p. 1113-1116.

Coogan, J.C., 1992, Thrust systems and displacement transfer in the Wyoming-Idaho-Utah thrust belt: Ph.D. dissertation, University of Wyoming.

Coogan, J.C., and Royse, F., Jr., 1990, Overview of recent developments in thrust belt interpretation, *in* Roberts, S., ed., Geologic field tours of western Wyoming and adjacent Idaho, Montana, and Utah: Geological Survey of Wyoming Public Information Circular 29, p. 89-124.

Cruz-Uribe, A., Hoisch, T.D., Wells, M.L., Vervoort, J., 2007, Adding the t to garnet P-T paths using the Lu-Hf method: Age constraints on thrusting and exhumation events in the hinterland of the Sevier orogen: AGU Annual Meeting, Abstract.

Davis, B.K., and Maidens, E., 2003, Archaean orogen-parallel extension: evidence from the northern Eastern Goldfields Province, Yilgarn Craton: Precambrian Research, v. 127, p. 229-248.

Davis, G.H., and Reynolds, S.J., 1984, Structural geology of Rocks and Regions: New York, John Wiley and Sons, 776p.

Decelles, P.G., 2004, Late Jurassic to Eocene evolution of the Cordilleran thrust belt, and foreland basin system, western U.S.A: American Journal of Science, v. 304, p. 105-168.

Dietrich, D., and Durney, D.W., 1986, Change of direction of overthrust shear in the Helvetic nappes of western Switzerland: Journal of Structural Geology, v. 8, p. 389-398.

Dixon, J.S., 1982, Regional structural syntheses, Wyoming salient of the western overthrust belt: American Association of Petroleum Geologists Bulletin, v. 6, p. 1560-1580.

Dudash, S.L., 2001, Polymetamorphism of a > 2.5 Ga pelitic schist in the Grouse Creek Mountains, northwestern Utah: M.S. thesis, Northern Arizona University.

Durney, D.W., and Ramsay, J.G., 1973, Incremental strains measured by sytectonic crystal growths *in* DeJong, K.A., and Scholten, R., eds., Gravity and Tectonics: New York, John Wiley and Sons, p. 67-96.

Egger, A.E., Dumitru, T.A., Miller, E.L., and Savage, C.F.I., 2003, Timing and nature of Tertiary plutonism and extension in the Grouse Creek Mountains, Utah: International Geology Review, v. 45, p. 497-532.

Ellis, M., and Watkinson, A.J., 1987, Orogen-parallel extension and oblique tectonics: The relation between stretching lineations and relative plate motions: Geology, v. 15, p. 1022-1026.

Engebretson, D.C., Cox, A., and Gordon, R.G., 1985, Relative motions between oceanic and continental plates in the Pacific Basin: Geological Society of America Special Paper 206, 59 p.

Etchecopar, A., and Malavieille, J., 1987, Computer models of pressure shadows: a method for strain measurement and shear-sense determination: Journal of Structural Geology, v. 9, p. 667-677.

Fergusson, C.L., Henderson, R.A., Withnall, I.W., Fanning, C.M., Phillips, D., and Lewthwaite, K.J., 2007, Structural, metamorphic, and geochronological constraints on alternating compression and extension in the Early Paleozoic Gondwanan Pacific margin, northeastern Australia: Tectonics, v. 26, TC3008.

Ferrill, D.A., 1991, Calcite twin widths and intensities as metamorphic indicators in natural low-temperature deformation of limestone: Journal of Structural Geology, v. 13, p. 667-675.

Ferrill, D.A., and Groshong, R.H., Jr., 1993, Kinematic model for the curvature of the northern Subalpine Chain, France: Journal of Structural Geology, v. 15, p. 523-541.

Fisher, D.M., and Byrne, T., 1992, Strain variations in an ancient accretionary complex: implications for forearc evolution: Tectonics, v. 11, p. 330-347.

Fisher, D.M., and Anastasio, D.J., 1994, Kinematic analysis of a large-scale leading edge fold, Lost River Range, Idaho: Journal of Structural Geology, v. 16, p. 337-354.

Fossen, H., and Tikoff, B., 1998, Extended models of transpression and transtension, and application to tectonic settings *in* Holdsworth, R.E., Strachan, R.A., and Dewey, J.F., eds., Continental transpressional and transtensional tectonics: Geological Society, London, Special Publications, v. 135, p. 15-33.

Frisch, W., Kuhlemann, J., Dunkl, I., and Bruegel, A., 1998, Palinspastic reconstruction and topographic evolution of the eastern Alps during late Tertiary tectonic extrusion: Tectonophysics, v. 297, p. 1-15.

Froitzheim, N., 1992, Formation of recumbent folds during synorogenic crustal extension (Austroalpine nappes, Switzerland): Geology, v. 20, p. 923-926.

Ghosh, S.K., and Ramberg, H., 1976, Reorientation of inclusions by combination of pure shear and simple shear: Tectonophysics, v. 34, p. 1-70.

Ghosh S.K., Hazra, S., and Sengupta, S., 1999, Planar, non-planar and refolded sheath folds in the Phulad Shear Zone, Rajasthan, India: Journal of Structural Geology, v. 21, p. 1715-1729.

Groshong, R.H., Jr., 1988, Low-temperature deformation mechanisms and their interpretation: Geological Society of America Bulletin, v. 100, p. 1329-1360.

Harris, C. R., 2003, A pressure-temperature path record of repeated thrusting and exhumation in the Sevier hinterland, Albion Mountains, Idaho: M.S. thesis, Northern Arizona University.

Harris, C.R., Hoisch, T.D., and Wells, M.L., 2007, Construction of a composite pressure-temperature path: revealing the synorogenic burial and exhumation history of the Sevier hinterland, USA: Journal of Metamorphic Geology, v. 25, p. 915-934.

Hoisch, T.D., Wells, M.L., and Hanson, L.M., 2002, Pressure-temperature paths from garnet-zoning: Evidence for multiple episodes of thrust burial in the hinterland of the Sevier orogenic belt: American Mineralogist, v. 87, p. 115-131.

Hudec, M.R., 1992, Mesozoic structural and metamorphic history of the central Ruby Mountains metamorphic core complex, Nevada: Geological Society of America Bulletin, v. 104, p. 1086-1100.

Jackson, J., 2002, Faulting, flow, and the strength of the continental lithosphere: International Geology Review, v. 44, p. 39-61.

Janecke, S.U., Vandenburg, C.J., and Blankenau, J.J., 1998, Geometry, mechanisms and significance of extensional folds from examples in the Rocky Mountain Basin and Range province, U.S.A.: Journal of Structural Geology, v. 20, p. 841-856.

Kelly, E.D., 2004, Pressure-temperature paths and isotopic dating along a major thrust, Sevier hinterland, Albion Mountains, Idaho: M.S. thesis, Northern Arizona University.

Kerrich, R., 1978, An historical review and synthesis of research on pressure solution: Zentralblatt fuer Mineralogie Geologie und Palaeontologie, v. 1, p. 512-550.

Knipe, R.J., 1989, Deformation mechanisms—recognition from natural tectonites: Journal of Structural Geology, v. 11, p. 127-146.

Koehn, D., Bons, P.D., and Passchier C.W., 2003, Development of antitaxial strain fringes during non-coaxial deformation: an experimental study: Journal of Structural Geology, v. 25, p. 263-275.

Koehn, D., Aerden, D.G.A., Bons, P.D., and Passchier, C.W., 2001, Computer experiments to investigate complex fibre patterns in natural antitaxial strain fringes: Journal of Metamorphic Geology, v. 19, p. 217-231.

Koehn, D., Hilgers, C., Bons, P.D., and Passchier, C.W., 2000, Numerical simulation of fibre growth in antitaxial strain fringes: Journal of Stuctural Geology, v. 22, p. 1311-1324.

Kwon, S., and Mitra, G., 2004, Strain distribution, strain history and kinematic evolution associated with the formation of arcuate salients in fold-thrust belts: the example of the Provo salient, Sevier orogen, Utah: Geological Society of America Special Paper, v. 383, p. 205-223.

Lacassin, R., and Mattauer, M., 1985, Kilometre-scale sheath fold at Mattmark and implications for transport direction in the Alps: Nature, v. 315, p. 739-741.

Lamb, S.H., 1994, Behavior of the brittle crust in wide plate boundary zones: Journal of Geophysical Research, v. 99, p. 4457-4483.

Lamerson, P., 1982, The Fossil Basin area and its relationship to the Absaroka fault system, *in* Powers, R.B., ed., Geologic studies of the Cordilleran thrust belt, vol. 1: Rocky Mountain Association of Geologists, p. 279-340.

Laubscher, H.P., 1972, Some overall aspects of the Jura dynamics: American Journal of Science, v. 272, p. 293-304.

Lister, G.S., and Davis, G.A., 1989, The origin of metamorphic core complexes and detachment faults formed during Tertiary continental extension in the northern Colorado River region, U.S.A.: Journal of Structural Geology, v. 11, p. 65-94.

Lush, A.P., McGrew, A.J., Snoke, A.W., and Wright, J.E., 1988, Allochthonous Archean basement in the northern East Humboldt Range, Nevada: Geology, v. 16, p. 349-353.

Malavieille, J., 1987a, Extensional shearing deformation and kilometer-scale "a" type folds in a Cordilleran metamorphic core complex (Raft River Mountains, northwestern Utah): Tectonics, v. 6, p. 423-448.

Malavieille, J., 1987b, Kinematics of compressional and extensional ductile shearing deformation in a metamorphic core complex of the northeastern Basin and Range: Journal of Structural Geology, v. 9, p. 541-554.

Mancktelow, N.S., 1992, Neogene lateral extension during convergence in the Central Alps: Evidence from interrelated faulting and backfolding around the Simplonpass (Switzerland): Tectonophysics, v. 215, p. 295-317.

Manning, A.H., and Bartley, J.M., 1994, Postmylonitic deformation in the Raft River metamorphic core complex, northwestern Utah: Evidence of a rolling hinge: Tectonics, v. 13, p. 596-612.

Marshak, S., 1988, Kinematics of orocline and arc formation in thin-skinned orogens: Tectonics, v. 7, p. 73-86.

Marshak, S., Wilkerson, M.S., and Hsui, A., 1992, Generation of curved fold-thrust belts: insight from simple physical and analytical models, *in* McClay, K.R., ed., Thrust tectonics: London, Chapman and Hall, p. 83-92.

McCaffrey, R., 1991, Slip vectors and stretching of the Sumatran fore arc: Geology, v. 19, p. 881-884.

McCaffrey, R., 1996, Estimates of modern arc-parallel strain rates in fore arcs: Geology, v. 24, p. 27-30.

McCaffrey, R., and Nabelek, J., 1998, Role of oblique convergence in the active deformation of the Himalayas and southern Tibet plateau: Geology, v. 26, p. 691-694.

McKenzie, D., 1979, Finite deformation during fluid flow: Geophysical Journal International, v. 58, p. 689-715.

McKenzie, D., and Jackson, J., 1983, The relationship between strain rates, crustal thickening, palaeomagnetism, finite strain and fault movements within a deforming zone: Earth and Planetary Science Letters, v. 65, p. 182-202.

Means, W.D., Hobbs, B.E., Lister, G.S., and Williams, P.F., 1980, Vorticity and non-coaxiality in progressive deformations: Journal of Structural Geology, v. 2, p. 371-378.

Merschat, A.J., Hatcher, R.D., and Davis, T.L., 2005, The northern Inner Piedmont, southern Appalachians, USA: kinematics of transpression and SW-directed mid-crustal flow: Journal of Structural Geology, v. 27, p. 1252-1281.

Miller, D.M., 1980, Structural geology of the northern Albion Mountains, south-central Idaho, *in* Crittenden, M.D., Jr., Coney, P.J., and Davis, G.H., eds., Cordilleran metamorphic core complexes: Geological Society of America Memoir 153, p. 35-77.

Miller, D. M., Repetski, J.E., and Harris, A.G., 1991, East-trending Paleozoic continental margin near Wendover, Utah, *in* Cooper, J.D., and Stevens, C.H., eds., Paleozoic Paleogeography of the Western United States, Volume II: Los Angeles, Pacific Section, SEPM (Society for Sedimentary Geology), Book 67, p. 439–461.

Miller, R.B., Paterson, S.R., Lebit, H., Alsleben, H., and Luneburg, C., 2006, Significance of composite lineations in the mid- to deep crust: a case study from the North Cascades, Washington: Journal of Structural Geology, v. 28, p. 302-322.

Mitra, G., 1994, Strain variation in thrust sheets across the Sevier fold and thrust belt (Idaho-Utah-Wyoming): implications for section restoration and wedge taper evolution: Journal of Structural Geology, v. 16, p. 585-602.

Molnar, P., and Tapponnier, P., 1975, Cenozoic tectonics of Asia: effects of a continental collision: Science, v. 189, p. 419-426.

Müller, R.D., Roest, W.R., Royer, J.Y., Gahagan, L.M., and Sclater, J.G., 1997, Digital isochrons of the world's ocean floor: Journal of Geophysical Research, v. 102, p. 3211-3214.

Müller, W., Aerden, D., and Halliday, A.N., 2000, Isotopic dating of strain increments: Duration and rates of deformation in shear zones: Science, v. 288, p. 2195-2198.

Murphy, M.A., Yin, A., Kapp, P., Harrison, T.M., Manning, C.E., Ryerson, F.J., Lin, D., and Jinghui, G., 2002, Structural evolution of the Gurla Mandhata detachment system, southwest Tibet: Implications for the eastward extent of the Karakoram fault system: Geological Society American Bulletin, v. 114, p. 428-447.

Nelson, S.T., Harris, R.A., Dorais, M.J., Heizler, M., Constenius, K.N., and Barnett, D.E., 2002, Basement complexes in the Wasatch fault, Utah, provide new limits on crustal accretion: Geology, v. 30, p. 831-834.

Onderdonk, N.W., 2007, Vertical-axis rotation controlled by upper crustal stress based on force balance analysis: a case study of the western Transverse Ranges of California: Tectonophysics, v. 436, p. 1-8.

Passchier, C.W., and Trouw, R.A.J., 2005, Microtectonics: Berlin, Springer, 366p.

Paulsen, T., and Marshak, S., 1999, Origin of the Uinta recess, Sevier fold-thrust belt, Utah: influence of basin architecture on fold-thrust belt geometry: Tectonophysics, v. 312, p. 203-216.

Platt, J.P., 1986, Dynamics of orogenic wedges and uplift of high-pressure metamorphic rocks: Geological Society of America Bulletin, v. 97, p. 1037-1053.

Platt, J.P., and England, P.C., 1993, Convective removal of lithosphere beneath mountain belts: thermal and mechanical consequences: American Journal of Science, v. 293, p. 307-336.

Ramberg, H., 1975, Particle paths, displacement and progressive strain applicable to rocks: Tectonophysics, v. 28, p. 1-37.

Ramsay, J.G., and Graham, R.H., 1970, Strain variation in shear belts: Canadian Journal of Earth Sciences, v. 7, p. 786-813.

Ramsay, J.G., and Huber, M.I., 1983, The Techniques of Modern Structural Geology Volume 1: Strain Analysis: London, Academic Press, 307p.

Rey, P., Vanderhaeghe, O., and Teyssier, C., 2001, Gravitational collapse of the continental crust: definition, regimes and modes: Tectonophysics, v. 342, p. 435-449.

Rosenberg, C.L., Brun, J.P., and Gapais, D., 2004, Indentation model of the Eastern Alps and the origin of the Tauern Window: Geology, v. 32, p. 997-1000.

Royse, F., Jr., 1993, An overview of the geologic structure of the thrust belt in Wyoming, northern Utah, and eastern Idaho: Geological Society of Wyoming Memoir, v. 5, p. 272-311.

Royse, F., Jr., Warner, M.A., and Reese, D.L., 1975, Thrust belt structural geometry and related stratigraphic problems Wyoming-Idaho-northern Utah, *in* Bolyard, D.W., ed., Deep drilling frontiers of the central Rocky Mountains: Denver, Rocky Mountain Association of Geologists, p. 41-54.

Saltzer, S.R., and Hodges, K.V., 1988, The Middle Mountain shear zone, southern Idaho: Kinematic analysis of an early Tertiary high-temperature detachment: Geological Society of America Bulletin, v. 100, p. 96-103.

Sanderson, D.J., 1982, Models of strain variation in nappes and thrust sheets: a review: Tectonophysics, v. 88, p. 201-233.

Sanderson, D.J., and Marchini, W.R.D., 1984, Transpression: Journal of Structural Geology, v. 6, p. 449-458.

Seyferth, M., and Henk, A., 2004, Syn-convergent exhumation and lateral extrusion in continental collision zones—insights from three-dimensional numerical models: Tectonophysics, v. 382, p. 1-29.

Sheely, J.C., 2002, Kinematics and timing of normal faulting in a metamorphic core complex: Grouse Creek Mountains, Utah: M.S. thesis, University of Nevada, Las Vegas.

Simpson, C., and DePaor, D.G., 1993, Strain and kinematic analysis in general shear zones: Journal of Structural Geology, v. 15, p. 1-20.

Stewart, J.H., Poole, F.G., Ketner, K.B., Madrid, R.J., Roldan-Quintana, J., and Amaya-Martinez, R., 1990, Tectonics and stratigraphy of the Paleozoic and Triassic southern margin of North America, Sonora, Mexico: Arizona Geological Survey Special Paper, p. 1-17.

Sullivan, W.A., and Snoke, A.W., 2007, Comparative anatomy of core-complex development in the northeastern Great Basin, U.S.A.: Rocky Mountain Geology, v. 42, p. 1-29.

Takasu, A., Wallis, S.R., Banno, S., and Dallmeyer, R.D., 1994, Evolution of the Sambagawa metamorphic belt, Japan: Lithos, v. 33, p. 119-133.

Teyssier, C., Tikoff, B., and Markley, M., 1995, Oblique plate motion and continental tectonics: Geology, v. 23, p. 447-450.

Tikoff, B., and Fossen, H., 1995, The limitations of three-dimensional kinematic vorticity number: Journal of Structural Geology, v. 17, p. 1771-1784.

Todd, V.R., 1980, Structure and petrology of a Tertiary gneiss complex in northwestern Utah, *in* Crittenden, M.D., Jr., Coney, P.J., and Davis, G.H., eds., Cordilleran metamorphic core complexes: Geological Society of America Memoir 153, v. 153, p. 349-383.

Vanderhaeghe, O., and Teyssier, C., 2001, Partial melting and flow of orogens: Tectonophysics, v. 342, p. 451-472.

Wallis, S., 1995, Vorticity analysis and recognition of ductile extension in the Sanbagawa belt, southwest Japan: Journal of Structural Geology, v. 17, p. 1077-1093.

Wallis, S.R., Banno, S., and Radvanec, M., 1992, Kinematics, structure and relationship to metamorphism of the east-west flow in the Sanbagawa Belt, southwest Japan: The Island Arc: v. 1, p. 176-185.

Wells, M.L., 1997, Alternating contraction and extension in the hinterlands of orogenic belts: An example from the Raft River Mountains, Utah: Geological Society of America Bulletin, v. 109, p. 107-126.

Wells, M.L., 2001, Rheological control on the initial geometry of the Raft River detachment fault and shear zone, western United States: Tectonics, v. 20, p. 435-457.

Wells, M.L., Dallmeyer, R.D., and Allmendinger, R.W., 1990, Late Cretaceous extension in the hinterland of the Sevier thrust belt, northwestern Utah and southern Idaho: Geology, v. 18, p. 929-933.

Wells, M.L., Spell, T.L., and Zanetti, K., 2000, Laserprobe Argon dating of strain fringes: Albion-orogen-parallel extension in the hinterland of the Sevier Orogen: Geological Society of America Abstracts with Programs, v. 32, p. A-106.

Wells, M.L., Hoisch, T.D., Hanson, L.M., Wolff, E.D., and Struthers, J.R., 1997, Large magnitude crustal thickening and repeated extensional exhumation in the Raft River, Grouse Creek, and Albion Mountains: BYU Geology Studies, v. 42, part 1.

Wells, M.L, Spell, T.L., Hoisch, T.D., Arriola, T., and Zanetti, K.A., 2008, Laserprobe $^{40}Ar/^{39}Ar$ dating of strain fringes: Mid-Cretaceous synconvergent orogen-parallel extension in the interior of the Sevier orogen: Tectonics.

Wells, M.L., Beyene, M.A., Spell, T.L., Kula, J.L., Miller, D.M., and Zanetti, K.A., 2005, The Pinto shear zone; a Laramide synconvergent extensional shear zone in the Mojave Desert region of the southwestern United States: Journal of Structural Geology, v. 27, p. 1697-1720.

Wheeler, J., and Butler, R.W.H., 1994, Criteria for identifying structures related to true crustal extension in orogens: Journal of Structural Geology, v. 16, p. 1023-1027.

Yonkee, A., 1997, Kinematics and mechanics of the Willard thrust sheet, central part of the Sevier orogenic wedge, north-central Utah: Brigham Young University Geology Studies, v. 42, p. 341-354.

Yonkee, A., 2005, Strain patterns within part of the Willard thrust sheet, Idaho-Utah-Wyoming thrust belt: Journal of Structural Geology, v. 27, p. 1315-1343.

Zartman, R.E., 1974, Lead isotopic provinces of the Cordillera of the western United States and the geologic significance: Economic Geology, v. 69, p. 792-805.

Zweigel, P., Ratschbacher, L., and Frisch, W., 1998, Kinematics of an arcuate fold-thrust belt: the southern Eastern Carpathians (Romania): Tectonophysics, v. 297, p. 177-207.

VITA

Graduate College
University of Nevada, Las Vegas

Tonia G. Arriola

Local Address:
9420 Kingsley Ct.
Las Vegas, NV 89149

Home Address:
3919 Blossom St.
Houston, TX 77007

Degrees:
Bachelor of Science, Geology, 2002
University of Nevada, Las Vegas

Awards:
UNLV Department of Geoscience, Death Valley Scholarship, 2006
UNLV Department of Geoscience, Bernarda E. French Scholarship, 2006
Geological Society of America Research Grant, 2006
UNLV Geosymposium 1st place poster presentation, 2006
UNLV Geosymposium 1st place oral presentation, 2007
Funding for this project was provided by a research grant awarded to Dr. Michael L. Wells.

Publications:
Wells, M.L., Spell, T.L., Arriola, T., and Hoisch, T.S., 2007, A mid-Cretaceous age for synconvergent orogen-parallel extension in the interior of the Sevier orogen constrained by laserprobe 40Ar/39Ar dating of strain fringes: Geological Society of America Abstracts with Programs.

Wells, M.L, Spell, T.L., Hoisch, T.D., Arriola, T., and Zanetti, K.A., 2008, Laserprobe $^{40}Ar/^{39}Ar$ dating of strain fringes: Mid-Cretaceous synconvergent orogen-parallel extension in the interior of the Sevier orogen: Tectonics.

Thesis Title: Kinematics and Timing of Orogen-Parallel Flow, Grouse Creek Mountains, Utah.

Thesis Examination Committee:
Chairperson, Dr. Michael L. Wells, Ph.D.
Committee Member, Dr. Terry Spell, Ph.D.
Committee Member, Dr. Thomas Hoisch, Ph.D.
Graduate Faculty Representative, Dr. Michael Pravica, Ph.D.